Ninevah University

College of Electronics

Electronic Department

Design and Simulation of High Efficiency Quantum-Dot Solar Cells Based on Nano-crystal Technology

Iman Mohsin Ahmed

A Thesis in

Electronic Engineering

Supervised by

Prof.

Dr. Qais Thanon Algwari

Assist. Prof.

Dr. Omar Ibrahim Alsaif

Design and Simulation of High Efficiency Quantum-Dot Solar Cells Based on Nano-crystal Technology

A Thesis Submitted by

Iman Mohsin Ahmed

To

The Council of the College of Electronics Engineering

Ninevah University

As a Partial Fulfillment of the Requirements

For the Degree of Master of Science

In

Electronic Engineering

Supervised by

Prof.

Dr. Qais Thanon Algwari

Assist. Prof.

Dr. Omar Ibrahim Alsaif

بِسْمِ اللهِ الرَّحْمَنِ الرَّحِيمِ

﴿يَرْفَعِ ٱللَّهُ ٱلَّذِينَ ءَامَنُواْ مِنكُمْ وَٱلَّذِينَ أُوتُواْ ٱلْعِلْمَ

دَرَجَٰتٍ وَٱللَّهُ بِمَا تَعْمَلُونَ خَبِيرٌ﴾

صَدَقَ اللهُ الْعَظِيمُ

(سورة المجادلة، الآية:11)

Committee Certification

We the examining committee, certify that we have read this dissertation entitled (**Design and Simulation of High Efficiency Quantum-Dot Solar Cells Based on Nano-crystal Technology**) and have examined the postgraduate student (**Iman Mohsin Ahmed**) in its contents and that in our opinion; it meets the standards of a dissertation for the degree of Master of Science in Electronic Engineering.

Signature:

Name: Prof. Dr. Khaled Khalil Muhammad

Head of committee

Date: /   /2024

Signature:

Name: Assist. Prof. Dr. Ahmed Mohammed Ahmed

Member

Date: /   /2024

Signature:

Name: Assist. Prof. Dr. Omar Ibrahim Alsaif

Member and Supervisor

Date: /   /2024

Signature:

Name: Assist. Prof. Dr. Mohammed Tariq Yasin

Member

Date: /   /2024

Signature:

Name: Prof. Dr. Qais Thanon Najim

Member and Supervisor

Date: /   /2024

The college council, in its   …………… meeting on   /   / 2024, has decided to award the degree of Master of Science in Electronic Engineering to the candidate.

Signature:

Name: Prof.   Khaled   Khalil Muhammad

Dean of the College

Date: /   /2024

Signature:

Name: Assist. Prof. Dr. Bilal A. jebur

Council registrar

Date: /   /2024

ABSTRACT

Renewable energy development led to an urgent requirement to use solar cells. However, the weakness in the power conversion efficiency of conventional solar cells turned the recent studies to finding a solar cell with high power conversion efficiency. Quantum dot (QD) solar cells are one of the most promising structures and they belong to the third-generation of solar cells. The current work involves the simulation investigation of the effect of inserting the quantum dot layers on the performance parameters of the solar cell. The p-i-n structure was implemented for a standard solar cell and made of GaAs, where p-layer represents the hole transport layer (HTL), the i-layer (intrinsic layer) represents the absorber layer, the n-layer represents the electron transport layer (ETL) and the quantum dot layers are made of InAs. In this work, the thickness of the i-layer is kept constant while adding the QDs layers inside it. To realize this objective, SILVACO-TCAD software was employed to implement the standard solar cell and quantum dot solar cell. The simulation results show that the proposed method of adding 1-layer of QDs and increasing the number of QDs layers to (5,10,15 and 20) respectively led to improvement in the performance of the solar cell and outperformed the standard solar cell in terms of J_{sc}, V_{oc}, **FF** and **PCE**. By comparing the results of the standard solar cells with the results of adding a single layer of QDs shows an improvement in the SC performance with an increase in PCE from 12.5158% to 26.7046%. Adding more layers of QD's rise the PCE but the increase starts saturate after 10 layers. The PCE increased to 29.0493% with 10 layers of QD's. The effect of temperature on the performance of the standard solar cell with the existence of different numbers of QDs layers was studied too. The results show that the temperature affects negatively the SC performance with increasing temperature the efficiency of the cell decreases even with the existence of

the QD's layers, where the PCE decreased to 25.6224% when the temperature increased to 360 $^{\circ}$K.

List of Contents

List of Figures

List of Tables

List of Abbreviations

ABBREVIATIONS	DESCRIPTION
AlGaAs	Aluminium Gallium Arsenide
AM	Air Mass coefficient
Augn	Auger constants for electron
Augp	Auger constants for hole
CdS	Cadmium sulfide
CdSe	Cadmium Selenide
CdTe	Cadmium Telluride
CIGS	Copper Indium Gallium Selenide
conmob	Mobility Concentration
consrh	Carrier recombination under Shockley – Read - Hall
DSCs	Dye – Sensitized Solar Cells
EHP	Electron-Hole pair
ETM	Electron Transport Medium
fldmob	Mobility depends on Electric field
GaAs	Gallium Arsenide
HTM	Hole Transport Medium
IBSC	Intermediate Band Solar Cell
InAs	Indium Arsenide
IPCE	Incident Photon to Current Efficiency
ITO	Indium-doped Tin Oxide

ABBREVIATIONS	DESCRIPTION
J-V	Current density-Voltage characteristics
MEG	Multiple Exciton Generation
NCs	Nano-Crystals
PbS	Lead Sulfide
PCE	Power Conversion Efficiency
PV	Photovoltaic
QDs	Quantum Dots
QDSCs	Quantum Dot – Sensitized Solar Cells
SC	Solar Cells
Si	Silicon
SK	Stransky Krastanov
Taun	Lifetimes for electron
Taup	Lifetimes for hole
TCAD	Technology Computer Aided Design
ZnSe	Zinc Selenide

List of Symbols

Symbols	DESCRIPTION
hv	Optical Power
h	Planck Constant
C	Speed of Light in the Vacuum
λ	Wavelength
E_g	Energy Gap
E_{ph}	Photon's Energy
λ_c	Cutoff Wavelength
θ	The incident light's angle
J	Current Density
J_0	Reverse Saturation Current Density
q	Electron Charge
V	Voltage
K_B	Boltzman constant
T	Temperature
J_L	Light Generated Current Density
J_{sc}	Short circuit Current Density
R_L	Load Resistance
V_{oc}	Open circuit Voltage
G	Generation Rate

Symbols	DESCRIPTION
L_n	Diffusion Length for Electron
L_p	Diffusion Length for Hole
P_{mp}	Maximum Power Output from the Solar Cell
J_{mp}	Maximum Current Density
V_{mp}	Voltage Maximum Power
FF	Fill Factor
η	Photovoltaic Efficiency
R_s	Series Resistance
R_{sh}	Shunt Resistance
E^{QD}	Energy Gap for Quantum Dot
E_g^{bulk}	Energy Gap for bulk material
R	Radius of Quantum Dot
m_e^*	Effective Mass of Electron
m_h^*	Effective Mass of Hole
ε	Permittivity
ε_0	Permittivity for Free Space
ρ	Charge Density
p	Concentration of Holes at Thermal Equilibrium
n	Concentration of Electrons at Thermal Equilibrium

Symbols	DESCRIPTION
N_A^-	Ionized Concentration of Acceptors Atoms
N_D^+	Ionized Concentration of Donors Atoms
μ_n	Mobility of Electron
μ_p	Mobility of Hole
E	Intensity of the Electric Field
D_n	Diffusion coefficient of Electrons
D_p	Diffusion coefficient of Holes
α	Constant value for each Material
β	Constant value for each Material
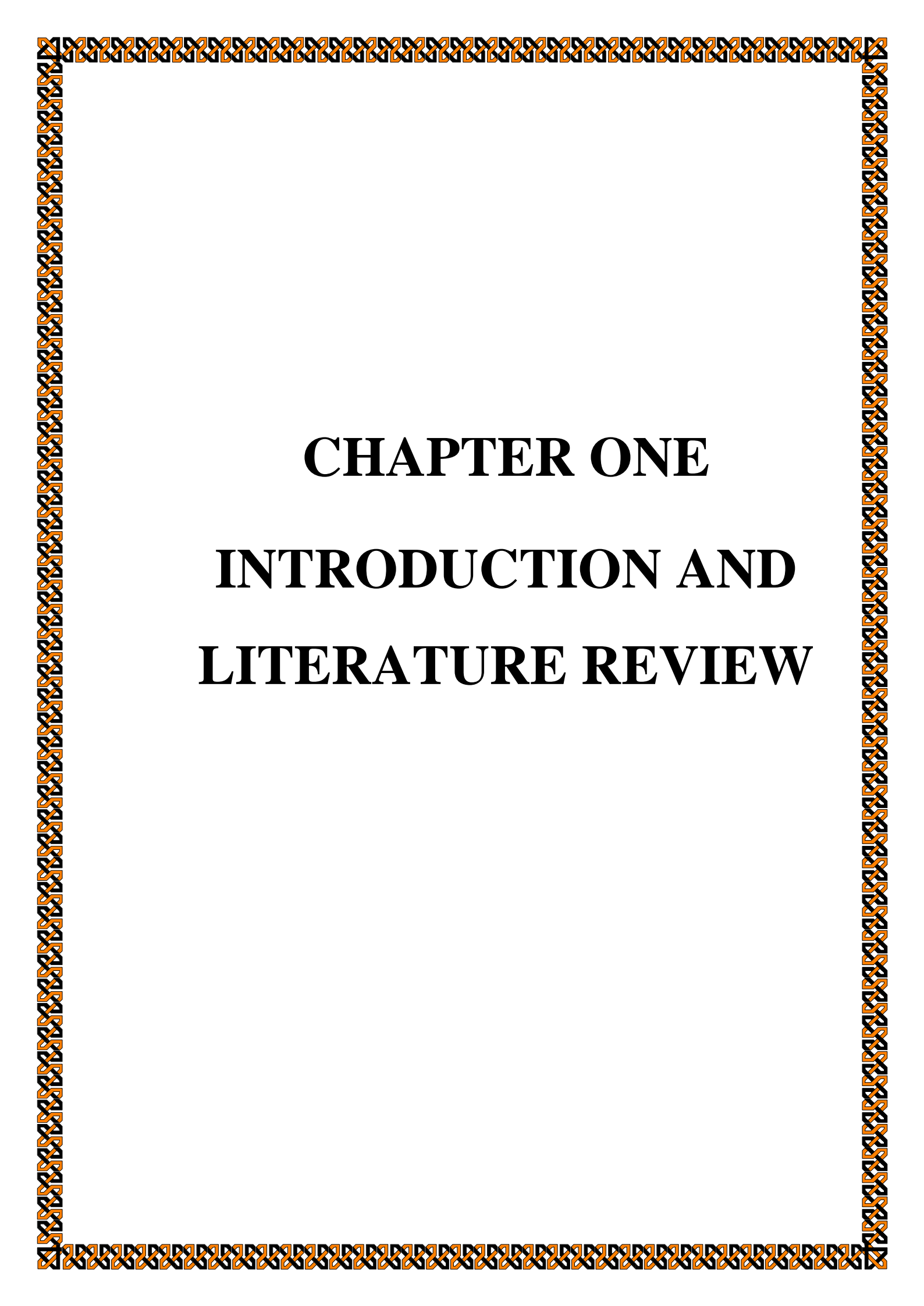
CHAPTER ONE

INTRODUCTION AND

LITERATURE REVIEW

CHAPTER ONE

INTRODUCTION AND LITERATURE REVIEW

1.1 Introduction:

Lack of energy is one of the environmental problems has led to the search for commercially viable energy alternatives that produce less pollution. Currently, coal and oil are the most widely used energy sources worldwide, but they are also the primary contributors to CO_2 depletion and other dangerous effluent emissions. Due to the finite nature of traditional energy sources, renewable energy sources have come to the forefront of global attention. Due to its simplicity of maintenance, lack of emissions, and lack of noise, solar energy will be the most dependable alternative source given the rising demand for clean energy worldwide [1]. Researchers are working to develop the most effective photovoltaic (PV) cells because of the rising global energy demand, the depletion of traditional energy sources, and the dangers posed by global warming. Utilizing photovoltaic or solar cells, it was created and is used to generate electricity based on the electronic radiative conversion theory [2]. In the past 50 years, there has been a lot of interest in photovoltaic (PV) technology-based solar cells because of their decentralized nature and sustainability [3].

Solar cells are the most important devices that were made to exploit solar energy, which is characterized by having renewable, sustainable, clean energy and their ease of installation in their places of use. Their technologies are not complicated, and they can be developed and used to develop other technologies. Using solar cells has created a wide job opportunity, and their material and environmental requirements are available significantly. It needed a large capital in the beginning, but it does not need raw materials due to its availability in nature, nor does it need continuous maintenance [4]. However, despite these advantages, it is still very expensive compared to

traditional electric energy. That is why great scientific and technical efforts have been made all over the world to make this technique cheap and available. Adams and Day, in 1877, described the photovoltaic effect in much more detail. When exposed to radiation, selenium electrodes developed an electrical potential [5] that allowed them to conduct current. As many specialized research laboratories in this field seek to improve the efficiency of these devices in terms of energy transformation on the one hand and to reduce their cost on the other hand [6]. It is important to remember that solar cells were first created for use in space, as they were also providing satellites with electrical energy based on photovoltaic conversion [7].

1.2 **Solar Cell Generations:**

By incorporating modern technologies, solar cells have advanced significantly over time. Generally speaking, solar cells can be divided into three generations. These generations of solar cells classified according to the materials used and how they are manufactured, and they all convert light energy into electrical energy.

1.2.1 **First-Generation Solar Cell:**

The first generation of solar cells, which employ silicon semiconductor as their substrate, are the most extensively used solar cells because of their high efficiency, extended lifespan (over 20 years), and marketability. A monocrystalline Si solar cell's maximum efficiency was 24%. A lower efficiency of about 19.5% is demonstrated using polycrystalline silicon. Defects in the crystal are what cause polycrystalline solar cells to have lesser efficiency than monocrystalline solar cells [8]. These solar cell varieties are the most prevalent on the market and are typically found on residential house's roofs. The benefit of these photovoltaic cells is manufactured from semiconductors, which are the most common and used silicon material due to their worldwide availability. The key to solar

cell technology is its high stability and optimal performance. It costs a lot of energy to produce, even though it is solid. It is still commercially dominant due to its efficiency and longevity compared to other cells. This generation includes two species [8]:

- **Monocrystalline Silicon Type**
- **Polycrystalline Silicon Type**

1.2.2 Second-Generation Solar Cell:

Thin film technology is used in second-generation solar cells. Thin film technologies can be produced or coated consecutively on inexpensive substrates like glass or plastic with few material (typically 1-2 μm thick). The three materials amorphous silicon, copper indium gallium selenide, and cadmium telluride are the most widely used thin film technologies today [8]. It has been avoided in the second generation of solar cells to use silicon wafers, and it was found that they have less consumption of materials, and this enables the production costs of this type of solar cell to be lower than those of the first generation. Additionally, it is possible to manufacture second-generation solar cells with some degree of flexibility. However, high-temperature treatments and discharge techniques are still used in the generation's solar cell production, in addition to this, it was founded that the second generation is dependent on rare elements, and the price reflects this.

- **Amorphous Silicon Solar Cells Type**
- **(Cadmium Telluride) CdTe Solar Cells**
- **(Copper Indium Gallium Selenide) CIGS Solar Cells**

1.2.3 <u>Third-Generation Solar Cell:</u>

The nanoparticles are used to power the third generation of solar cells. The production processes and operating principles are very different from those used in Si solar cells. The implications of nanotechnology present enormous potential for third-generation solar cells, even though they haven't quite reached the efficiency levels of Si solar cells [8]. It is anticipated that they would use a variety of organic components, such as tiny molecules or pigment, and exhibit a wide range of creativity. As a result, dye solar cells are an organic solar cell subclass. Additionally, the third generation includes prototype solar cells, costly and high-execution solar cells that set a world record for efficiency. Due to its high production cost, this type only has minimal commercial applicability. Current researches on a new class of thin-film solar cells show that solar can achieve record efficiencies of over 20% in a very small area. The third generation SCs under consideration include perovskite, hybrid polymer, and polymer fullerene SCs. The nature of the acceptor phase, which is the primary difference between the first two SC types, allows us to compare and evaluate these SC types. Perovskite SCs are included to allow comparison of hybrid polymer and mixed molecular (perovskite) SC technology [9]. Although nanotechnology may be able to boost solar cell efficiency, the most promising use of the technology is to decrease the production costs [10]. Despite the fact that this approach is tried-and-true, the world is beginning to develop new technology by increasing productivity and cutting costs in manufacturing. Despite having restricted performance and stability compared to first- and second-generation solar cells, third-generation solar cells have a lot of potential and are now on the market [9]. This generation includes a lot of types:

- **Organic Solar Cells.**
- **Dye-Sensitized Solar Cells.**

- **Tandem or Stacked Multilayers.**
- **Quantum Dots Solar Cells.**

1.3 Literature Review:

- In (2011), it has been designed and fabricated of 3-terminal tandem solar cell (Si-Si: Ge) to replace the standard Si solar cell to improve their performance and reduce costs. Initial findings demonstrate that Si solar cells and Si:Ge solar cells can both function well in this configuration. The finest Si solar cell exhibits a V_{oc} of 598.5 mV, a J_{sc} of 22.9 mA/cm^2, and an FF of 77.3% under a single sun using a silicon filter, a Si:Ge solar cell displays a V_{oc} of 189 mV and a J_{sc} of 3.26 mA/cm^2 [11].

- Multi-junction cell that can absorb visible and IR wavelengths was proposed in 2011. The bottom unit of the proposed structural cell, which consists of two sub-cells, is a 20-period GaAs-Ge super lattice embedded in a GaAs/Ge bulk solar cell. The AlAs/AlGaAs/GaAs cell, appropriate for short wavelengths, is proposed at the top of this cell. Through a typical tunnel junction that connects the two sections in series and collection efficiency is expected to rise above the current threshold 42% (under one sun circumstances) [12].

- In (2011), a quantum dot sensitized solar cell was used, where the CuInS$_2$ material was used as a quantum dot layer with a thickness of (3.5 nm), a surface layer of TiO$_2$, a CdS layer as a coating, and the last layer of ZnS for passivation. Through the results, the efficiency of conversion reached about 4.2%. The cell's optical absorption and incident photon conversion efficiency (IPCE) spectra are both extended to a longer wavelength of about 800 nm by the heterojunction between the CuInS$_2$ QDs and CdS, which also offers an IPCE of almost 80% at 510 nm [13].

- In (2014), a standard GaAs solar cell and 40-layers of InAs/GaAs p-i-n QD were modeled and simulated using SILVACO TCAD and compared with experimental data for fabricated solar cells, where the conversion

efficiency increased from 14.1% to 18.6% due to the use of QD. Additionally, the absorption range edge of low-energy photons increased from 875 nm to 1200 nm. All of the findings in this thesis demonstrate that embedded quantum dots have favorable impacts on solar cells and can raise their conversion efficiency [14].

- In (2015), the impact of temperature on photovoltaic characteristics was assessed. For poly-crystalline silicon, the maximum power decreased by (17%) as temperature increased from (15℃ to 60℃). With an increase in light intensity, the maximum current rose linearly. The measurements were carried out in a weather-related outdoor setting [15].

- GaAs p-i-n was structured and 40 – layers of GaSb QD were inserted inside the i – region and compared with the results of standard GaAs solar cells. It was noticed that the conversion efficiency increased from 16.48% to 22.4% (a relative increase of about 36.3%) in 2015. The edge of the absorption range for low-energy photons was also expanded from 900 to 1200 nm. The findings show that compared to p-i-n junction solar cells, the GaSb/GaAs quantum dot solar cell has a significantly higher power conversion efficiency [16].

- ITO/TiO$_2$/P$_3$HT, PCBM/Ag, ITO / TiO$_2$ / CdS / P$_3$HT and PCBM/Ag were structured and simulated using SILVACO TCAD in 2016. The simulation results of the fabricated solar cell, where the efficiency of this cell reached 1.8%, it was close to the experimental results. This means that when CdS QD is inserted, the light absorption will increase, and thus the efficiency will improve [17].

- In (2017), InAs QD material was inserted into the i-region of GaAs solar cell (p-i-n) hetero-structure, and thus an increase in efficiency was obtained by 3.885%, and an increase in FF from 83.27% to 88.0538%. The structure was lighted with AM 1.5 G solar spectrum, and it was discovered that the inclusion of a quantum dot layer extended the absorption edge of the

solar cell, resulting in a good photo-generation rate and increasing the efficiency of the solar cell [18].

-        In comparison between the performance of CdZnS solar cells without the ZnO buffer layer and the performance of the similar devices with a ZnO buffer layer that is transparent in 2019 has seen a conversion efficiency boost of up to 1.8%. This resulted in the front contact being able to regulate light, which improved the J_{sc} and therefore the efficiency of photovoltaic conversion. These findings are intriguing because prior research on CdTe solar cells did not describe how manipulating the extremely resistive transparent buffer layer could enhance photocurrent and device performance [19].

-        In (2019), a numerical analysis of the photovoltaic behavior of single-junction solar cells made of p-InGaN and n-InGaN is reported. The SCAPS (Solar Cell Capacity Simulator) software was used to simulate this solar cell. By adjusting the bandgap energy and doping concentrations along with each layer, specifically the n- and p- InGaN layers, the electrical characteristics and photovoltaic performance of the InGaN solar cells, were investigated. The optimal conversion efficiency of (15.32%), which corresponds to (64%) of the indium compositions, was validated at a band-gap of (1.32 eV) [20].

-        In (2019), The realization of InAs/GaAs solar cells was studied in the case of Quantum Wells and Quantum Dots. InAs/GaAs QW was simulated using MATLAB software, as the efficiency of this cell reached 18.52%, compared to the standard solar cell, where the efficiency was 16.78%. For InAs/GaAs QD solar cell, it was simulated using SILVACO TCAD, where the efficiency in the ideal case reached 43.05%, while in the practical case, the efficiency of this cell reached 9.1%, taking into account the presence of the valence band tail and discrete electron and by improving the number of Quantum Dots layers and doping it is possible to improve the efficiency of the solar cell to 11.29% [21].

- With a notable increase in cell efficiency of about (19%), in 2020, band-gap grading and an array of Au plasmonic nanoparticles were used to assess the high performance of the ultra-thin CIGS solar cell. Plasmonic nanoparticles are capable of limiting, absorbing, navigating, or scattering incident light. Results indicated that output characteristics such as open-circuit voltage (V_{oc}), short-circuit current (I_{sc}), fill factor (FF), and power conversion efficiency (η) were significantly improved [22].

- In (2020), the effect of the performance of InGaAs/GaAs-based quantum dot intermediate band solar cells (QDIBSCs) was studied with the cap and passivation layers. AlGaAs was used as a cap layer and Si_3N_4 was used as a passivation layer. The results showed that the use of these layers improved the efficiency of the solar cell, as it changed from 21.6% to 27.8%. As the rate of recombination was decreased when using the cap layer and the reflection decreased by improving the rate of photovoltaic generation of the cell by using the passivation layer, thus increasing the efficiency [23].

1.4 Aims of the Study:

The goals of the work are:

1. To simulate a GaAs p-i-n structure Solar Cell based on the Quantum Dot Solar Cell concept.

2. To study the effect of adding Quantum Dot layers inside the i-region of the Solar Cell on its performance.

3. To determine the optimum number of QDs layers that give the best solar cell performance.

4. To study the temperature impact on the solar cell performance with existence the QDs layers.

1.5 Organization of Thesis:

There are five chapters in the thesis. The following is a summary of the chapters' outline:

- Chapter One includes a general introduction to solar cells and the literature review.

- Chapter Two covers, in general, the essential characteristics of solar cells and Quantum Dots solar cells

- The Third Chapter describes how to use SILVACO-TCAD software and create a reference cell model with optimal values.

- The Fourth Chapter deals with the simulation results of the impact of the Quantum Dots on the standard solar cell.

- Finally, in Chapter Five, the conclusions and recommendations for further works are presented.
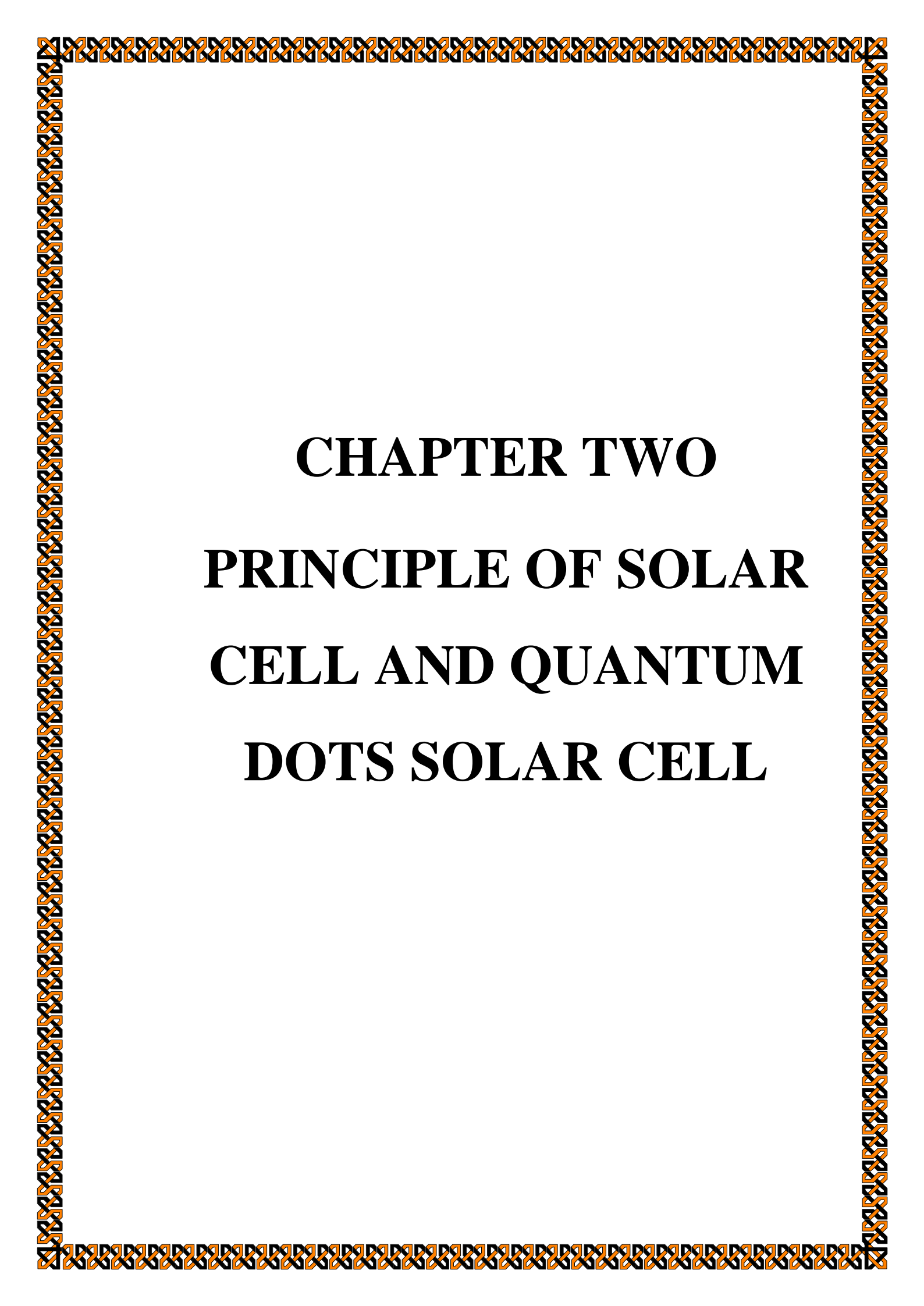
CHAPTER TWO

PRINCIPLE OF SOLAR CELL AND QUANTUM DOTS SOLAR CELL

CHAPTER TWO

PRINCIPLE OF SOLAR CELL AND QUANTUM DOTS SOLAR CELL

2.1 Introduction:

A semiconductor material converts sunlight directly into electrical energy in a solar cell, also known as a photovoltaic cell. Solar photovoltaic systems are crucial for the use of solar energy to produce electricity [24]. First, a substance must absorb light to raise an electron to a higher energy state. Second, the higher energy electron must be transported from the solar cell onto an external circuit [25]. The French physicist Edmund Becquerel made the discovery of the photovoltaic phenomenon in 1839 [26]. In 1954, the first silicon solar cell was created, heralding the emergence of p-n junction solar cells. It is usually understood to be the development of an electric potential between two electrodes connected to a solid or liquid system in response to the application of light to the system [26]. The depletion region separates the p-n junction, which is the most basic component of a solar cell. Each photon of light that strikes a solar cell is absorbed by the semiconductor material, producing an electron-hole pair (EHP) as a result, as shown in Figure (2.1). The excited electrons should push away and send into an external circuit prior to (EHP) recombination occurring. After releasing their energy in the external circuit, the electrons subsequently return to the solar device. The operation of a photovoltaic (PV) cell requires three basic attributes:

1. The absorption of light, generating either electron-hole pairs or excitons.
2. The separation of charge carriers of opposite types.
3. The separate extraction of those carriers to an external circuit.

This process entails the employment of a substance that absorbs light and raises an electron's energy level; this higher energy electron is then transported from the solar device onto an external circuit. All solar energy conversion uses P-N junction semiconductor materials [27].
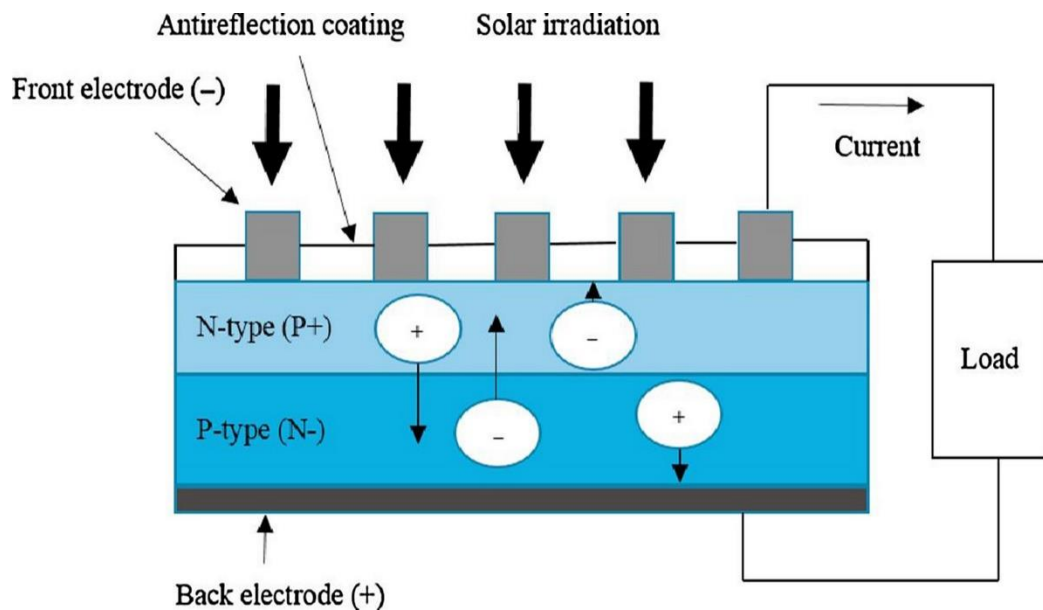
Figure (2.1) p-n junction solar cell [28].

2.2 **Photovoltaic Effect:**

The creation of a potential as a result of radiation ionizing the area in or close to a semiconductor's inherent potential barrier is known as the photovoltaic effect. In a semiconductor, a potential barrier can form through a variety of techniques. The two methods that photovoltaic cells are mainly interested in are [29]:

i. The metal-semiconductor barrier created by the evaporation or sputtering of a suitably transparent metallic coating over a semiconductor, such as in a selenium cell.

ii. The p-n junction, which is created by adding an appropriate type of impurity to a semiconductor that contains an impurity of the opposite kind.

Due to the fact that unabsorbed photons will not contribute to the creation of electricity, reflection and transmission of photovoltaic systems are typically regarded as loss mechanisms. The photon has the potential to excite an electron from the valence band to the conduction band if it is absorbed. The energy of the photon is a crucial component in deciding whether it is absorbed or transmitted. Equation (2-1) displays the energy of photons calculation as shown below:

$$E = hv = \frac{hc}{\lambda} \qquad (2-1)$$

h is the constant of Plank = 4.1357×10^{-15} eV s, c is the light's speed in vacuum = 3×10^8 m.s^{-1}, E is the photon's energy in eV and λ is the wavelength in nm.

Equation (2-2) displays the necessary light wavelength of the light that satisfies the absorption criteria in terms of wavelength [30].

$$\lambda(\mu m) \leq \frac{1.24}{E_g} \qquad (2-2)$$

Based on their energy in relation to the semiconductor band-gap, the photons that strike semiconductor material can be divided into three categories [30].

- $E_{ph} < E_g$ Photons with energies E_{ph} below the bandgap energy E_g interact with the semiconductor only faintly, behaving as though it were transparent. These photons have wavelengths greater than the cut-off wavelength (λ_c), hence they won't be absorbed and will flow through the semiconductor.

- $E_{ph} = E_g$ is effectively absorbed and has just enough energy to produce an electron-hole pair.

- $E_{ph} > E_g$ Photons with energies significantly higher than the band gap are substantially absorbed. However, photovoltaic applications squander photon energy above the band gap because electrons quickly thermalize back down to the conduction band boundaries.

To put it another way, the photovoltaic effect happens when a semiconducting material is exposed to photons of light with an energy greater than or equal to that energy gap of the semiconductor [31].

2.3 <u>Solar Radiation:</u>

Local climatic circumstances affect the amount of solar radiation that can reach Earth's surface. For the right design of building energy systems, solar energy systems, and a good evaluation of the thermal environment within buildings, knowledge of the local solar radiation is crucial. The incident light that is available to terrestrial PVCs may be lessened by the atmospheric factors. The spectral distributions of solar radiation outside the atmosphere (AM 0) and at the surface of the Earth (AM 1.5) are shown in Figure (2.2) [32]. Photons contain enormous amounts of energy and motion yet lack physical substance. Light waves of various photons have various wavelengths. The blue and red line (AM 1.5) in Figure (2.2) shows how the solar radiation has been absorbed and scattered by air molecules and dust in the atmosphere, as well as by O_2, O_3, H_2O, and CO_2.
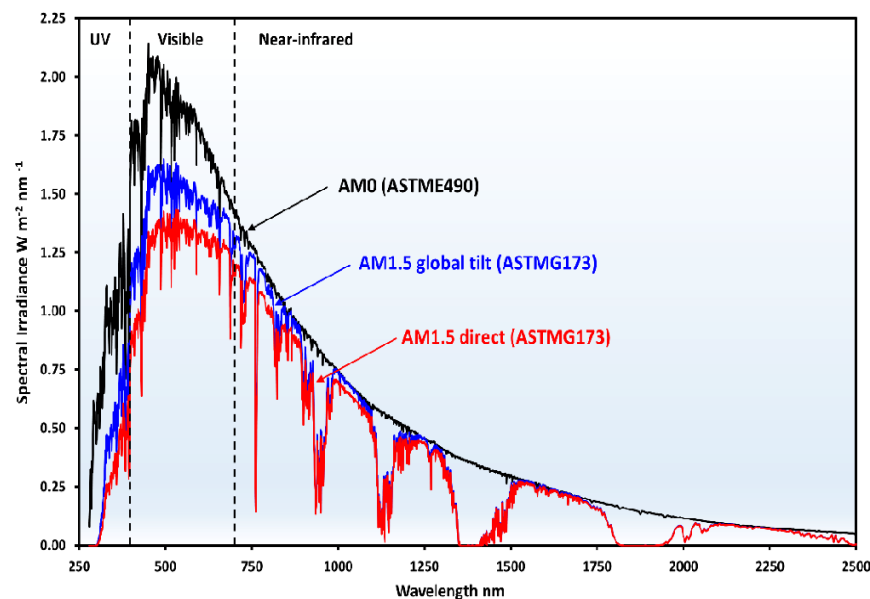
Figure (2.2) Solar radiation from the outside (AM 0, black), (AM 1.5 Global, blue), and (AM 1.5 Direct, red).

The performance of solar modules has been compared using the air mass coefficients (AM), as a parameter that primarily considers the impact of wavelength allocation on photon flow [33], which fluctuates based on meteorological factors including water, vapor, and dust [34]. The distance that sunlight must travel through the atmosphere to reach the surface of the Earth when the sun is overhead is referred to as the Air Mass (AM). AM's equation is as follows:

$$AM = \frac{1}{cos\theta} \qquad\qquad (2-3)$$

The angle of the Sun determines the AM. When the angle (θ) from above is zero, AM equals 1. While if (θ) is 48.2° from the horizon, AM = 1.5. For evaluating photovoltaic devices, this serves as the industry-standard sunlight spectrum [32][35][36].
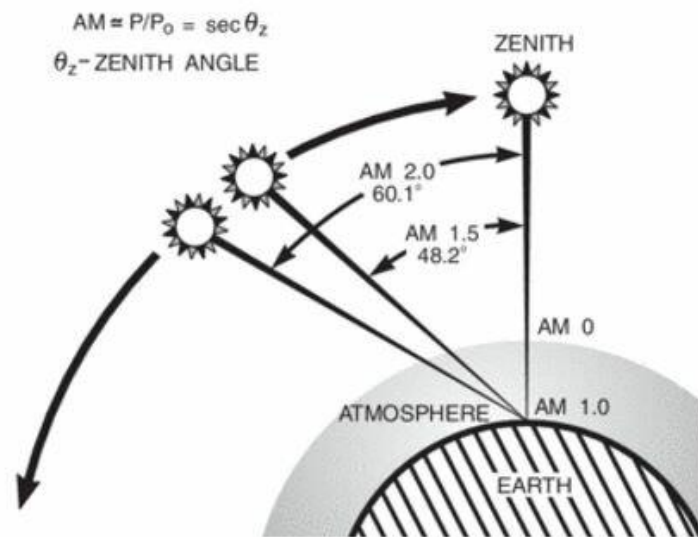
Figure (2.3) The Air Mass that Radiation Must Pass Through Before Impacting the Surface of the Earth [30].

2.4 P-N Junction Under Illumination:

As shown in Figure (2.4), P-N junctions are created by connecting n-type and p-type semiconductor materials. Electrons diffuse from the n-type side to the p-type side because the n-type region has a high electron concentration and the p-type region has a high hole concentration. A junction is the interface plane at the boundary where two semiconductor areas meet. In the junction plane, donors and acceptors should have an equal density [37]. When a grain is made up of two distinct components and PN connections are produced in a single semiconductor crystal through a doping procedure, a grain boundary is introduced. The following three events occur at the intersection [37]:

i. Across the junction, a space charge area, depletion region, or transition zone is established.

ii. Potential barrier is created across the p-n junction.

iii. Junction and diffusion capacitances are caused by the presence of the depletion layer.
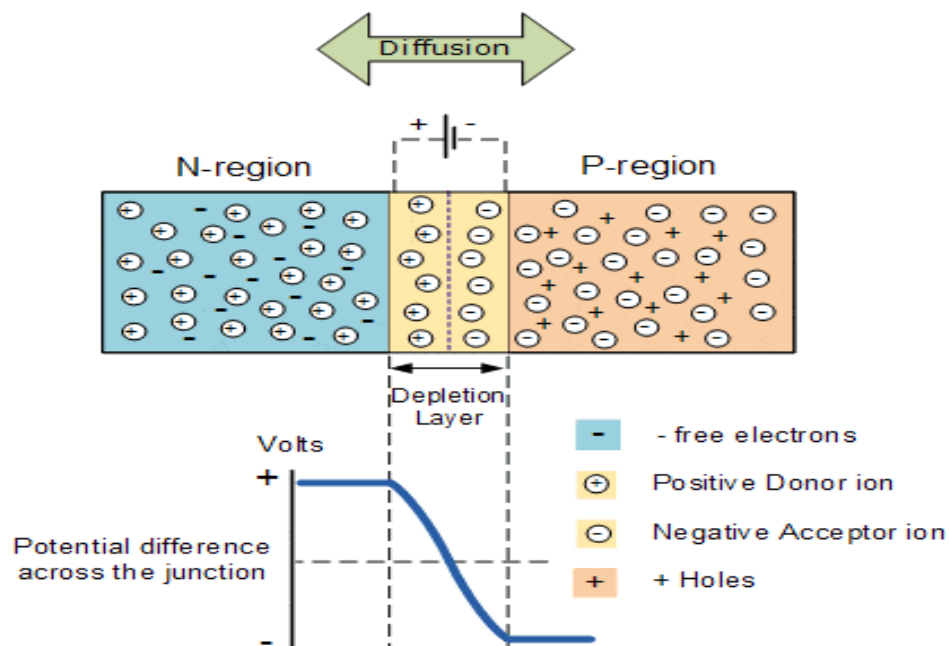
Figure (2.4) p-n junction semiconductor diode [36].

2.5 J-V Characteristic of Solar Cell:

A photovoltaic cell functions as a current source when it absorbs incident light, and when it is dark, it functions as a diode. As a result, photovoltaic cells in the dark can be described using the ideal diode law.

$$J = J_\circ \left[\exp\left(\frac{qv}{K_B T}\right) - 1 \right] \qquad (2-4)$$

Where J stands for the p-n junction current density, while J_0 stands for the saturation current density (the diode's leakage current density when there is no light), V for voltage, q for electron charge (1.6×10^{-19} Coulombs), K_B for the Boltzmann constant (1.38×10^{-23} J/K), and T for temperature in Kelvin. Photovoltaic cells' J-V curve is shown in Figure (2.5) (blue line) as a diode in the dark [38].

When photovoltaic cells absorb incident light, the light effect is added to the diode law. The photovoltaic effect is shown in the following equation (2-5) when there is light irradiation:

$$J = J_\circ \left[\exp\left(\frac{qv}{K_B T}\right) - 1 \right] - J_L \qquad (2-5)$$

J_L represents the light-generated current. Figure (2.5) illustrates how the J-V curve (blue line) is moved toward the fourth quadrant by absorbed light [32].
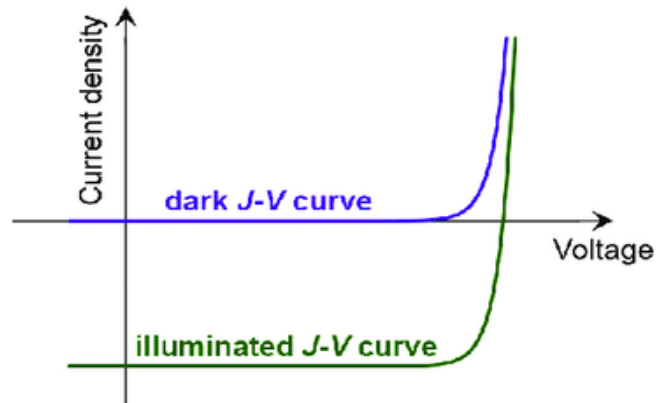
Figure (2.5) Incoming light's effect on photovoltaic cells' J-V curve.

2.6 Solar Cell Parameters:

Several factors, referred to as solar cell parameters, can be retrieved from the photovoltaic cell's J-V curve to characterize the solar cell's conversion of sunlight into energy. These parameters are as follows:

2.6.1 Short Circuit Current Density:

Short-circuit current density (J_{sc}) is the greatest current that can pass through a solar cell when it is shorted out or under maximum load conditions ($R_L = 0$). The voltage of a solar cell will be zero at the greatest value of J_{sc} [39]. If the current density flows in the other direction, producing a positive current density rather than a negative current density, the J-V curve of the photovoltaic cell under incident light can be re-defined and written in the first quadrant as shown in Equation (2-6) below:

$$ J = J_L - J_0 \left[exp\left(\frac{qv}{K_B T}\right) - 1 \right] \qquad (2-6) $$

The J-V curve can be generated in the first quadrant using equation (2-6), as shown in Figure (2.5). The J-V curve crosses the x-axis at V_{oc} and the y-axis at J_{sc}, respectively [32].
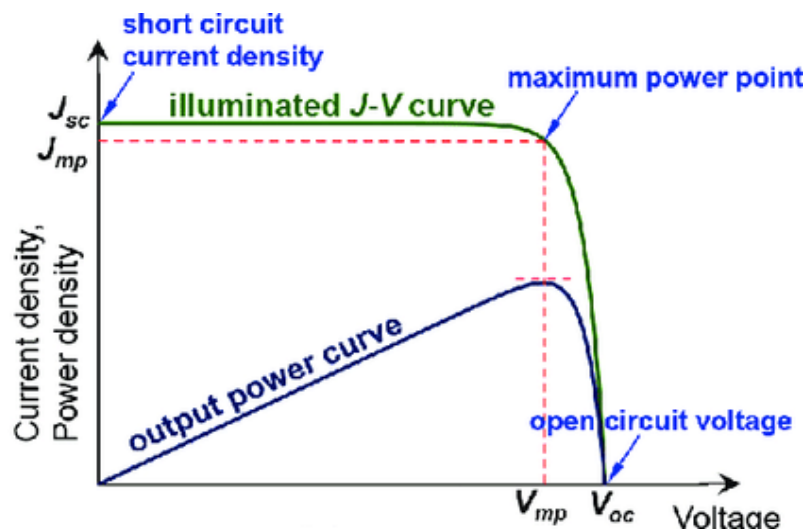
Figure (2.6) Solar cell J-V curve (green line) and power curve (blue line).

The highest current that flows through the cell circuit while there is no voltage across the solar cell is known as the short circuit current density *(Jsc)*. When *V=0*, the short circuit current density (**Jsc**) value is identical to *(JL)* value. The short-circuit current density is determined by a number of variables, including:

- The short-circuit current density *(Jsc in mA/cm²)* is more frequently employed than the short-circuit current itself to avoid dependence on the solar cell's surface area.
- The quantity of photons (the intensity of the light source incident). The amount of light a solar cell absorbs directly correlates to its output.
- The incident light's spectrum: Most solar cell measurements are standardized using the *AM1.5* Spectrum.
- Absorption and reflection properties of the solar cell.
- Probability that a solar cell will collect: The generation rate and diffusion length for electrons and holes, respectively, are also factors that affect the *Jsc*, as shown by equation (2-7).

$$J_{sc} = qG(L_n + L_p) \qquad\qquad (2-7)$$

where G indicates the generation rate and L_n and L_p, respectively, stand for the electron and hole [31][32].

2.6.2 The Open Circuit Voltage:

The open-circuit voltage *(Voc)* is the greatest voltage that can exist on a cell when no current is flowing. As illustrated in Figure (2.5), *Voc* is equal to the voltage across the solar cell when there is no current flowing through it, or when the circuit is open.

Putting the net current in the solar panel at zero results in the definition of a V_{OC} the formula, which is:

$$V_{oc} = \frac{K_B T}{q} \ln\left(\frac{J_L}{J_o} + 1\right) \qquad\qquad (2-8)$$

In this case, J_0 stands for the saturation current density, whereas J_L stands for the photo generated current density, which is directly related to the photon flux impinge on the cell and its reliance on the wavelength of light.

In Figure (2.7), the highest power point is shown. The power equation states that the maximum power *(P_{mp})* is theoretically the result of the product of *J_{SC}* and *V_{OC}* under ideal circumstances, but this is not practical due to device resistance. However, maximum power is typically computed by multiplying a value for *V_{mp}* on the V-axis between zero and *V_{OC}*, and another value for *J_{mp}* on the J-axis between zero and *J_{SC}*. The maximum current density and voltage, respectively, are indicated at the *P_{mp}* by the symbols *J_{mp}* and *V_{mp}* [37].
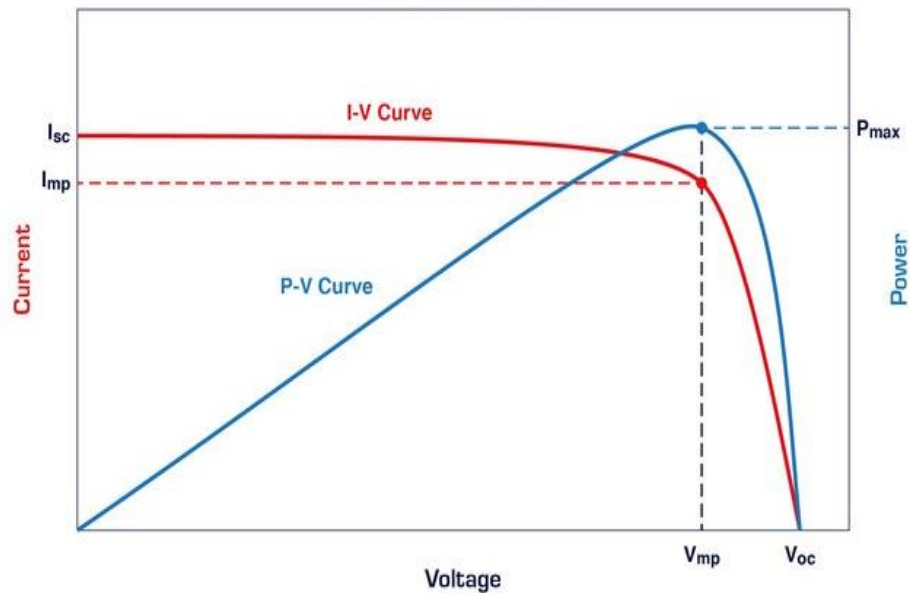
Figure (2.7) Maximum power curve of solar cell.

2.6.3 Fill Factor:

According to Figure (2.8), the Fill Factor (**FF**), which is the ratio of the maximum power output (J_{mp}, V_{mp} Green rectangular) to the theoretical power output (J_{SC}, V_{OC} Blue rectangular), is used to describe the performance quality of the solar cell. This implies that the best solar cells are produced when the value of **FF** is near to 1 [40].

$$FF = \frac{J_m V_m}{J_{sc} V_{oc}} \qquad\qquad (2-9)$$
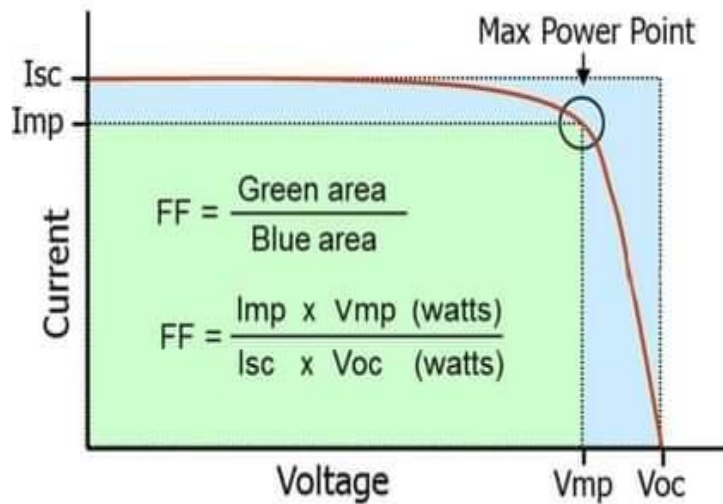
Figure (2.8) The regions where the FF formula is used (FF is the green zone over the blue region) [36].

2.6.4 Power Conversion Efficiency (η):

Power conversion efficiency, also known as **PCE**, is the most widely used metric to compare the performance of two solar cells. Its definition states that it is the proportion of a solar cell's output power to the incoming power from the sun [41]. Efficiency is significantly influenced by the temperature variation, and light spectrum and intensity. Because of this, it is necessary to compare solar cell performance to that of other cells by measuring it under similar circumstances. Photovoltaic devices are measured at the earth's surface in **AM 1.5** conditions (light output from the solar

simulator is 100 mW/cm^2) and at 300°K. Equation (2-10) can be used to define efficiency:

$$\eta = \frac{P_{out}}{P_{in}} = \frac{P_{max}}{P_{in}} = \frac{J_{sc}V_{oc}\text{FF}}{P_{in}} \qquad (2-10)$$

Where P_{in} is the solar cell's input power and P_{out} is P_{max}, or the greatest power output the cell is capable of producing at maximum efficiency [42]. **PCE** is influenced by factors such as the amount of incident sunlight, the operating temperature of solar cells, and the type of spectrum. Therefore, it is crucial to carefully control the conditions in which **PCE** is measured in order to compare two or more solar cells.

2.7 **The Electrical Model of Solar Cell:**

Making an electrically similar model is necessary to comprehend the operation of a solar cell. Figure (2.9), which depicts the perfect solar cell in its simplest form, shows a parallel-connected diode and a constant current source. In order to drive electrons into the external circuit, constant current sources operate similarly to generators.
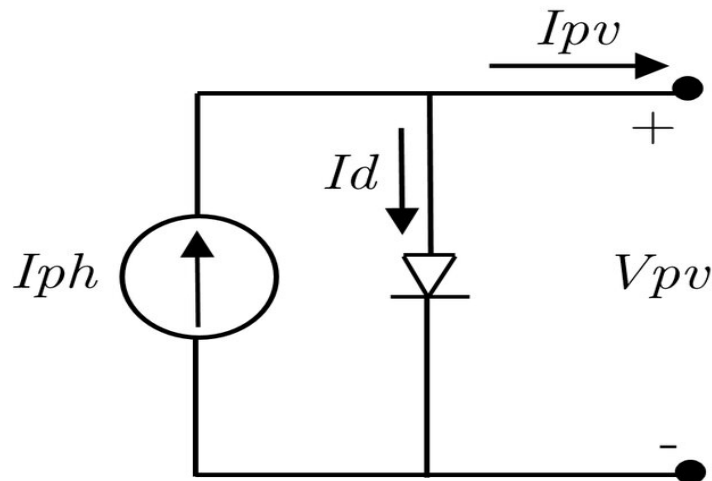
Figure (2.9) The ideal solar cell [36].

Photovoltaic cells are not really optimal. As a result, the equivalent circuit is expanded with shunt and series resistance components. Figure (2.10) shows the next equivalent circuit. It is known as the "four parameters model" and includes a current source, a diode, a series resistance, and a parallel resistance. This model is the corresponding circuit diagram of the PV system.
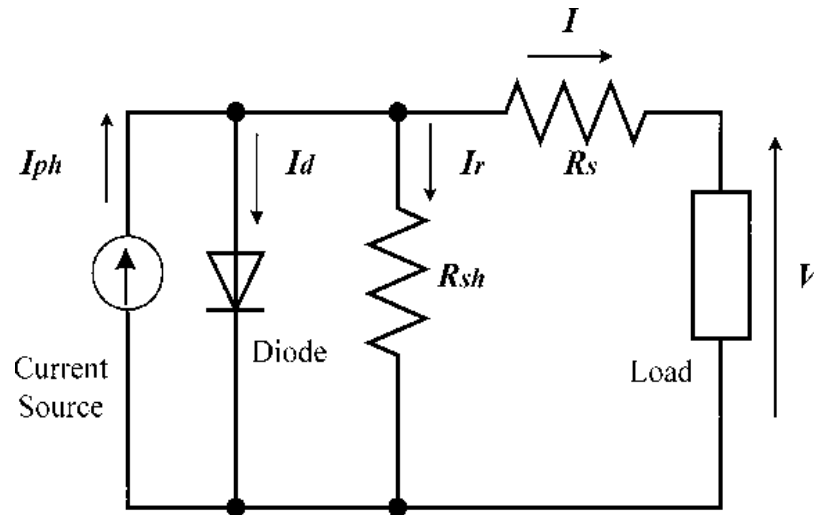
Figure (2.10) The equivalent circuit of a solar cell [43].

The diode depicts the nonlinear impedance of the PN junction. The series R_S resistance exposes internal electrical losses. The shunt R_{Sh} resistance represents the current that leaks to the ground. The current source refers to the light that the solar cell has absorbed [38]. It is possible to depict the cell current density by include the resistances as shown in equations (2-11).

$$J = J_L - J_\circ \left[\exp\left(\frac{V + JR_s}{\frac{K_B T}{q}} \right) - 1 \right] - \frac{V + JR_s}{R_{sh}} \qquad (2-11)$$

2.7.1 Series Resistance:

Metal-semiconductor contact resistance, ohmic resistance in the metal contacts, and ohmic resistance in the semiconductor material are some of the elements that contribute to series resistance. Figure (2.11) shows how series resistance affects the J-V properties of the solar cell. The fill factor is most affected. The J_{sc} current declines as R_s value rises, lowering solar cell efficiency. To attain the highest level of efficiency, the series resistance must be kept as low as feasible [38].
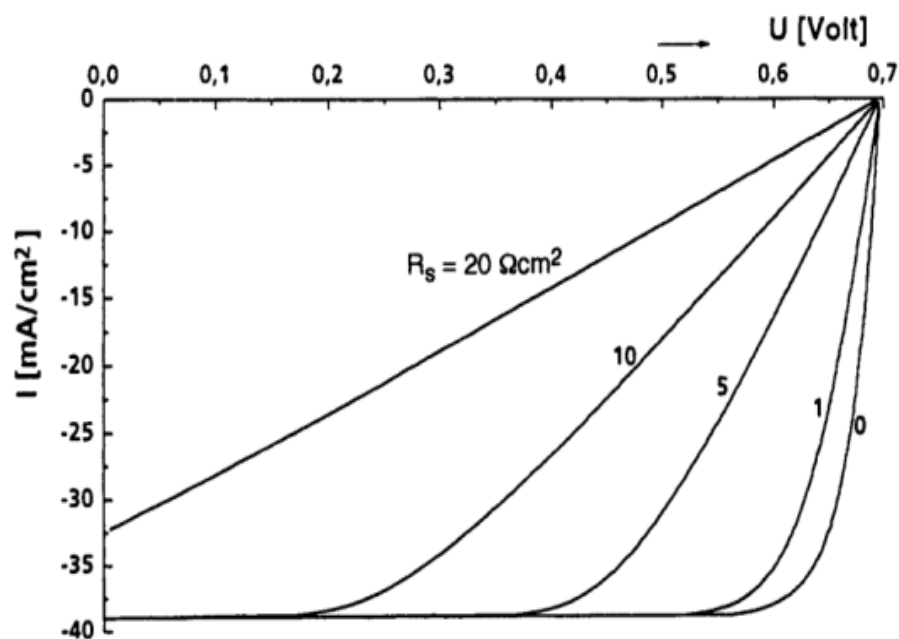
Figure (2.11) Characteristics of solar cells affected by series resistance [37].

2.7.2 Shunt Resistance:

Shunt resistance simulates the leakage across the p-n junction and the presence of contaminants there, such as those near the cell's edge. The impact of shunt resistance is shown in Figure (2.12). As demonstrated in Figure (2.12), V_{OC} will drop if R_{sh} is reduced sufficiently. Additionally, whereas parallel resistance has no impact on short-circuit current, resistance reduction reduces the fill factor (FF) [32].
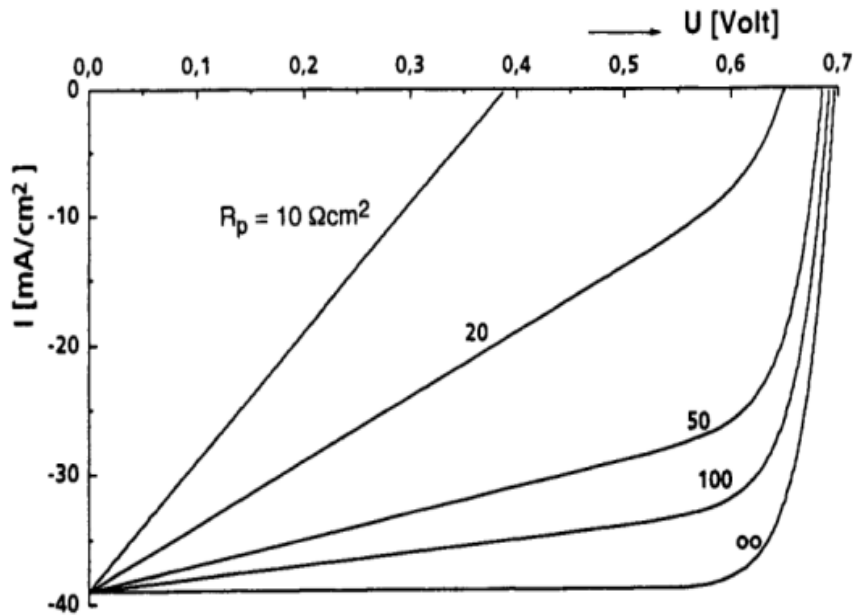
Figure (2.12) Characteristics of solar cells affected by shunt resistance [37].

2.8 Solar Cell Industry based on (III–V Group) Technique:

At the beginning of the twentieth century, it was believed that the devices based on Nano-electronics would enable the manufacture of more solar cells, in addition, that it would have a great impact in meeting global energy requirements. GaAs is more efficient than Si in solar cells, both theoretically and practically. GaAs has already demonstrated an efficiency of 25.1% compared to Si's 24.0%, as per widely-accepted efficiency figures. In addition, III-V solar cells have superior radiation resistance. As a result, III-V compound semiconductor-based solar cells are dominating more and more space applications [44]. The absence of harmful heavy metals like cadmium and lead is significant since it provides III-V NCs a strong alternative material platform for uses in biological imaging and optoelectronic devices. Despite these qualities, the synthesis of III-V is still less advanced than that of II-IV and VI-IV, mostly because of the environment of more covalent bonds, which makes it harder to crystallize in the solution phase [45].

2.9 **Quantum Dots Solar Cells:**

Quantum dot semiconductors have excellent optoelectronic properties such as tunable bandgap, multiple exciton generation (MEG), and high extinction coefficient. Because of this, due to their potential to produce very efficient solar cells, these materials have received a lot of interest. Quantum dot solar cells have a conversion efficiency of 16.6%, which is the most efficiency possible, as opposed to the theoretical value of roughly 66%. To handle the difference between the actual and theoretical energy conversion efficiencies, strategies have been proposed to understand the relationship between the element composition properties, synthesis methods, and physical structures [46]. Numerous extraordinary features can be attained if the dimensions of a semiconductor are shrunk to the nanoscale scale. These nanoparticles behave significantly differently from normal materials. Many nanomaterials have been created in the previous 20 years, including quantum wells, quantum wire, and quantum dots. A nanostructure known as quantum dots (QDs) is described as having lower dimensions in three dimensions than the De-Broglie exciton wavelength [47].

The photovoltaic concepts of the intermediate band and multi-exciton generation solar cells are created to provide a performance greater than that of single gap solar cells. The fundamental ideas behind its operation revolve around synthesizing a semiconductor material with an electronic band located within the band gap, carrier recombination between bands should be much slower than the relaxation within the bands for capture and use of photons with energies below the bandgap, or synthesizing a semiconductor with intraband transitions equivalent to the bandgap of semiconductor for greater benefit and use of photons with energies above the bandgap [21].

The notion of the intermediate band solar cell (IBSC), first put forth theoretically by Luque and Mart, has revolutionized the traditional single

junction and multiple junction solar cell technologies [48]. The great majority of QD-IBSC prototypes created up until this point have utilized type-I QDs. The two-step absorption mechanism in many materials, including the InAs/GaAs QD system [49], GaAs/AlGaAs [50], and InAs/AlGaAs [51], has been extensively studied experimentally. Recently, one single InAs/GaAs QD with the same method was reported [52]–[56]. The most crucial characteristic that provides measured energy levels is the quantum effect. It is possible to tailor the electrical and optical properties of this sort of material by manipulating its dimension and form. The distinction between these sorts is the quantity of the limited directions. One of the methods most frequently employed to increase the photovoltaic conversion efficiency of solar cell technology is the employment of quantum dot solar cells. One of the most active study areas in the third-generation solar cell at the moment is quantum dot solar cells. When compared to a quantum well, a quantum dot has stronger 3-dimensional quantum confinement effects [16].

The third-generation solar cell's conversion efficiency can be greatly increased in two ways by using quantum dot solar cells. One result is that a photon with high energy can generate many excitons. Another result is that intermediary band can be offered to assist in the absorption of lower energy photons. Both of the two phenomena are caused by the quantum dot's quantized level energy, which also has other benefits including a slower cooling rate for hot electron-hole couples. Additionally, the law of conservation of momentum need not be upheld during the transition phase for those carriers that are constrained in three dimensions [57].

2.9.1 <u>Quantum Dots Properties:</u>

In 1980, Alexei Ekimov and Alexander Efros discovered Quantum dots which became important [58], because of their extraordinary quantum confinement-derived features. They are three-dimensional semiconductors

that are constrained. The sizes of quantum dots range from 1 to 100 nm. The properties of quantum dots are dependent on the size of the nanocrystals. The quantum confinement effect is the change in the bandgap's size backward proportional to how big quantum dots are. One of the most significant elements affecting the effectiveness of solar cells is the process of absorbing high-energy photons because the substance is transparent to photons with energies below the bandgap, but the photons whose energy is the same as or greater than the bandgap will be absorbed, producing an electron-hole pair that needs to be separated. In the bulk of the semiconductors, when high-energy photons are absorbed, they will generate a high-energy charge carrier, which are called hot carriers. When it returns to its steady stable (relaxation) it will cause efficiency losses via what is called heat release [59].

In quantum dots, the capture of a single high-energy photon will generate multiple charge carriers (multiple excitation generation) because it suppresses the development of heat carriers, and thus the thermal losses in efficiency will decrease and the efficiency of the solar cell will increase [60].

2.9.2 **Quantum Dot Materials:**

Different materials can be used to manufacture quantum dots, but the selection of a semiconductor must take into account the absorption range of photon energy, in addition to other important properties. The energy of photons in solar radiation ranges between (0.5 eV and 4 eV). The energy of the sunlight corresponds to infrared radiation by 49%, 46% with the energy of visible light, and only 5% with ultraviolet radiation. The band gap of quantum dots must be within the energy range corresponding to infrared radiation to obtain high conversion efficiency.

In addition, MEG (Multiple Exciton Generation) is an important factor in the quantum semiconductor of solar cells. It also requires a higher cooling time for the exciting to separate the charge carriers and extract them before

recombining them [61]. Finally, to ensure optimal long-term performance, quantum materials must be extremely stable.

Table 2.1 Semiconductor resources used usually in quantum dot for solar cells arranged according to Bohr radius [62].

Semiconductor	Excitation Bohr Radius (nm)	Bandgap Energy (eV)
PbS	40.0	0.41
InAs	34.0	0.354
GaAs	28.0	1.43
CdTe	15.0	1.50
CdSe	10.6	1.74
ZnSe	8.4	2.58
CdS	5.6	2.53

2.9.3 <u>Synthesis of Quantum Dots:</u>

Numerous composition techniques have been created to produce high-quality components at the lowest feasible cost, with the least amount of environmental damage, and with the least amount of technological needs. The variety of these techniques, as well as temperature and pressure, are controlled by the materials utilized in the production of quantum dots. These techniques could be chemical or physical. Quantum dots may be produced on a big scale and at a lower cost using chemical processes. The quality of the quantum dots, film thickness, and homogeneity are controlled using physical techniques. They are usually more expensive, but due to the high quality of the particles, they have become a good choice for researchers. One of the most common physical methods is Stransky- Krastanov, or SK method [63], where this method is used to fabricate quantum dots of high quality with the molecular beam epitaxy technique. For better control of the particle

size, synthesis protocols have been used, as well as passivation techniques have been used to control surface defects. Temperature, pressure, reaction duration, and reactant concentrations are synthesis parameters that can change quantum dot characteristics and defect density. The most well-known techniques in quantum dot fabrication are consecutive ionic layer absorption, chemical bath deposition, and seller interaction. To enhance optoelectronic quantum dots' characteristics, it is necessary to reduce defects on their surfaces.

2.9.4 **Quantum Dot Solar Cells Design:**

The requirements for reducing electricity generation costs by photovoltaic devices are to explore new materials and to design new devices to achieve remarkable progress. The structures of solar cells affect the materials employed, technology requirements, and manufacturing costs. The following are types of quantum dot solar cells:

1. **Schottky Solar Cells based on Metal/Semiconductor Junctions:**

The term Schottky junction quantum dots solar cells also refers to metal-semiconductor junction solar cells. These represent the first class of QDSC to reach 1% efficiency [64]. Between the indium-doped tin oxide (ITO) counter electrode and the metallic electrode are sandwiched quantum dots in the form of thin films. A photo electrode is formed by the ITO-based counter electrode. Figure (2.13) displays a schematic of a solar cell with a metal-semiconductor connection [65].
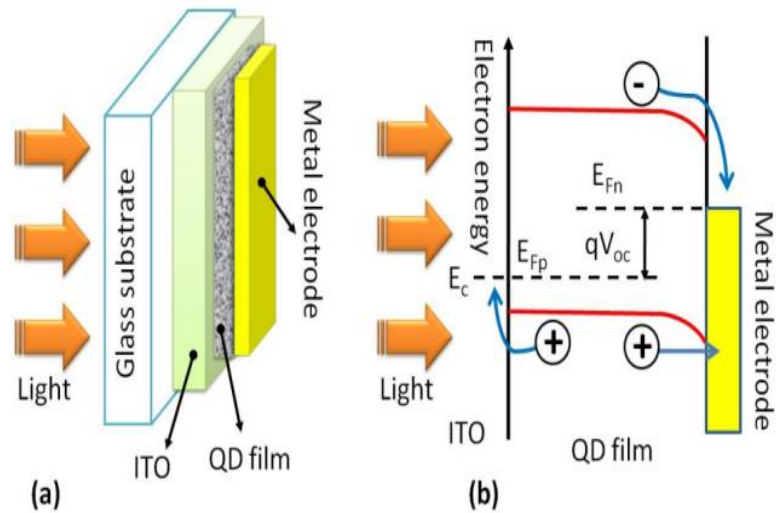
Figure (2.13) Schottky Solar Cells

a) Schematic of Schottky barrier quantum dots based solar cell.

b) Band diagram of Schottky solar cell.

2. Depleted Heterojunction Quantum Dots Solar Cells:

Widely controllable bandgaps provided by colloidal quantum dot photovoltaics allow for the processing of both single-junction cells with ideal bandgaps and multi-junction layouts. Additionally, size-effect tuning makes it possible to use cheap, plentiful ultralow-bandgap semiconductors that would not otherwise be suitable for solar energy conversion. The design of depleted heterojunction QDs is shown in Figure (2.14) [66].
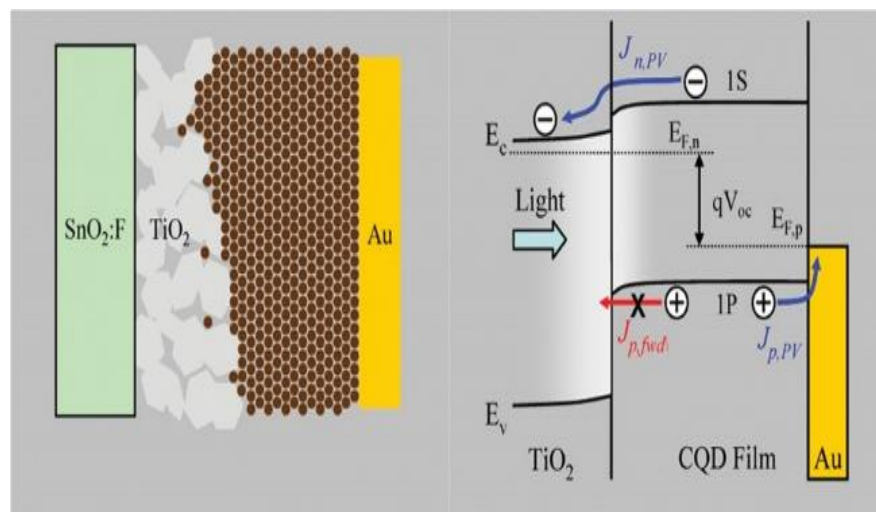
Figure (2.14) The depleted heterojunction design.

3. Quantum Dot-Sensitized Solar Cells:

With a minor modification, quantum dots are utilized in quantum dot-sensitized solar cells (QDSCs) instead of dye as a current injector, the operating principle of quantum dot-sensitized solar cells (QDSCs) is nearly identical to that of dye-sensitized solar cells (DSCs). According to Figure (2.15), the three crucial components of the quantum dot-sensitized solar cell are the counter electrode, the photo anode, which has a nanostructured TiO2 layer with quantum dots on it, and the electrolyte [65].
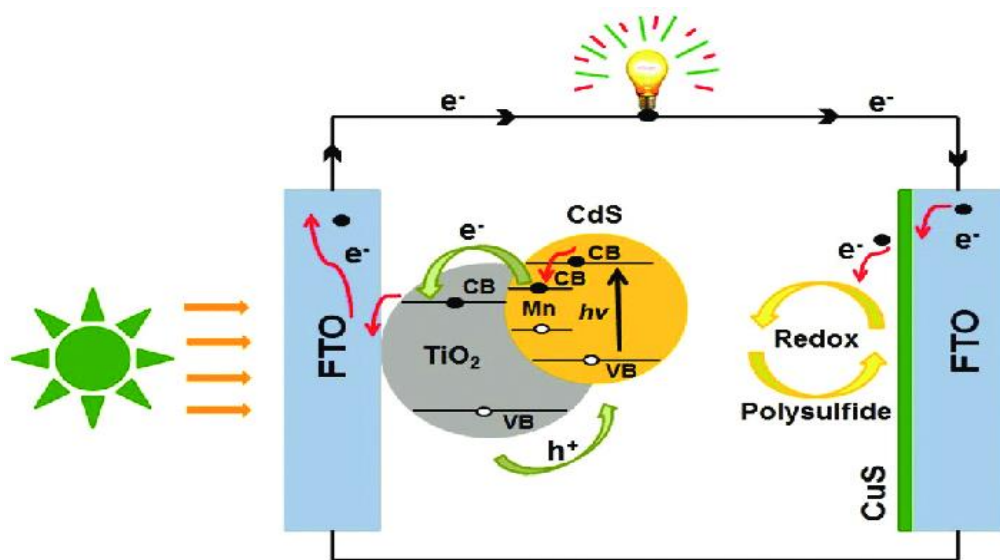
Figure (2.15) Schematic of Quantum Dot sensitized solar cell [65].

2.10 Quantum Dots Solar Cell Structure:

A unique family of semiconductors known as quantum dots may confine electrons (quantum confinement) and are nanocrystals made of periodic groups of II-VI, III-V, or IV-VI materials. The most pervasive consequence of quantum confinement is the radical alteration of a semiconductor's band gap and consequently its absorption properties. The greatest potential efficiency of solar cells based on intermediate bandgap materials is anticipated to reach 65% [67]. As illustrated in Figure (2.16), a quantum dot solar cell structure is made up of front and rear electrodes, a

hole transport medium (HTM), a Quantum Dots layer (also known as an absorption layer), and an electron transport medium (ETM).
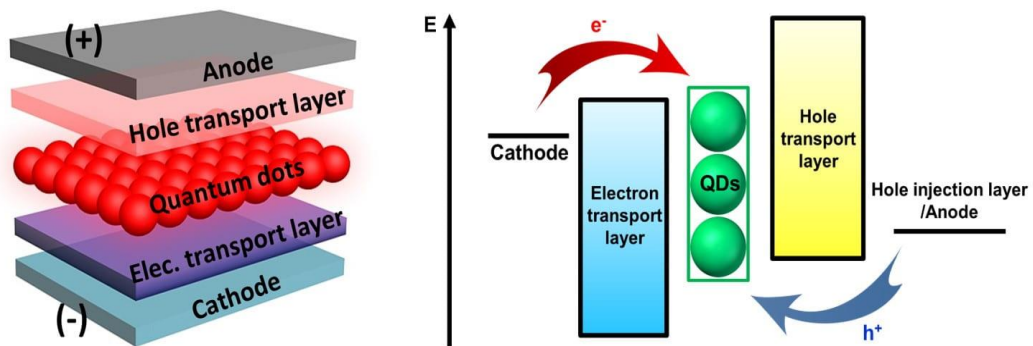
Figure (2.16) Quantum Dots Solar Cell structure.

2.11 Physics of Quantum Dot Solar Cell:

2.11.1 Multiple Excitation Generations:

Since electrons and holes in a bulk semiconductor are unrestrained and free to migrate, they have continuous energy values. Energy levels in a bulk semiconductor are packed closely together, forming energy bands, and the band-gap is determined by the material used. Before the excited electron (hot carrier) reaches the base of the conduction band, it goes through a number of non-radiative relaxations (thermalization: multi-phonon emission) [56]. When a single photon with enough energy is absorbed by a quantum dot solar cell, the action of collision ionization may cause the generation of many electron-hole pairs. An additional electron and a positive-charged ion are produced as a result of the photon's extra-high energy, which causes collision ionization [68]. As a result, there is a significant reduction in the rate of energy relaxation, which strengthens the impact of collision ionization [69]. Figure (2.17) depicts the multiple exciton generation (MEG) that takes place in a quantum dot solar cell [70]. One electron-hole pair (located on the leftmost) was produced by a single, very energetic photon, as shown in

Figure (2.17). The quantized QD energy levels in the conduction band and valence band are to blame.

<div align="center">(a)   (b)</div>
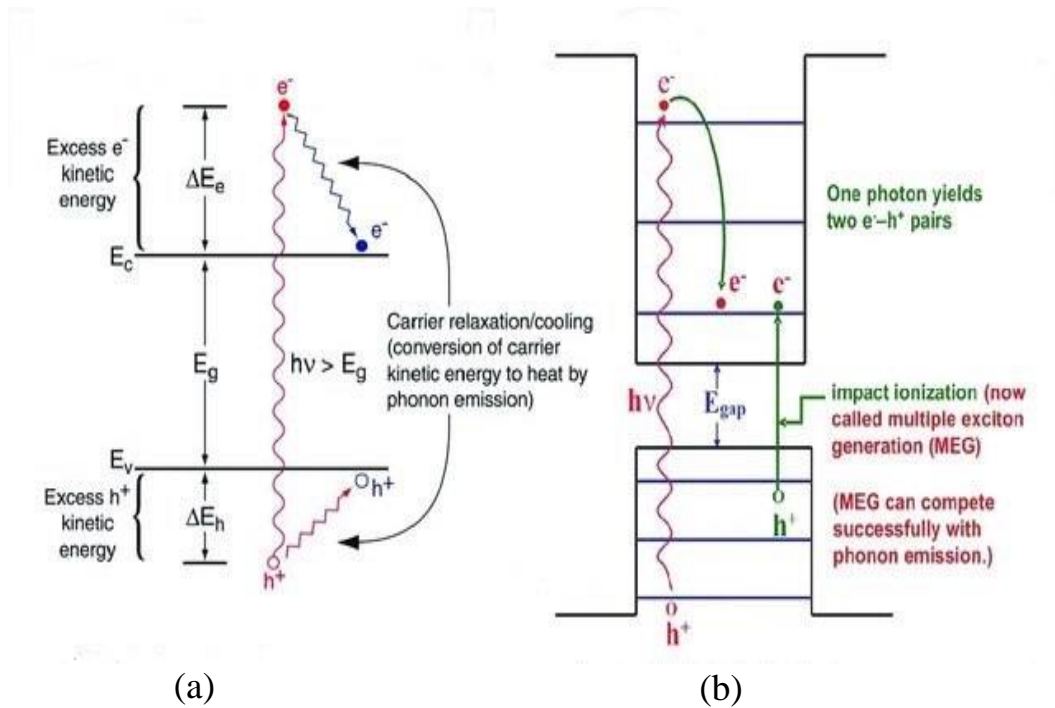
<div align="center">Figure (2.17) Multiple exciton generation [41].</div>

a) Hot carriers in a bulk semiconductor thermalizing.
b) Quantum dot impact ionization (MEG).

2.11.2 Intermediate Band in The Band Gap:

Quantum confinement effect in three dimensions causes the energy levels of quantum dots to be quantized. The small potential barriers caused by the tightly packed quantum dots allow electrons to flow together. After that, a sub-band known as the intermediate band forms in the band gap between the conduction band and the valence band. The so-called intermediate band can be produced using quantum dot structured material. It has been suggested that the intermediate band solar cell (IBSC) utilize photons with less energy than the bandgap [71]. Inserting nanometer-sized quantum dots into the semiconductor materials will produce the intermediate band. While semiconductors create the potential barrier, quantum dots create the potential well. Quantum effects, such as varying band gaps and distances

between quantized energy levels, can be changed by altering the size of quantum dots [58], as shown in Figure (2.18).
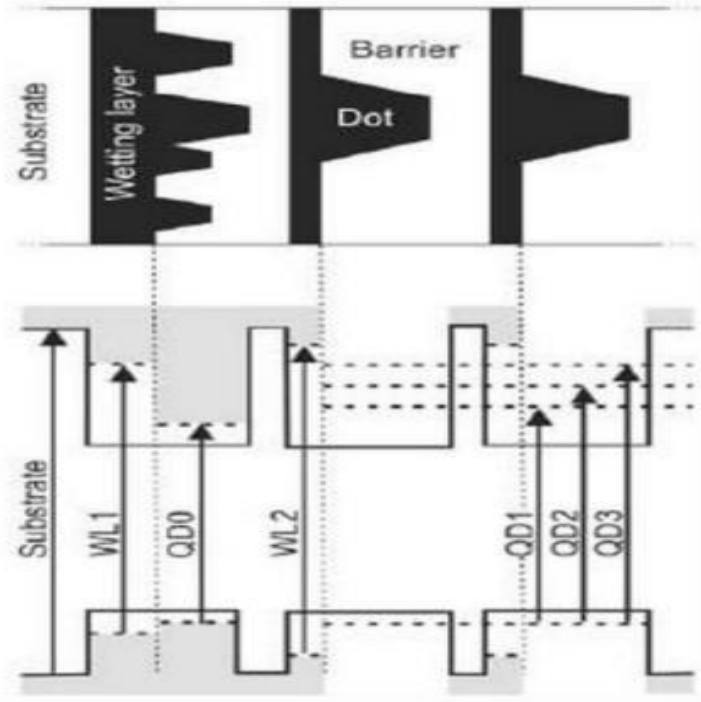
Figure (2.18) Quantum dot solar cell with intermediate band energy level structure [46].

Taking into account the spherical shape of a quantum dot with radius R and the effective mass model for colloidal quantum dots created by Louis Brus. The band gap E^{QD} can be roughly calculated using [72]:

$$E^{QD} = E_g^{bulk} + \frac{\hbar^2 \pi^2}{2R^2}\left(\frac{1}{m_e} + \frac{1}{m_h}\right) - \frac{1.8e^2}{4\pi\varepsilon\varepsilon_0 R} \qquad (2-12)$$

Where ε is the relative permittivity, and $\varepsilon_\circ = 8.854 * 10^{-14}$ F.cm^{-1} the permittivity of free space. According to Equation (2-12), the first component on the right-hand side describes the energy bandgap value of the bulk, the second term is a particle in a box quantum confinement model, and the third term describes the Coulomb attraction between the electron and the hole

(exciton). Compared to the second component in computations, the Coulomb attraction term may be ignored when the quantum dot's radius decreased. As a result, Equation (2-12) shows that the bandgap energy eigen values rise as the quantum dot size declines [43].

The middle band Quantum Dot Solar cells have a very high theoretical conversion efficiency, but their actual measurement findings are not very accurate. This is due to the fact that the quantized energy levels put into the band gaps would result in an unexpected non-radiative recombination center, lowering the performance of the solar cell. Despite some successes, there are still a lot of issues that need to be resolved. For instance, a closely arranged quantum dot arrangement is necessary for a quantum dot solar cell with an intermediate band in order to provide a constant energy level. Additionally, a high quantum dot density is necessary to absorb more photons. However, the self-assembling nature of the current quantum dot growth and fabrication technology makes it extremely challenging to control the size and shape of quantum dots.
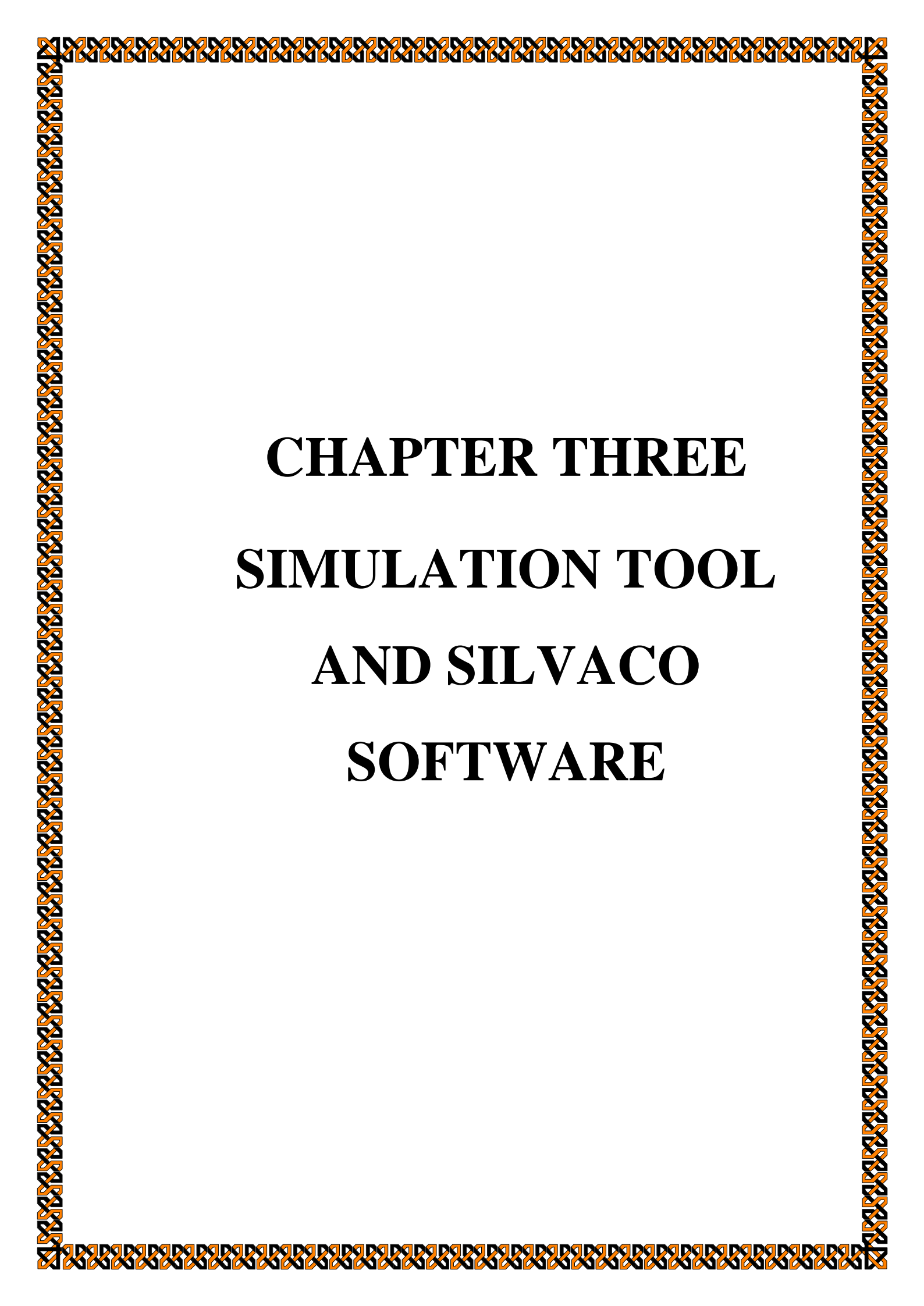
CHAPTER THREE

SIMULATION TOOL AND SILVACO SOFTWARE

CHAPTER THREE

SIMULATION TOOL AND SILVACO SOFTWARE

3.1 Introduction:

V. Aroutiounian created the p-i-n quantum dot model in 2001, to enhance the current, he created many layers of quantum dots inside the i-layer. The quantum confinement effect quantizes the energy level in quantum dots, which has been crucial to understanding quantum dots [18]. It would seem fair to think about whether a low-dimensional structure, such as a quantum dot p-i-n structure, could offer a fresh method for solving the challenge of high-efficiency solar cells [73]. These solar cells' drawbacks include the nature of electronic states as a function of interdot gaps, transportation characteristics, array form, order, and disorder, and quantum dot orientation [74]. The existence of very few atoms in a quantum dot, where excitons are restricted to a considerably smaller space on the order of the exciton Bohr radius of the material, is what causes quantum confinement. The effective band gap of the material is raised by the quantum confinement of charge carriers (electrons and holes) in variable-size quantum dots that make up the i-layer [75]. The type-I InAs/GaAs QD solar cells, which can extend the spectral response to longer wavelengths beyond the GaAs absorption edge, have been the subject of several investigations [75][76]. The type -I QDs feature strong carrier recombination in addition to high optical absorption due to the significant electron-hole wave function overlap. Numerous studys' findings about various quantum dot solar cells (QDSCs) made of various materials and structures have been presented. There have been various attempts to investigate the behavior of QDs and flaws in this class of materials, however, the maximum reported conversion efficiency of manufactured QDSCs has only achieved 19.4%, which is under two-sun illumination [78]. As far as the study is aware, virtually all theoretical

publications addressing the IBSC only take cubic geometry into account when figuring out the characteristics of this new type of photodiode. In this work, the study examines the behavior of various parameters and features of a multiple quantum dots solar cell (MQDSC) structure [79].

3.2 Theory Approach:

Basic semiconductor equations had to be solved to assess the performance of the solar cell; these equations have a real-valued function. The following equations, which explain the physical models utilized for this simulation, can be used to describe solar cell operation [80]:

a) The Poisson equation, which connects charge to electrostatic potential, is the governing equation. Equation (3-1) contains the Poisson Electrostatic Potential equation [37].

$$\frac{d^2 E}{dx^2} = \frac{\rho}{\varepsilon} \qquad\qquad (3-1)$$

Where ρ is the charge density (C.cm^{-3}), and ε is the material permittivity. Equation (3-2), which is derived from the charge neutrality equation, can be written as the dopant is fully ionized.

$$\rho = q(p - n + N_D^+ - N_A^-) \qquad\qquad (3-2)$$

Equation (3-2) yields equation (3-3) when it is combined with equation (3-1) [37]:

$$\frac{d^2 E}{dx^2} = \frac{q(p - n + N_D^+ - N_A^-)}{\varepsilon} \qquad\qquad (3-3)$$

b) The second equation is a continuity equation, which is also known as a governing equation because it considers generation, recombination, drift, and diffusion simultaneously. The continuity equation for the change in electron and hole concentration is represented by equations (3-4) and (3-5) [37]:

$$\frac{\partial n}{\partial t} = G_n - R_n + \frac{1}{q} \cdot \frac{\partial J_n}{\partial x} \qquad\qquad (3-4)$$

$$\frac{\partial p}{\partial t} = G_p - R_p - \frac{1}{q} \cdot \frac{\partial J_p}{\partial x} \qquad\qquad (3-5)$$

Where J_n is the electron's current density, J_p is the hole's current density, G_n, G_p is the generation rate for electrons and holes, and R_n, R_p is the recombination rate for electrons and holes respectively.

c) Electric currents are generated in semiconductors because electrons and holes move charges around. The ability to solve the drift-diffusion equation for current in a solar cell is necessary for calculating the current and properties of a solar cell simulator.

- **Drift:** it is the electric field proportional to the velocity of charged particles. The carrier's acceleration is frequently destabilized by collisions with ionized impurity atoms and thermally vibrating lattice atoms. The drift-current densities for electrons and holes J_n and J_p drift are described by equations (3-6) and (3-7), respectively, and the overall drift current is described by equation (3-8)

$$J_{n\ drift} = -qn v_{dn} = qn\mu_n E \qquad\qquad (3-6)$$

$$J_{p\ drift} = qp v_{dp} = qp\mu_p E \qquad\qquad (3-7)$$

$$J_{drift} = J_{n\ drift} + J_{p\ drift} = q.E.\left(n\mu_n + p\mu_p\right) \qquad (3-8)$$

Where μ_n and μ_p are the mobility of electron and hole respectively.

- **Diffusion:** it is a phenomenon whereby particles tend to spread from areas of high particle concentration to areas of low particle concentration as a result of erratic thermal motion. Equations (3-9) and (3-10) are used to express the diffusion-related currents that are proportional to the gradient in

particle concentration, and equation (3-11) is used to define the total diffusion current [81].

$$J_{n\,diff.} = qD_n\nabla n \qquad\qquad (3-9)$$

$$J_{p\,diff.} = -qD_p\nabla p \qquad\qquad (3-10)$$

$$J_{diff.} = J_{n\,diff.} + J_{p\,diff.}$$

$$J_{diff.} = q(p\mu_p + n\mu_n)E + q(D_n\nabla n - D_p\nabla p) \qquad\qquad (3-11)$$

3.3 The Silvaco Atlas Simulator:

To create solar cell models and simulate solar energy conversion, SILVACO TCAD Software is used in this project. A robust device design and simulation tool, SILVACO TCAD (Technology Computer Aided Design) includes both device and semiconductor process simulation. For the business and scientific communities, having the ability to precisely replicate a semiconductor device is essential. The ATLAS simulation program was created specifically for modeling semiconductor components in 2D and 3D using their physical attributes, such as their electrical, optical, and thermal characteristics. It offers a library of predefined materials and lets the user define more materials of their choosing.

3.4 Atlas Inputs and Outputs:

Two types of input files are used by Atlas:

- An Atlas command file in text form.
- A structure file that specifies the model's structure.

Three different output file types are generated by Atlas:

- The runtime output displays errors and cautions as the simulation progresses.
- The log file is used to keep track of voltages and currents.
- The structure file contains 2D and 3D information about the values of the solution variables. Figure (3.1) shows the inputs and outputs for the SILVACO ATLAS.
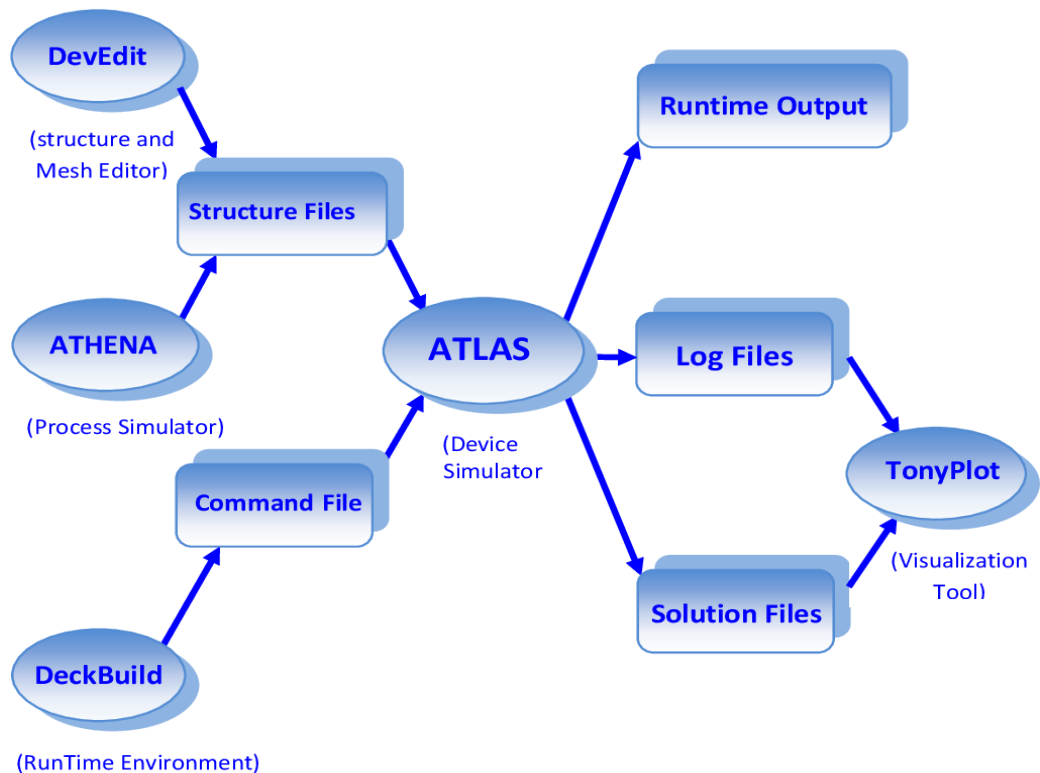
Figure (3.1): Atlas inputs and outputs [82].

Figure (3.1) demonstrates that the device simulator ATLAS is the main component of the SILVACO TCAD program. It can completely replicate many semiconductor device features, such as electrical behavior, optical behavior, thermal behavior, and so forth. A physics-based, user-friendly, modular, and extendable platform is offered by ATLAS. Additionally, ATLAS provides users with access to a variety of physical calculation models [83].

3.5 Operating Atlas within Deckbuild:

The extended "*.in*" signifies the run-time environment known as Deckbuild, which is used to enter command files or decks. Using the command line is the first step towards running ATLAS inside the Deck Build environment:

go atlas

It is crucial to consider the statements' order in an ATLAS input file. The right sequence of five groups of statements must be used. The input file must thereafter adhere to the pattern shown in Figure (3.2) after that command.

```
Group                              Statements

                                   MESH
                                   REGION
1. Structure Specification  ──────  ELECTRODE
                                   DOPING

                                   MATERIAL
                                   MODELS
2. Material Models Specification ──────  CONTACT
                                   INTERFACE

3. Numerical Method Selection ──────  METHOD

                                   LOG
                                   SOLVE
4. Solution Specification   ──────  LOAD
                                   SAVE

                                   EXTRACT
5. Results Analysis         ──────  TONYPLOT
```

Figure (3.2) Primary statements for each group of ATLAS Commands.

3.6 Structure Specification:

The mesh, region, electrodes, and amounts of doping are defined to create the structure's specification.

3.6.1 Mesh:

First, the command "*MESH*" can be used to control how the grids are divided, and it must be:

MESH SPACE.MULT=<Value>

Then, as illustrated below, a sequence of **X.MESH** and **Y.MESH** assertions is made.

x.m l =0.0 s=0.05

x.m l =0.1 s=0.05

y.m l =0 s=0.01

y.m l =3.0 s=0.5

Grid definitions for landscape and portrait orientations are done with (**x.m**) and (**y.m**), respectively. The grid exit point is indicated by (*l*), while the density or distance between two succeeding nodes is indicated by (*s*). The mesh density definition is crucial. The calculating pace will be slow if it is dense. The precision and convergence will suffer if it is coarse. Consequently, it is important to define the grid density accurately. As an illustration, the density should be sparse inside the substrate but dense near the p-n junction and interfaces.

3.6.2 Regions:

Second, the command "*REGION*" can be used to control how regions are defined, as demonstrated by the examples below:

region number=<integer> <material type> <position parameters>

for example:

region num=2 material=GaAs x.min=0 x.max=0.1 y.min=0 y.max=0.5

Region statements must each begin with a region number of 1, increasing thereafter. In ATLAS, one can have up to 200 distinct areas. There are numerous materials available. The **REGION** statement additionally allows for the x and y composition fractions to be supplied if a composition-dependent material type is defined [82].

3.6.3 Electrodes:

Electrodes are the subject of the structural definition which will considered in the current work. The anode and cathode are the only defined electrodes in this simulation, as is customary. The maximum number of electrodes that can be defined for Silvaco Atlas is 50. This is how electrodes should be defined:

ELECTRODE NAME =< electrode name>< position_parameters>

for example:

electrode name=anode top

electrode name=cathode bottom

When specifying the position of an electrode, there are a few shortcuts that can be used. The electrode is considered to be at the top of the structure if no Y-coordinate data are provided.

3.6.4 Doping:

Doping is the final part of structure specification that requires definition. The Atlas statement is written in the following format:

doping <distribution type><dopant_type><position parameters>

for example:

doping uniform region=1 p.type conc=2e18

3.7 <u>Materials Model Specification:</u>

It is Including the material set up specifications such as (band gap, absorption coefficient, minority lifespan, electron affinity, etc.), selecting the physical models, defining the contact qualities, and specifying the contact characteristics.

3.7.1 <u>Materials:</u>

First, by using the command "***MATERIAL***," which is illustrated in the example below, the parameters and properties of materials used in simulation models can be defined:

material <localization> <material_definition>

for example:

material material=GaAs eg300=1.424 permittivity=13.1 affinity=4.07 nc300=4.7e17 nv300=7e18 augn=1e-30 augp=1e-30 taun0=1e-8 taup0=1e-8

"***Eg300***" denotes the energy gap at ***300K*** (measured in eV) among them. "***Permittivity***" refers to the dielectric constant. "***affinity***" stands for electron affinity (measured in eV). Effective densities of states in the conduction band and valence band, respectively, are denoted by "***nc300***" and "***nv300***" (in units of cm^{-3}). "***augn***" and "***augp***" stand for the respective Auger constants for electrons and holes (unit: cm^6 /s). "***taun0***" and "***taup0***" stand for the lifetimes of electrons and holes under the Shockley Read Hall recombination condition (measured in seconds).

3.7.2 <u>Models:</u>

Carrier statistics, impact ionization, mobility, recombination, and tunneling are the five categories into which the physical models are divided. The model statement has the following expression:

models <model flag><general parameter> /<model dependent parameters>

The model selected will rely on the simulation materials selected. The example that follows turns on various models.

for example:

models conmob fldmob consrh print

The term "*conmob*" refers to the concept where mobility is dependent on impurity concentration. *"Fldmob"* refers to the model that mobility depends on electric field. *"consrh"* refers to the carrier recombination model which is under Shockley-Read-Hall condition and also depends on concentration. All models and material parameters will output in tabular form, and other models will not be referred to by the term "*print*" instead.

3.7.3 Contact:

The characteristics of the electrode are governed by contact. The following is the expression for contact:

CONTACT NUMBER= |NAME=|ALL

An illustration of a contact statement is given below.

contact name=anode

contact name=cathode

3.7.4 Interface:

The "*INTERFACE*" command can be used to define the surface recombination rate, as in the example below:

interface s.p=100 s.n=100

"*s.p=100*" means the recombination velocity for holes is 100 cm/s, and "*s.n=100*" means the recombination velocity for electrons is 100 cm/s.

3.8 Numerical Method Selection:

Numerical calculation is the foundation of computer simulation. The right numerical approach should be chosen to ensure that the calculation can converge. There are four different iteration techniques used in Atlas: Newton, Gummel, Block, and combination techniques [84]. For example:

method newton autonr trap maxtrap=10

The whole system of unknowns is solved via the NEWTON technique. When the system of equations is strongly coupled and converges quadratically, the NEWTON technique is helpful. However, this approach could take more time to solve for quantities that are essentially constant or weakly connected. Additionally, to achieve convergence, a more precise starting guess is needed for the problem. In the METHOD statement, use the **autonr** parameter to activate the automated Newton-Richardson Method. Dopant concentration should be regarded as a trap state density, according to the trap specification. **Maxtrap** indicates how many times the trap procedure will be carried out in the event of divergence. **MAXTRAPS** may have a value between 1 and 10.

3.9 Solution Specification:

The solution specification comes next after the numerical method selection is finished. The four statements of the solution specification are: log, solve, load, and save.

3.9.1 <u>Log:</u>

Terminal characteristics derived by Atlas are stored in log files (*.log*). DC or AC data created via a ***SOLVE*** statement after a ***LOG*** statement is saved. The ***LOG*** file is specified as the following:

LOG OUTFILE=<file name>.log

In the given example, the current-voltage data is saved to the specified

<file name>.log

3.9.2 <u>Solve:</u>

The LOG statement is followed by the SOLVE statement. In order to solve, the beam should be defined as the following:

beam num=1 x.origin=0.05 y.origin=-1.0 angle=90.0 AM1.5 Back.Ref quantum.eff=1

The centers of the "light beam" are indicated by the variables "*x.origin*" and "*y.origin*" among them. "*Angle*" refers to the slope of a light beam. When "*angle=90.0*", for instance, the illumination is vertical incident. The command *"num=1"* is used to assign numbers to light beams, and it will come in handy when one of the light beams is called in the commands that follow. A quantum efficiency factor called "*quantum.eff*" describes how many carrier pairs are produced for each absorbed photon. After applying the light source (beam statement), the solution may be attained at various electrode voltages to establish the I-V solar cell curve:

solve b1=1.0

solve vanode=-1 name=anode. vstep=0.1 vfinal=1

3.9.3 Load and Save:

As a first guess for other bias spots, the *LOAD* statement inputs past solutions from files. All node point data is input into an output file via the *SAVE* command. These *LOAD* and *SAVE* statement examples can be found below:

SAVE OUTF=<file name>.STR

For example:

save outf=GaAsQD1.str

Specifically, *<file name>.STR* stores data following a *SOLVE* statement. Then, in an additional experiment, run *<file name>.STR*, this is how the file can be loaded:

LOAD INFILE=<file name>.STR

3.10 Results Analysis:

The steps "*tonyplot*" and "*extract*" are used for plotting and extracting the results when the calculation is complete and the results have been saved in records files. To get the features we want, we must first tell Atlas what they are. In the following example, it will be used the command *"output"* to demonstrate this step:

output opt.int charge band.param con.band val.band

"*opt.int*" refers to optical intensity, "*band.Param*" refers to all band parameters (including Eg, n_i, N_c, and N_v), "*val.band*" and "*con.band*" refer to the valance band and conduction band, respectively. For instance, the J-V characteristic log file contains many crucial details about a solar cell, just like the file *"<file name>.log"* that we obtained from ATLAS calculations. When plotting this file with the "*TONYPLOT*" command alone, the J-V curve figure can only obtain. The following examples demonstrate how

further information can be extracted from this file using the command "***EXTRACT***":

extract init infile= "<file name>.log"

extract name="Jsc" max(curve(v."anode", i."anode"))

extract name="Voc" x.val from curve(v."anode", i."anode") where y.val=0.0

extract name="Pm" max(curve(v."anode",(v."anode"*i."anode")))

tonyplot <file name>.log

3.11 <u>Modeling and Simulation of Standard p-i-n Solar Cell:</u>

Using Atlas, one first simulates a typical p-i-n GaAs solar cell with the same structural layout as shown in Figure (3.3) [85]. There are six layers in the solar cell, the first and fifth of which are InGaP with a thickness of 50 nm (p-type and n-type, respectively), and are referred to as the window layer and the rear surface field layer. Utilizing these two layers has the advantages of lowering surface recombination at the top and bottom of the solar cell and blocking minority carriers [80].

The second, third, fourth, and sixth layers, which have thicknesses of 500 nm, 410 nm, 1960 nm, and 250 nm, respectively, are the emitter-region (p-type), i-region, base-region, and epitaxial seed layer. The respective doping of these layers is: $2x10^{18}$ cm^{-3}, $1x10^{18}$ cm^{-3}, $1x10^{17}$ cm^{-3}, $1x10^{18}$ cm^{-3} and $1x10^{18}$ cm^{-3}.

P-type (InGaP), doping 2×10^{18} cm^{-3}, and thickness (50 nm)

(GaAs) p-type, 1×10^{18} cm^{-3} doping, 500 nm thickness

i-region (GaAs), 410 nm thick

n-type (GaAs), thickness (1960 nm), doping 1×10^{17} cm^{-3}

Materials
InGaP
GaAs
Conductor

Doping 1×10^{18} cm^{-3}, thickness (50 nm), n-type (InGaP)

n-type (GaAs), thickness (250 nm), doping 1×10^{18} cm^{-3}

Microns
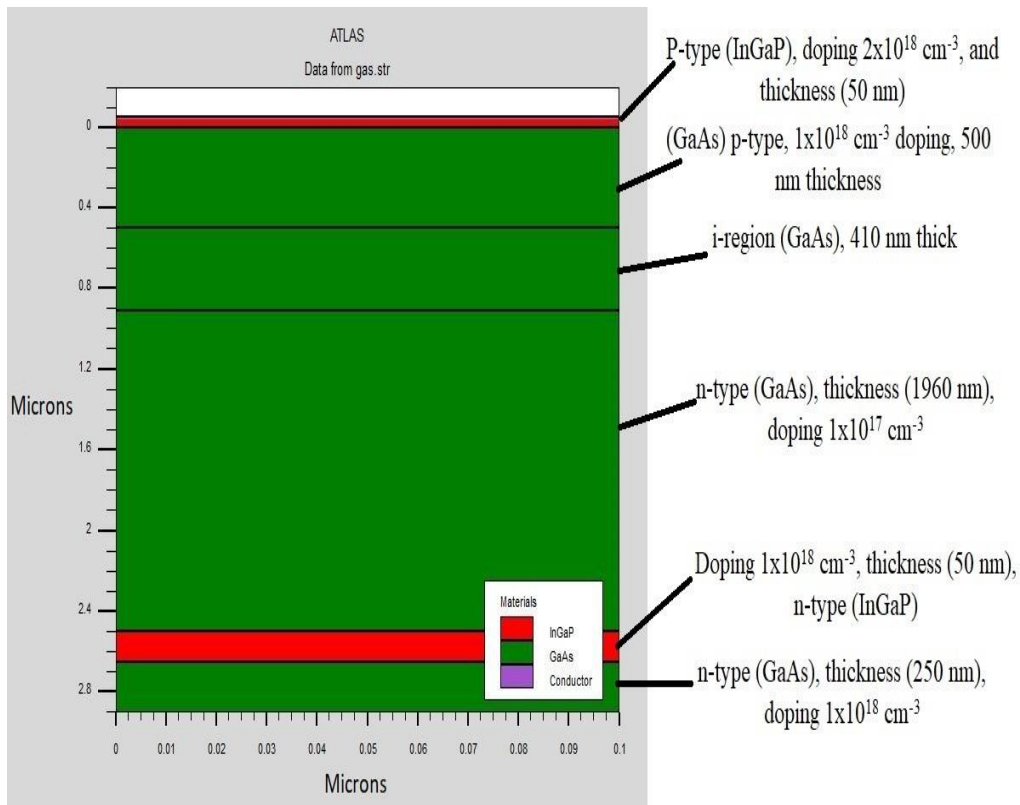
Figure (3.3) Structure of standard p-i-n solar cell.

3.12 Modeling and Simulation of p-i-n Quantum Dots Solar Cell:

The simulation using Atlas is run for the InAs/GaAs QD solar cell in this work for the QD solar cell. The typical p-i-n GaAs structure is used for the solar cell, and one layer of QD is embedded in the intrinsic region of the cell. Using the same p-i-n structure as before, it was explored how quantum dots affected the performance of the solar cell. In Figure (3.4), the structure of p-i-n QDs is depicted. The use of quantum dots is intended to increase the parameters that control the solar cell's properties by producing a large number of electron-hole pairs in the intrinsic region.
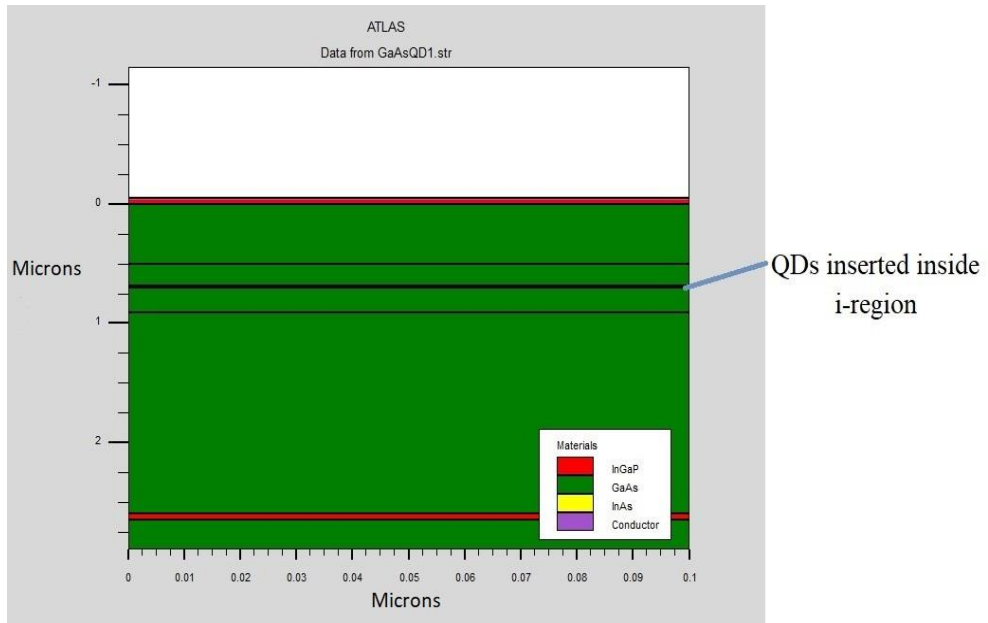
Figure (3.4) Structure of InAs/GaAs quantum dots solar cell with 1-layer embedded in the intrinsic region.

For ease of calculation, each QD is represented by a rectangle with a diameter and height of 10 nm and 5 nm, respectively [86]. The distance between the layers is 6.5 nm for the upper barrier and 4.5 nm for the lower barrier. The distance between QDs within the same layer is 10 nm, and the intrinsic region's thickness is 410 nm, as shown in Figure (3.5).
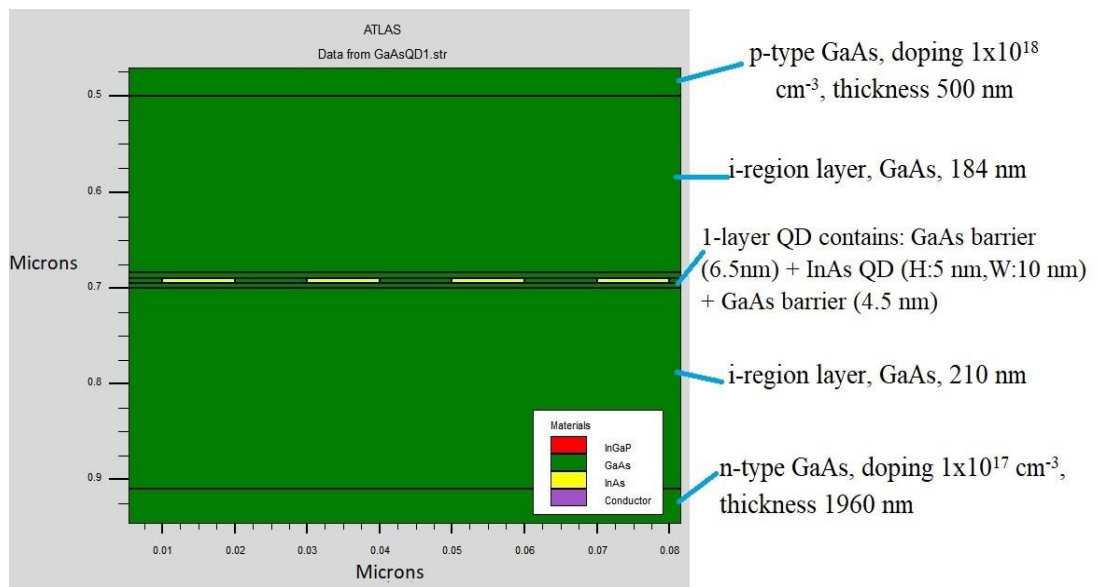
Figure (3.5) (a) Zoomed-in view of 1-layer quantum dots inserted in the intrinsic region.
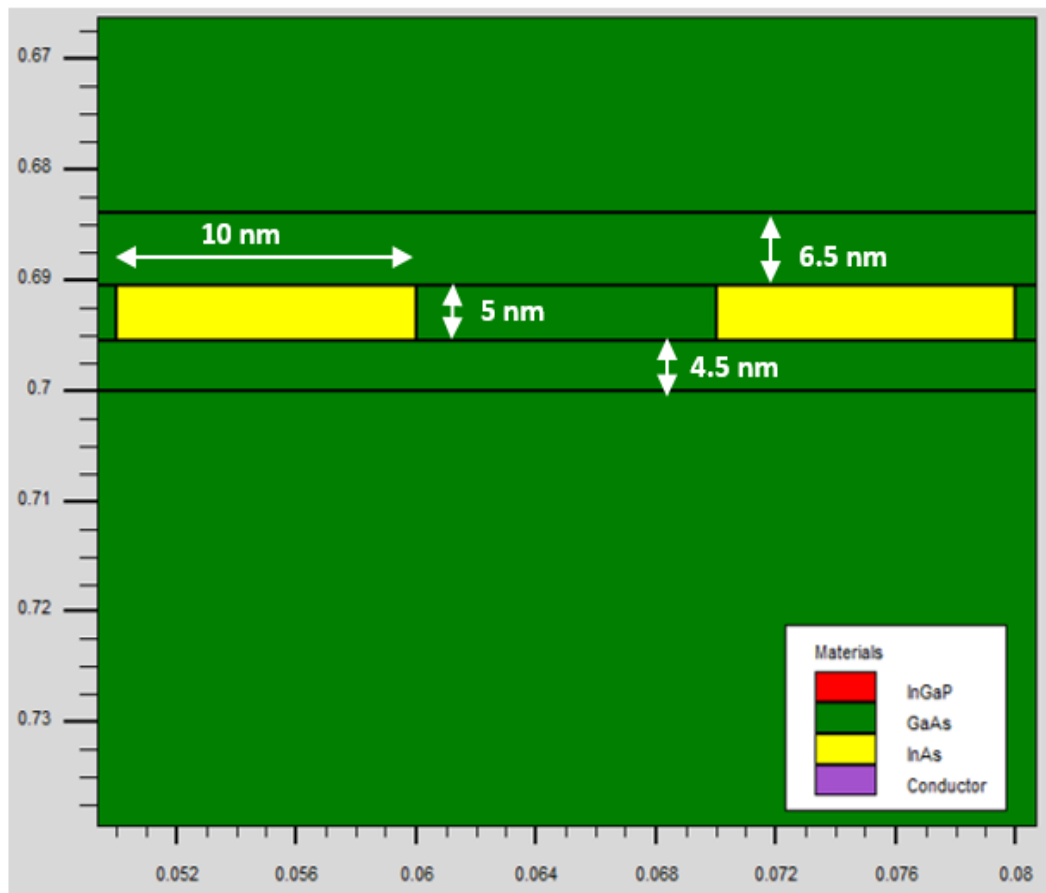
Figure (3.5) (b) Sizes of quantum dots and barriers in one layer.

This quantum dot layer structure, which includes a GaAs capping layer, an InAs QD array layer, and barrier layers, was inspired by the construction of an actual, produced quantum dot solar cell [77][86]. The sizes of them in detail are shown in Figure (3.5) (b). Based on the reference values from Dr. Bailey's research, all of these thickness and size numbers have been calculated [77][86].

ATLAS provides a variety of physical calculation models for simulation in several study fields. Users can pick the materials they require to aid in creating their simulation models. In addition to building the multiple-layer quantum dot structure, when simulating quantum dot solar cells, one also needs to select an appropriate physical calculation model to apply the effect of quantum dots. Several further quantum effects exist. ATLAS has physical simulations that can be used to simulate a variety of

quantum confinement effects. The physical model of the general quantum well is one of them. The quantum confinement effects can be applied using this model to those quantum well light emitting components, such as quantum well solar cells [82]. These bound state energies and wave functions, which can be used to describe optoelectronic gain, radiative recombination, and absorption, are calculated in this model by solving the Schrodinger equation [82]. The "*QWELL*" command must be specified in the "*REGION*" statement to allow this model, as in the example below:

region num=6 material=InAs x.min=0.01 x.max=0.02 y.min=0.6905 y.max=0.6955 qwell

This region will be used as a model for a quantum well computation that may be simulated after being specified. Carriers in quantum dots essentially have zero degrees of freedom. As a result, the primary goal of our approximation method is to roughly apply the three-dimensional quantum confinement effect using the quantum well physical model. ATLAS can successfully implement this concept and approximation technique due to two things:

At first, the Schrodinger equation in the quantization direction is solved in ATLAS along discrete slices of the calculation grid [82]. Here, the flag "*2DXY.SCHRO*" on the "*MODELS*" statement allows the quantization direction to be adjusted and the 2D orientation to be set. When this flag is raised, ATLAS is informed to solve the Schrodinger equation in the XY plane.

Second, this thesis's research makes use of a 2D simulation. There is no movement for carriers in the Z-axis direction since ATLAS of SILVACO TCAD can only calculate in the two-dimensional XY plane for two-dimensional device simulations. The density of the calculating grid should also be taken into consideration. Since quantum dots are nanometer-sized,

they are substantially thinner than other typical solar cell layers. As a result, the mesh density defined by the command "*MESH*" (as stated before) around quantum dots may be coarse, which lowers the accuracy of simulation results. To address this issue, the study may utilize the "*MODELS*" statement's "*WELL.NX*" and "*WELL.NY*" commands to create an auxiliary mesh that will improve the precision of calculations made inside or near quantum dots. As in the following illustration:

models well.nx=15 well.ny=15
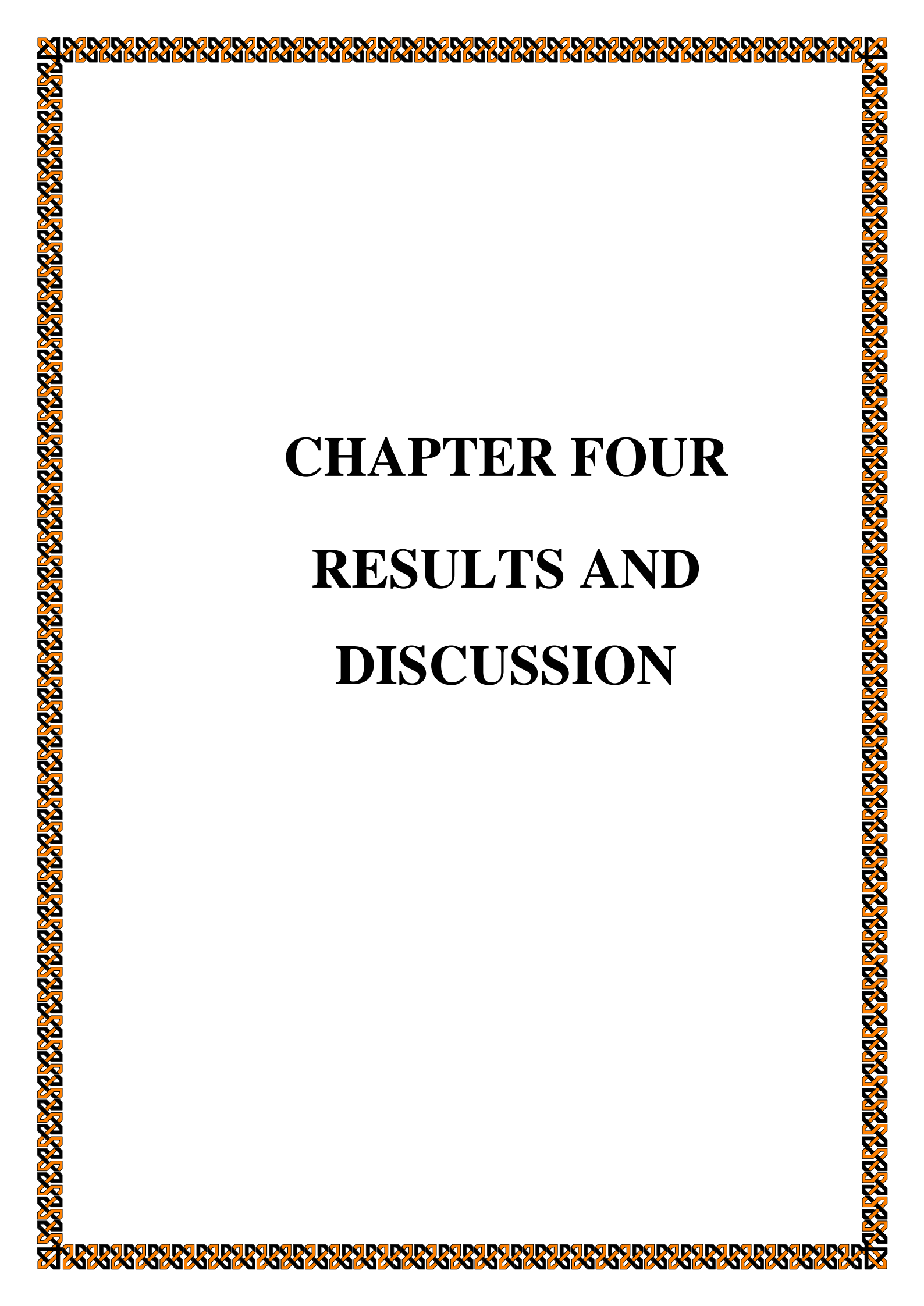
CHAPTER FOUR

RESULTS AND DISCUSSION

CHAPTER FOUR

RESULTS AND DISCUSSION

4.1 Introduction:

The solar cell with structure of QDSC (InAs/GaAs) is simulated using SILVACO ATLAS software to obtain the SC performance parameters. One-sun AM1.5G illumination condition has been chosen for this simulation. At first, a typical p-i-n GaAs solar cell was simulated. The impact of adding a different quantum dots layers (up to 20 layers) was then recorded to investigate the impact of QD on the solar cell performance.

4.2 Standard GaAs p-i-n Solar Cell:

The simulation results of the standard p-i-n GaAs solar cell will be presented, discussed in this section. The results of the current study will compare with the similar study achieved by Boqun Dong's [14]. Although the current structure is similar to the structure of reference [14] but the most important point that differentiates the present work is the thickness of the i-layer. In the Boqun Dong's study, the thickness of the i-layer was changed when the QDs layers were added and this led to the impact of a two-parameter on the solar cell performance simultaneously which gives an unclear vision of the role of each parameter individually and it was used an illumination source AM0 while in the present work the thickness of the i-layer was kept constant during adding the QD layers with the illumination source AM1.5. The J-V characteristic curve of the standard GaAs p-i-n solar cell is shown in Figure (4.1).
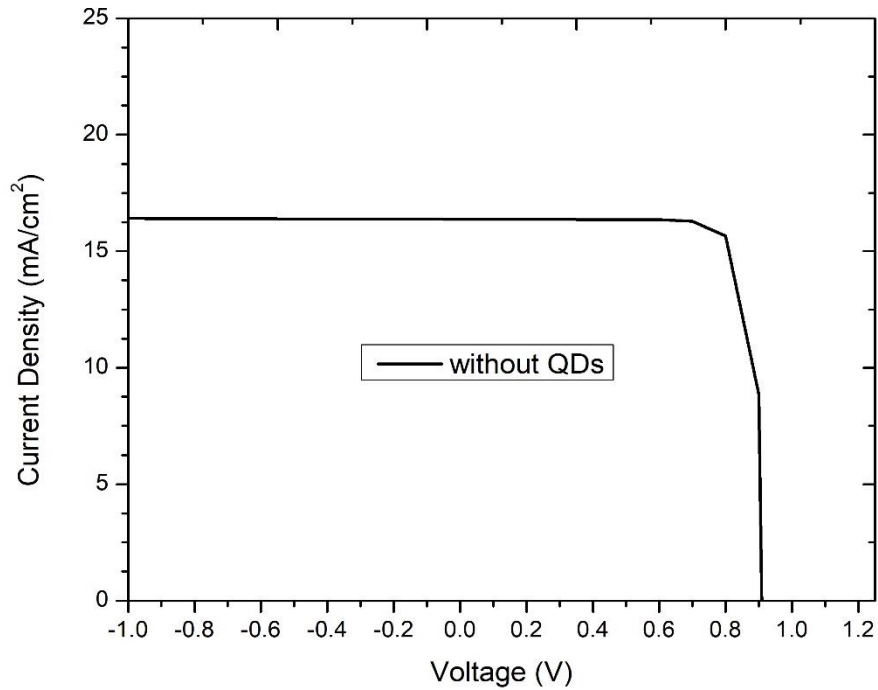
Figure (4.1) J-V characteristics of standard GaAs p-i-n solar cell.

The extracted solar cell parameters from Figure (4.1) shows that the vaules of J_{sc} is **16.4047 mA/cm²**, V_{oc}**=0.90884 V** , **FF=83.9773%** and **PCE=12.5158%.** By comparing the current results with the results obtained by Boqun Dong's in his study for validation it can be observed that the results of the current study are relatively less than the results that obtained by Boqun Dong's (details in table 4.1) [14]. The difference in these values can be attributed to the dissimilarity in thickness of the i-layer; where the i-layer thickness is 410 nm in the current study whilst it is 100 nm in the study of reference [14].

Table 4.1 The simulation results of standard GaAs p-i-n solar cell.

Device	J_{sc} (mA/cm²)	V_{oc} (V)	FF (%)	PCE (%)
Standard p-i-n solar cell	16.4047 (22.5309)[*]	0.90884 (0.9827)[*]	83.9773 (83.9786)[*]	12.5158 (14.1289)[*]

[*] The simulation results of standard GaAs p-i-n solar cell for Boqun Dong's research [14].

Figure (4.2) shows the photo-generation rate for standard p-i-n solar cell. It can be seen the high rate of photo-generation by ~3.69x10^{19} cm^3.s^{-1} at the intrinsic region
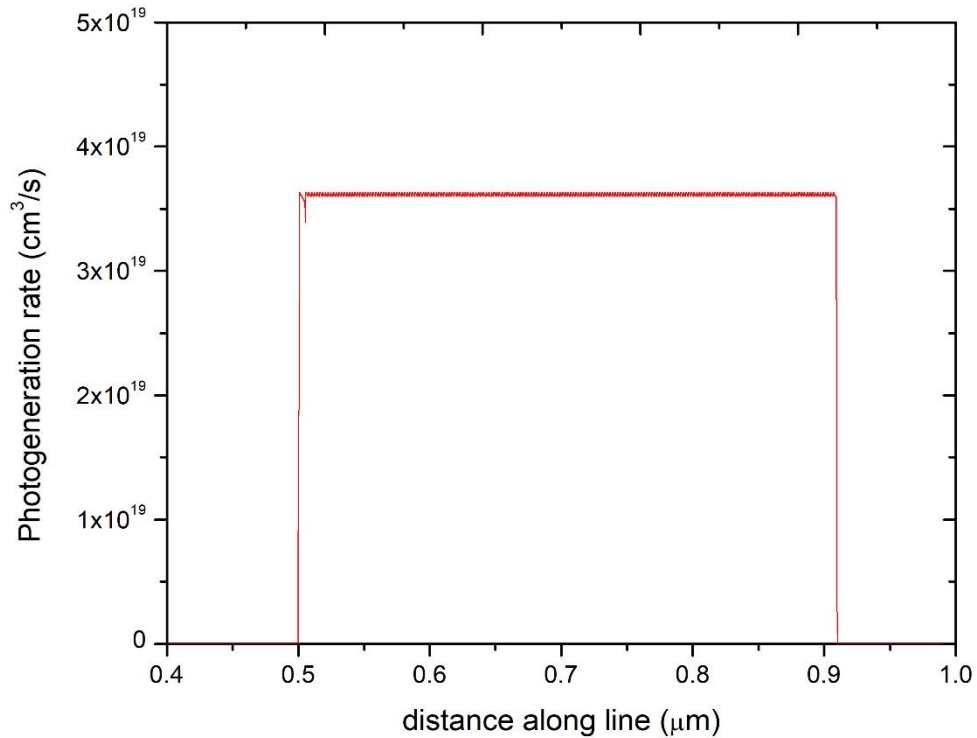
Figure (4.2) Photo-generation rate curve for standard p-i-n solar cell.

4.3 Impact the Quantum Dots on the Solar Cell Parameters:

To understand the QD's impact on InAs/GaAs solar cell performance, the current study involved investigating the influence of the number of QD's layers on the solar cell parameters. The results are compared with the standard solar cell (i. e. without QD's layer).

4.3.1 Adding One Layer of Quantum Dots:

As a first step a single layer of InAs was added at mid of the intrinsic layer. This layer has a dimension of 5nm × 10nm. The details of InAs/GaAs solar cell structure with a single quantum dots layer have been explained in details in chapter 3. It is worth mentioning that the thickness of the i-region

is kept constant in the conventional p-i-n solar cell structure even when the QDs layer(s) are added. Figure (4.3) shows the J-V curve for the standard solar cell and the solar cell structure with a single quantum dot solar layer. This figure shows that adding a single QD layer produces a noticeable improvement in the SC performance. The value of J_{sc} has increased from **16.4047 mA/cm²** to **34.1625 mA/cm²** (a relative increasing is approximately 208%), while the **FF** has increased from **83.9773%** to **84.2137%** (a relative increasing is 1%). The J-V curves in figure (4.3) show that the V_{oc} is almost unaffected by adding a QD layer. The increase in the J_{sc} and **FF** of the SC is reflected on the **PCE** which is increased from **12.5158%** to **26.7046%**. The comparison between the solar cell parameters with and without QDs is summarized in Table 4.2. It can be concluded that the existing of a single QDs-layer helps to absorb more of the incident photons with low energy (wavelength) consequently increasing in the generated number of electron-hole pairs.
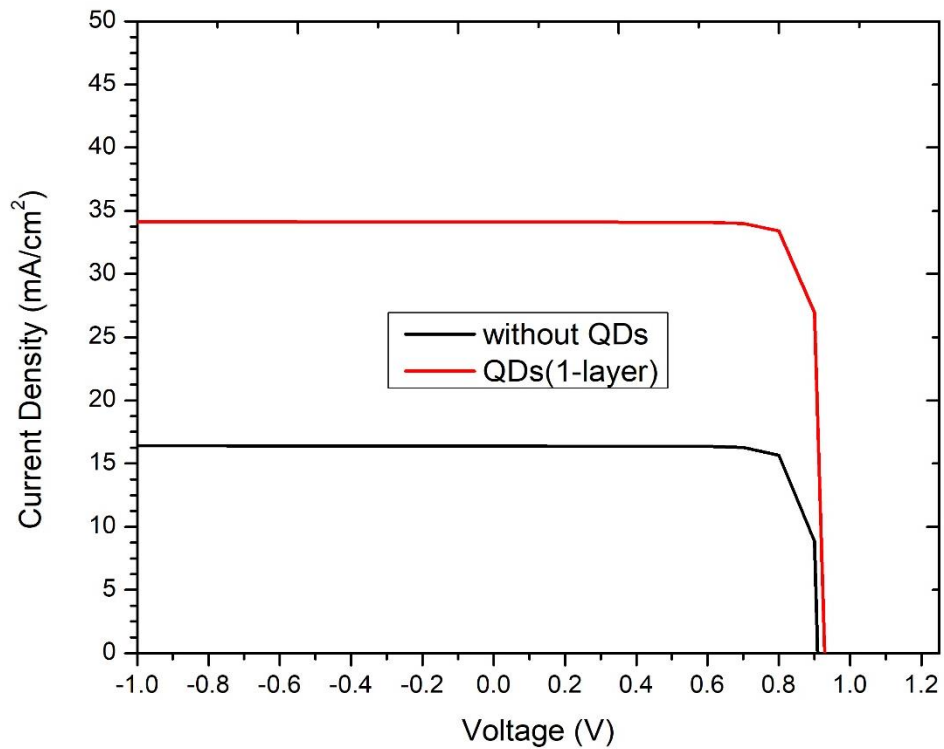
Figure (4.3) J-V characteristics of standard GaAs p-i-n solar cell and QDs solar cell with 1-layer.

Table 4.2 Simulation results of 1-layer QDs solar cell.

Device	J_{sc} (mA/cm²)	V_{oc} (V)	FF (%)	PCE (%)
p-i-n without QD	16.4047	0.90884	83.9773	12.5158
QDs solar cell with 1-layer	34.1625	0.92856	84.2137	26.7046

Figure (4.4) shows the photo-generation rate with existence a single QD layer. It is noticed the increasing in the rate of photo-generation by ~5.7x10²¹ higher around the 1-layer of QDs.
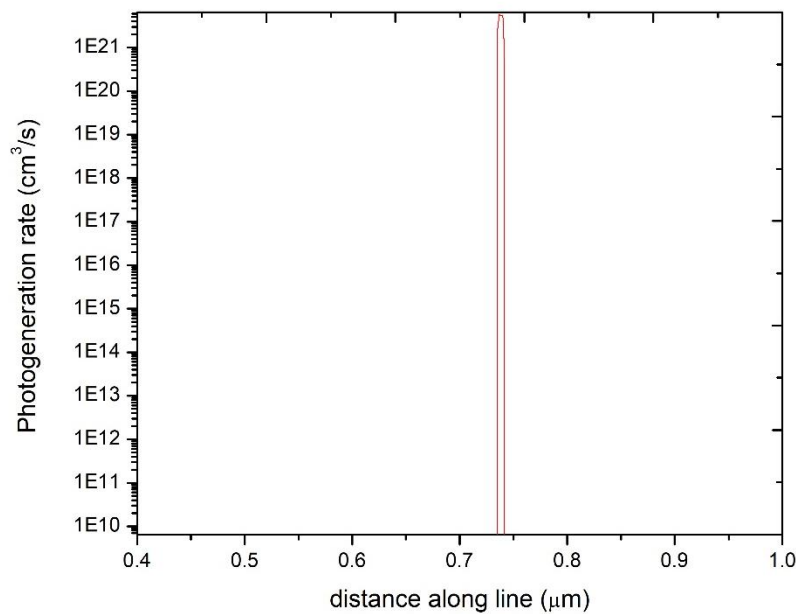
Figure (4.4) Photo-generation rate curve for QDs solar cell with 1-layer.

4.3.2 Adding 5-Layers of Quantum Dots:

To obtain the best insight into the impact of QDs layers on the solar cell performance, the layer's number of QDs was increased to 5-layers. The structure of InAs QDs with five QD layers is shown in Figure (4.5). The thickness of each layer is 5 nm and it is separated from the adjacent layer by

11 nm. The total thickness of the five layers with the space between them is 80 nm.
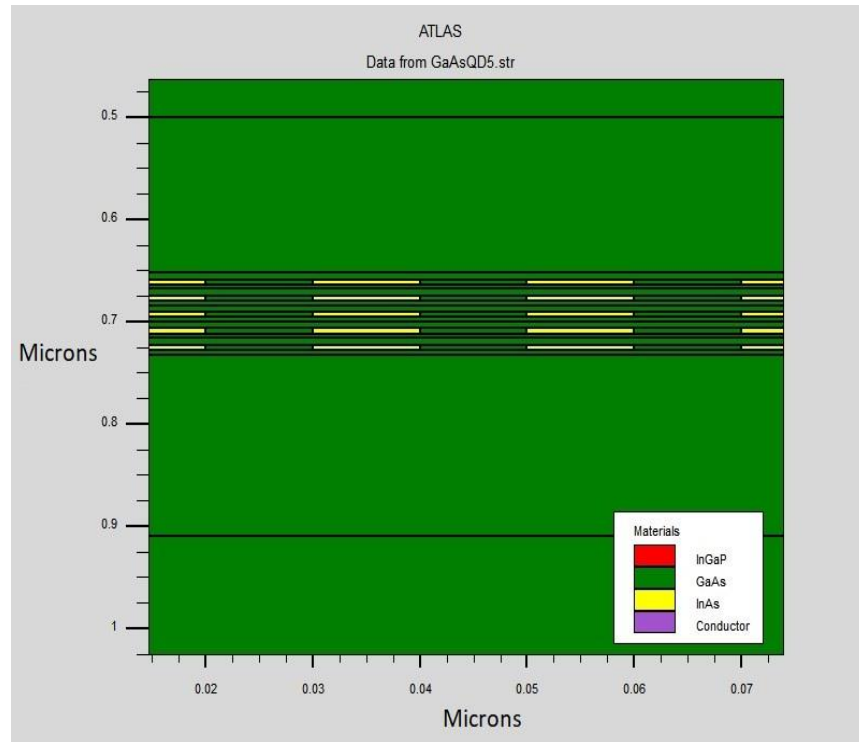
Figure (4.5) The structure of InAs/GaAs QDs solar cell with 5-layers.

Figure (4.6) shows the J-V characteristics of InAs/GaAs QDs solar cell with 5-layers in comparison with the standard GaAs p-i-n solar cell.
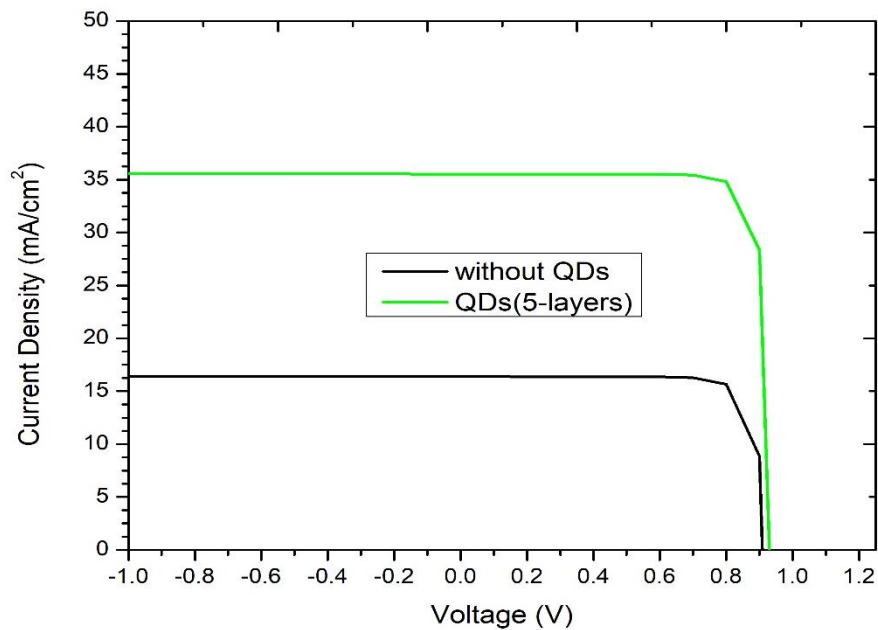
Figure (4.6) J-V characteristics of 5-layers QDs solar cell with standard solar cell.

From the J-V characteristics curves, it can be noticed that adding five QDs layers produces an enhancement in the performance of the solar cell. It can be seen that the J_{sc} increased by approximately 216% where the J_{sc} increased from **16.4047 mA/cm²** to **35.5917 mA/cm²**. Moreover, the value of **FF** rises from **83.9773%** to **84.15279%**. Similarly, in term of **PCE,** a noticeable enhancement in the SC efficiency has been obtained where it is increased from **12.5158%** to **27.8457%,** whereas V_{oc} value was kept almost constant. The increase in J_{sc} can be ascribed to the decrease in the effective bandgap of the solar cell [88]. Table 4.3 summarizes the simulation results for QDs solar cell with 5-layers.

Table 4.3 Simulation results of 5-layers QDs solar cell.

Device	J_{sc} (mA/cm²)	V_{oc} (V)	FF (%)	PCE (%)
p-i-n without QD	16.4047	0.90884	83.9773	12.5158
QDs solar cell with 5-layers	35.5917	0.93004	84.15279	27.84579

Figure (4.7) shows the photo-generation rate curve. It is noticed the increasing values of the photo-generation with increasing QDs layers to 5-layers at the solar cell.
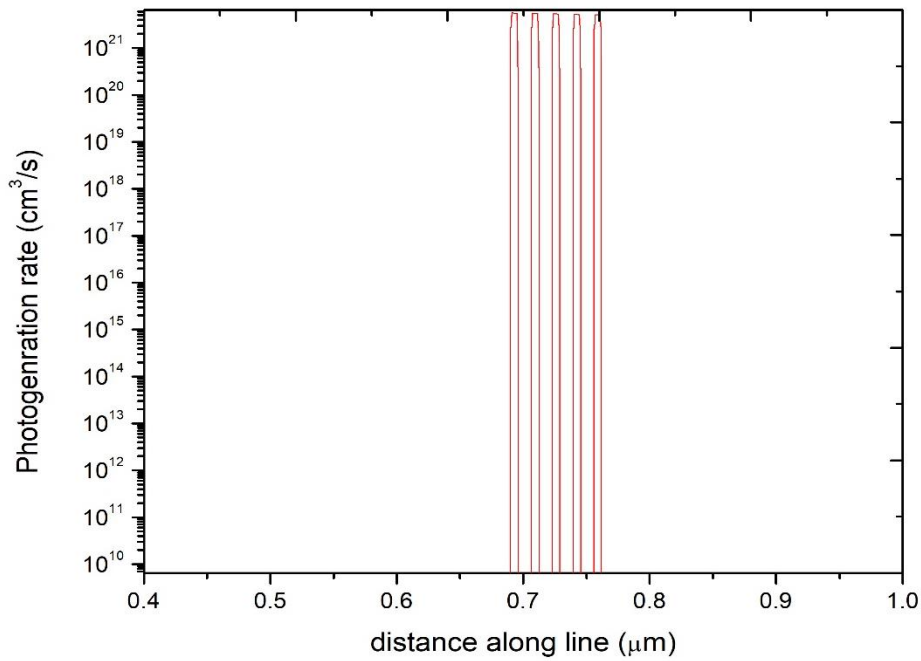
Figure (4.7) Photo-generation rate curve for QDs solar cell with 5-layers.

Although the range of photo-generation rate increased higher around the 5-layers of QDs same as the single layer but exist five layers give enhancement in the electron hole pair generation. One of the most interesting findings in Figure (4.7) is that the photo-generation rates at the five layers are not equal. The relatively small decrease in photo generation can be ascribed to the reduction in the number of low-energy photons due to its absorption in the earlier layer.

4.3.3 Adding 10-layers of Quantum Dots:

The number of QDs layers has been increased to 10-layers to reveal the extent of the improvement of the performance of the solar cell. The structure of InAs/GaAs QDs solar cell with 10-layers is seen in Figure (4.8). The total thickness of these layers is 160 nm and the layers are located at 120 nm distance in the upper side of insulator layer.
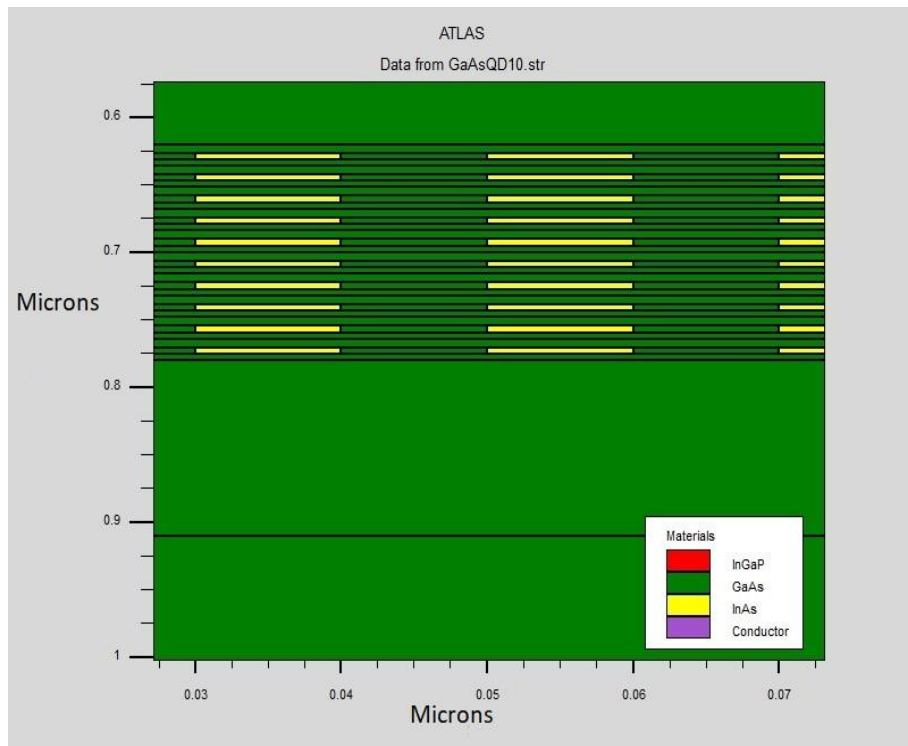
Figure (4.8) The structure of 10-layers QDs solar cell

J-V curve features of this structure is shown in Figure (4.9). From the curves, an increase in the performance of the solar cell after increasing the number of QDs layers can be noticed.
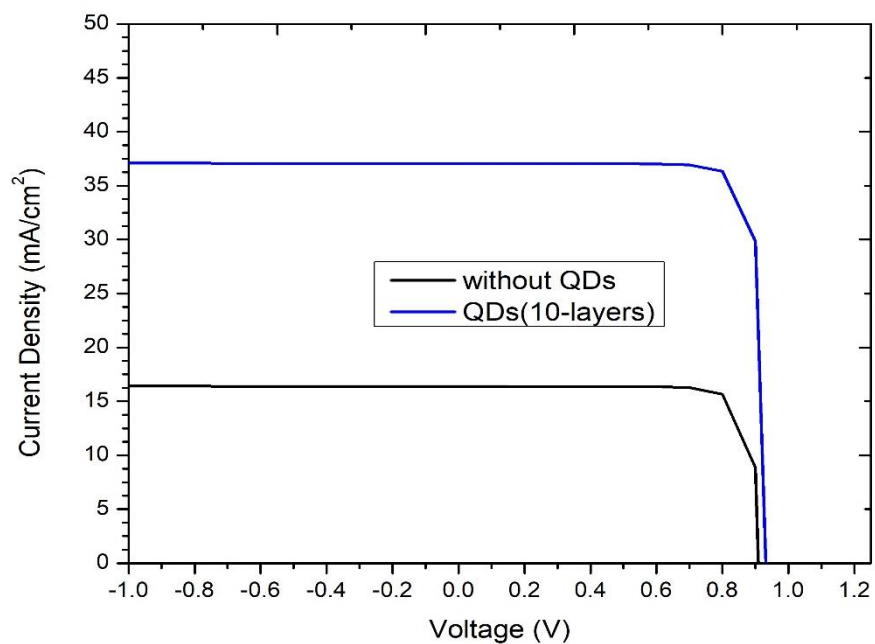
Figure (4.9) J-V characteristics of QDs solar cell with 10-layers and standard solar cell.

Noticeable improvement in the performance of the solar cell with increasing the number of QDs layers can be obtained. Impact of the 10-layers QDs on SC performance appears clearly on the main SC parameters, where the J_{sc} increases from **16.4047 mA/cm²** to **37.1026 mA/cm²**, the improvement is approximately 226%. Furthermore, **FF** raises from **83.9773%** to **84.07935%,** where the improvement ratio is about 1%. By contrast, the improvement is about 232% in term of **PCE,** where the result exceeds from **12.5158%** to **29.0493%.** Finally, in term of V_{oc}, there is a slight changing in its value from **0.90884 V** to **0.92856 V**. Table (4.4) displays the simulation results for InAs/GaAs QDs solar cell with 10-layers.

Table 4.4 Simulation results of QDs solar cell with 10-layers.

Device	J_{sc} (mA/cm²)	V_{oc} (v)	FF (%)	η (%)
p-i-n without QD	16.4047 (22.5309[*])	0.90884 (0.982732[*])	83.9773 (83.9786[*])	12.5158 (14.1289[*])
QDs solar cell with 10-layers	37.1026 (25.0959[*])	0.931544 (0.993139[*])	84.07935 (84.0565[*])	29.0493 (15.9187[*])

[*] The simulation results of standard GaAs p-i-n solar cell for Boqun Dong's research [14].

Figure (4.10) shows the rate of photo-generation curve. It is noticed increasing the range of photo-generation rate with increasing QDs layers to 10-layers at the solar cell which could be stand behind the noticeable enhancement in the SC performance. Similar to Figure (4.7), the photo-generation rates at the 10 layers are not equal. This confirm that the relative decrease in photo generation can be ascribed to the reduction in the number of low-energy photons due to its absorption in the earlier layer.
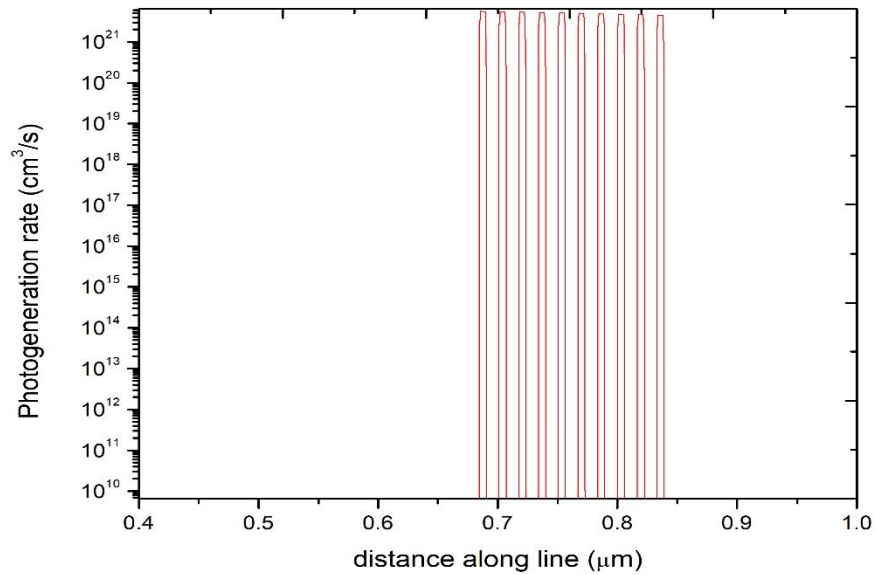
Figure (4.10) Photo-generation rate curve for QDs solar cell with 10-layers.

4.3.4 <u>Adding 15-layers of Quantum Dots:</u>

In order to characterize the impact of QDs layers on the solar cell performance in a more details a 15-layers of QDs is inserted to the i-region of the solar cell. Figure (4.11) shows the structure of QDs solar cell with 15-layers. It can be seen that the thickness of these layers is 240 nm. The J-V characteristics of this structure is shown in Figure (4.12), presenting a further improvement in the solar cell with increasing of QDs layers.
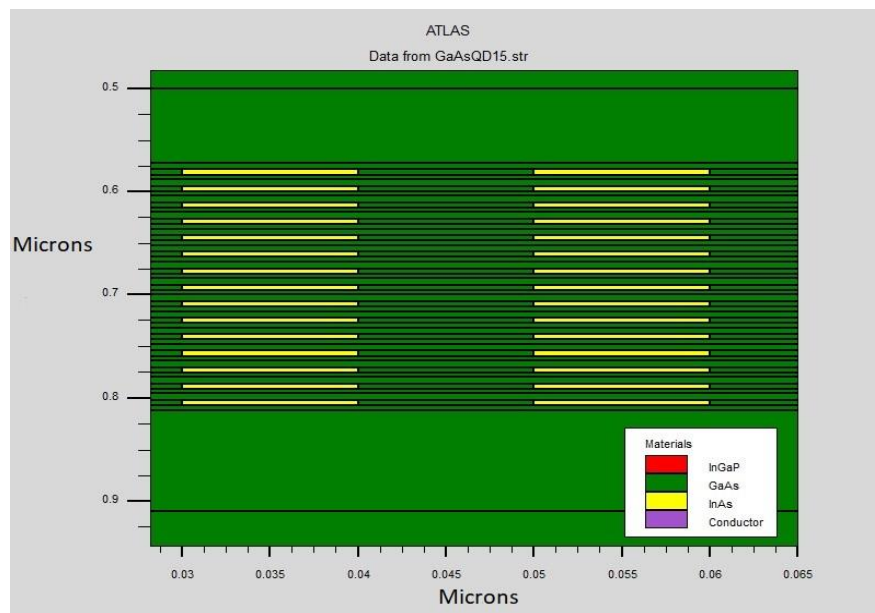
Figure (4.11) The structure of 15-layers QDs solar cell.
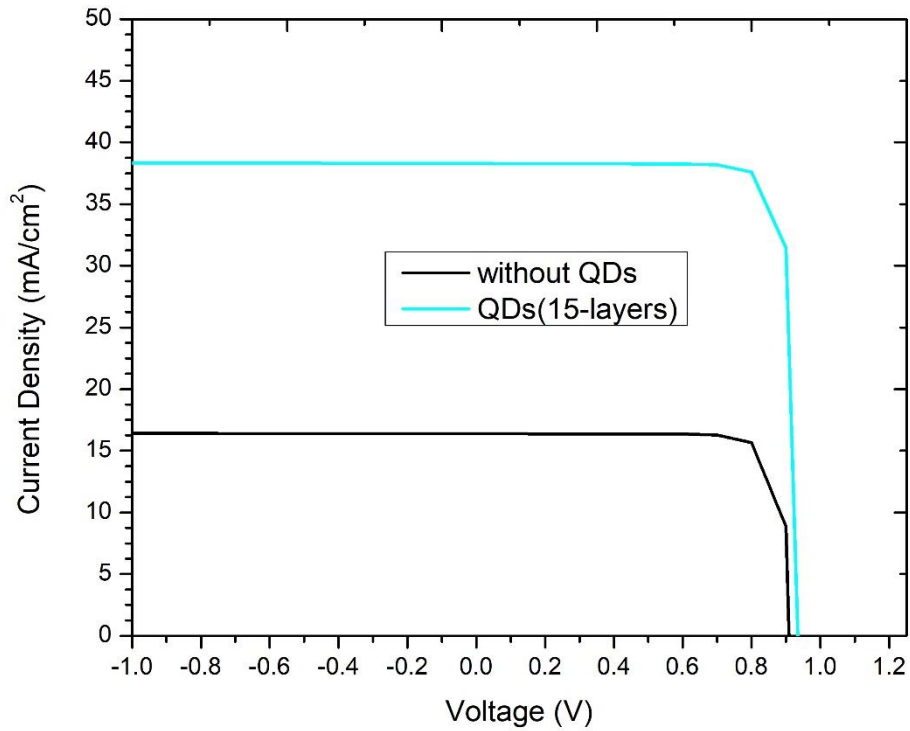
Figure (4.12) J-V characteristics of 15-layers QDs solar cell.

The improvements in the solar cell parameters are summarized in Table 4.6. By comparing the solar cell parameters after adding a 15 QDs layer with the case of solar cell without QDs layer it can be noticed that the J_{sc} increased from **16.4047 mA/cm²** to **38.3309 mA/cm²**, while a noticeable increase in the V_{oc} was obtained where its value increased from **0.90884 V** to **0.93456 V** whilst the FF value decreases slightly from **83.9773%** to **83.9353%.** As a result, the *PCE* raised from **12.5158%** to **30.0569%**.

Table 4.5 Simulation results of 15-layers QDs solar cell.

Device	J_{sc} (mA/cm²)	V_{oc} (V)	FF (%)	PCE (%)
p-i-n without QD	16.4047	0.90884	83.9773	12.5158
15-layers QDs solar cell	38.3309	0.93456	83.9353	30.0569

Figure (4.13) shows the rate of photo-generation with existence of 15 QDs layers. Similar to the previous cases the photo-generation range increases at each layer and since the number of layers increases these will cause an increase in the total photo-generation and hence an increase in the J_{sc}.

By comparing the results of 15 QDs layer with the previous case of 10 QDs layer it can be seen that the impact on increasing the QDs layers on the improvement in the SC efficiency becomes weak. This indicates that reaching saturation and adding more QD layers will not be useful. As a last stage and to confirm this assumption adding a 20 QDs layers will be investigated.
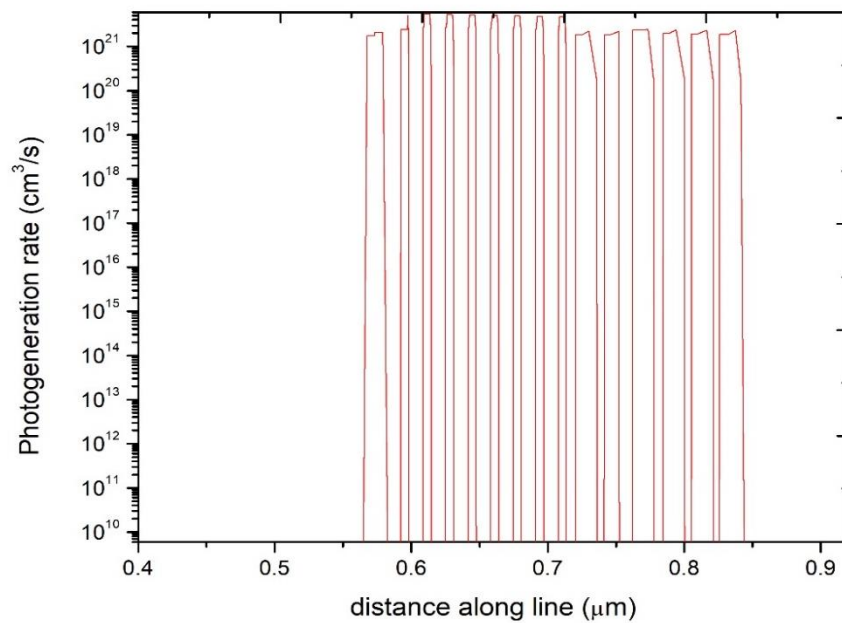
Figure (4.13) Photo-generation rate curve for QDs solar cell with 15-layers.

4.3.5 Adding 20-layers of Quantum Dots:

The number of InAs QDs layers increases to 20-layers at the i-region to find out the improvement extent for the solar cell performance. The thickness of these layers is 320 nm and the structure of QDs solar cell with 20-layers is shown in Figure (4.14).
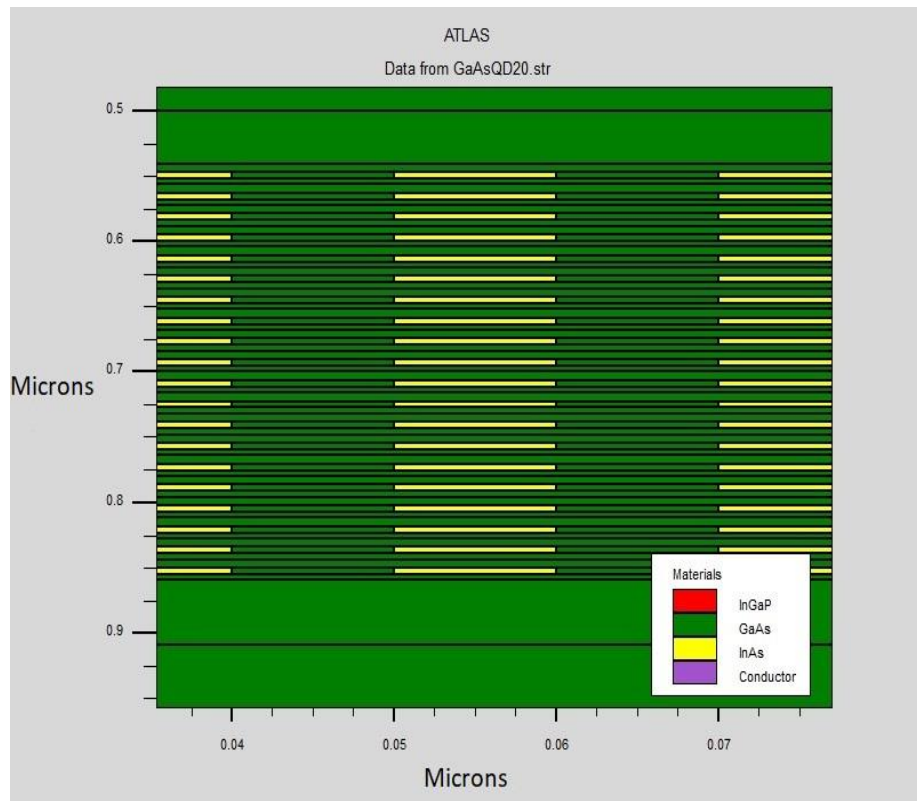
Figure (4.14) The structure of 20-layers QDs solar cell.

The features of the J-V curve of this structure are shown in Figure (4.15).
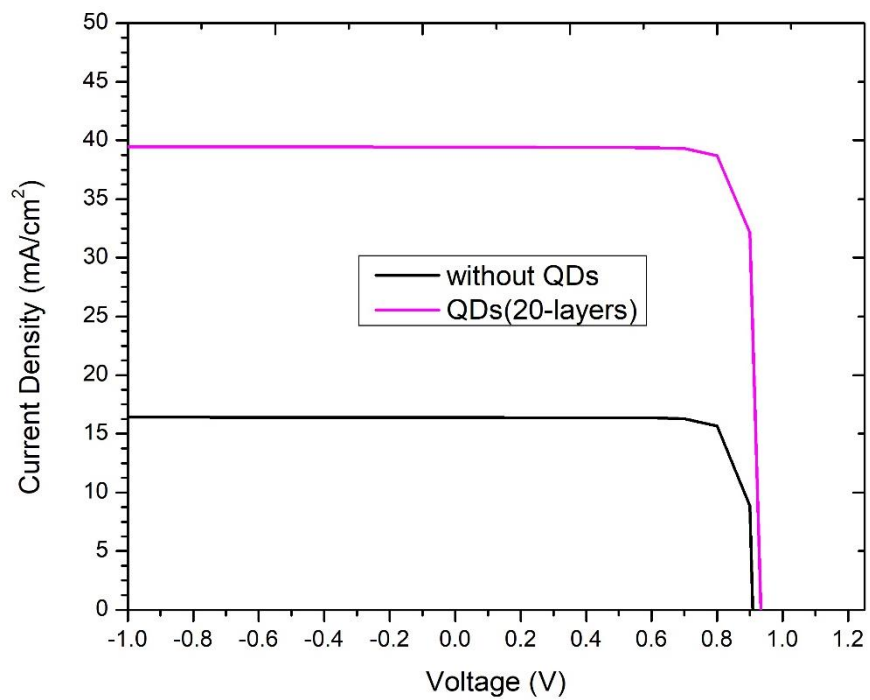
Figure (4.15) J-V characteristics of 20-layers QDs solar cell.

As it was mentioned in the last section that adding this number of layers is to inspect the role of adding more layer, thus the results of adding 20 QDs layer will compare with previous case (i.e., 15 QDs layer), The J_{sc} increases from **38.3309 mA/cm²** to **39.4775 mA/cm²**, while indescribable change in the V_{oc} was obtain where its values changed from **0.93456 V** to **0.9337 V**. The *FF* affect by adding more QDs layers is similar to the V_{oc} where it value changed from **83.9353%** to **83.97019%.** As a result of that the *PCE* was not much affected by adding more QDs layer where its value changed from **30.0569%** to **30.94025%**. The results of 20 QDs layers are compared with the those of Boqun Dong's study [14]. It has been noticed that the performance parameters of the solar cell are improved significantly after adding >10-layers of QDs, compared with Boqun Dong's study results at the same number of QDs layers, due to increasing the number of QDs layers to 20-layers which increases the wavelength absorption rate. Table 4.7 summarizes the simulation results of the current work.

Table 4.6 Simulation results of QDs solar cell with 20-layers.

Device	J_{sc} (mA/cm²)	V_{oc} (V)	FF (%)	PCE (%)
p-i-n without QD	16.4047 (22.5309)[*]	0.90884 (0.92856)[*]	83.9773 (83.9786)[*]	12.5158 (14.1289)[*]
20-layers QDs solar cell	39.4775 (26.9626)[*]	0.9337 (0.996407)[*]	83.97019 (83.7614)[*]	30.94025 (17.0988)[*]

[*] The simulation results of standard GaAs p-i-n solar cell for Boqun Dong's research [14].

Figure (4.16) shows the rate of photo-generation curves. Increasing the range of photo-generation rate has been noticed with increasing QDs layers to 20-layers at the solar cell.
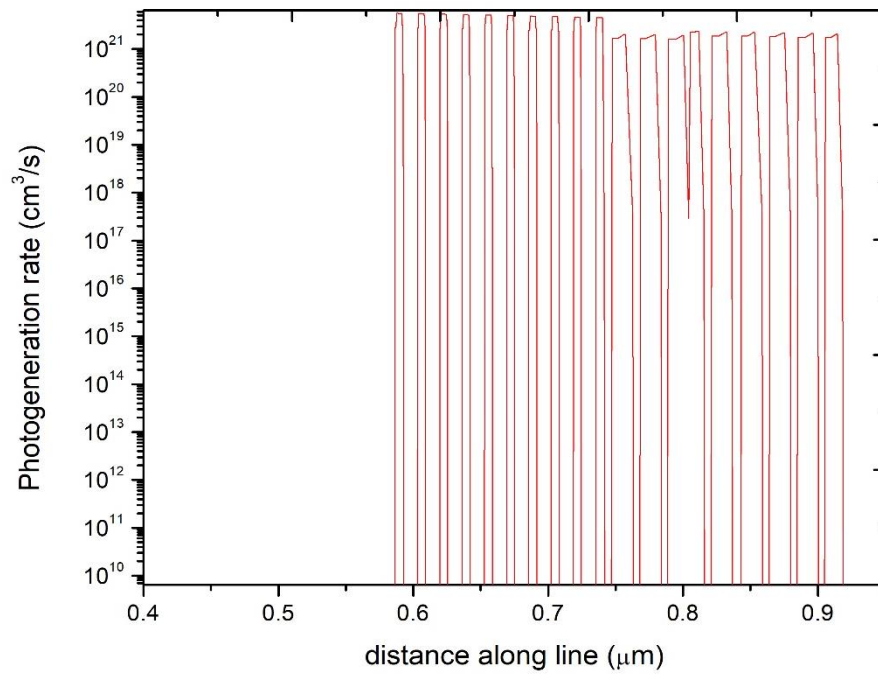
Figure (4.16) Photo-generation rate curve for QDs solar cell with 20-layers.

Figure (4.17) shows the comparison between the photo-generation rate for each case, where the photo-generation rate for standard p-i-n solar cell is along the i-region and at the same level. After inserting QDs layers, the photo-generation has become confined at QDs layers
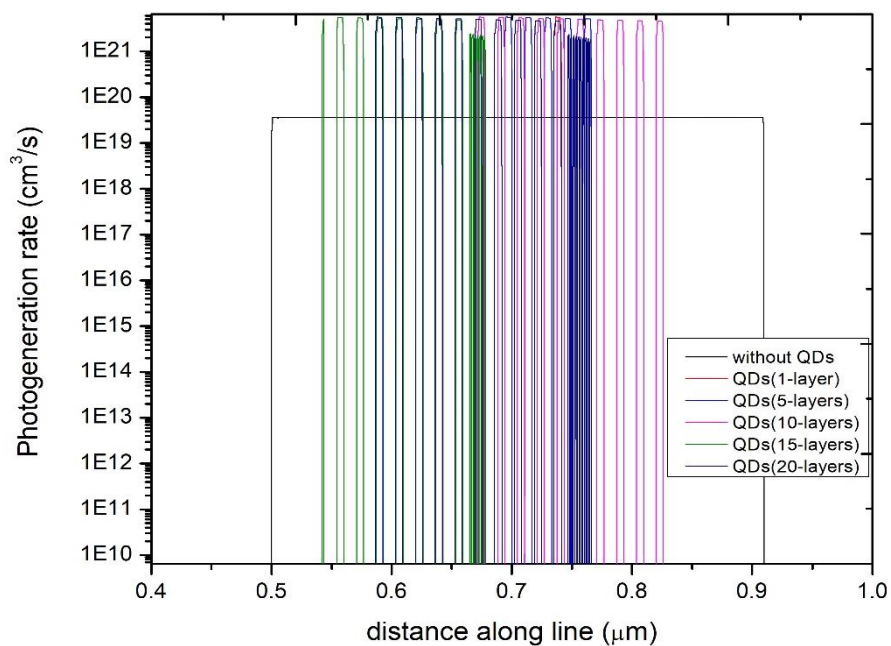
Figure (4.17) Photo-generation rate curves for standard solar cell and for QDs solar cell with different no. of layers.

The photo-generation process is followed by the recombination process. The basic condition to ensure that the solar cell works correctly is that the photo-generation rate must be greater than the recombination rate. Figure (4.18) shows the recombination rate for standard p-i-n solar cell and QDs solar cell with different number layers.
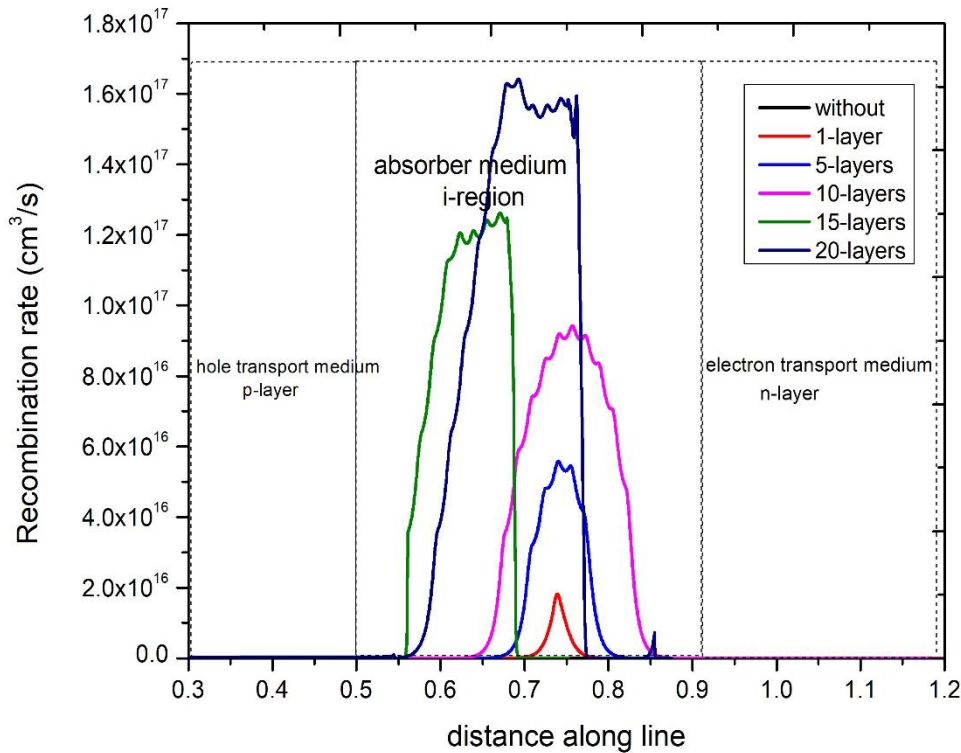
Figure (4.18) Recombination rate curves for standard solar cell and for QDs solar cell with different no. of layers.

As seen in Figure (4.18), the recombination rate for standard solar cell is low where its value reaches 0.95×10^{15} comparing to the recombination rate for quantum dot solar cell with 1-layer, its value is 1.65×10^{16}. For 20-layers quantum dot solar cell the recombination rate is 1.64×10^{17}.

4.4 Effect of Number of Quantum Dots Layers:

Through the previous sections, it has been noticed that the performance of the solar cell differs from each case to the other. For standard solar cell, the performance parameters are low, because of the absorption of a certain range of wavelengths. After inserting 1-layer of InAs QDs inside

the i-region, the improvement in the performance of this solar cell occurs through its parameters, whereas this layer helps to increase the absorption of more incident photons. In other words, it expands the range of absorbed wavelengths. After that, the number of layers is increased to 5-layers up to 20-layers. With each case, there is an improvement in the performance of solar cell. The light harvesting efficiency can be extended beyond the host material's energy bandgap limit thanks to the restricted states of QDs embedded in the intrinsic region of p-i-n structures [89]. The acquired J-V features for different conditions are shown in Figure (4.19). With increasing the QDs layers number, J_{sc} and **PCE** increase while *FF* increases slightly. V_{oc} almost keeps the same level.
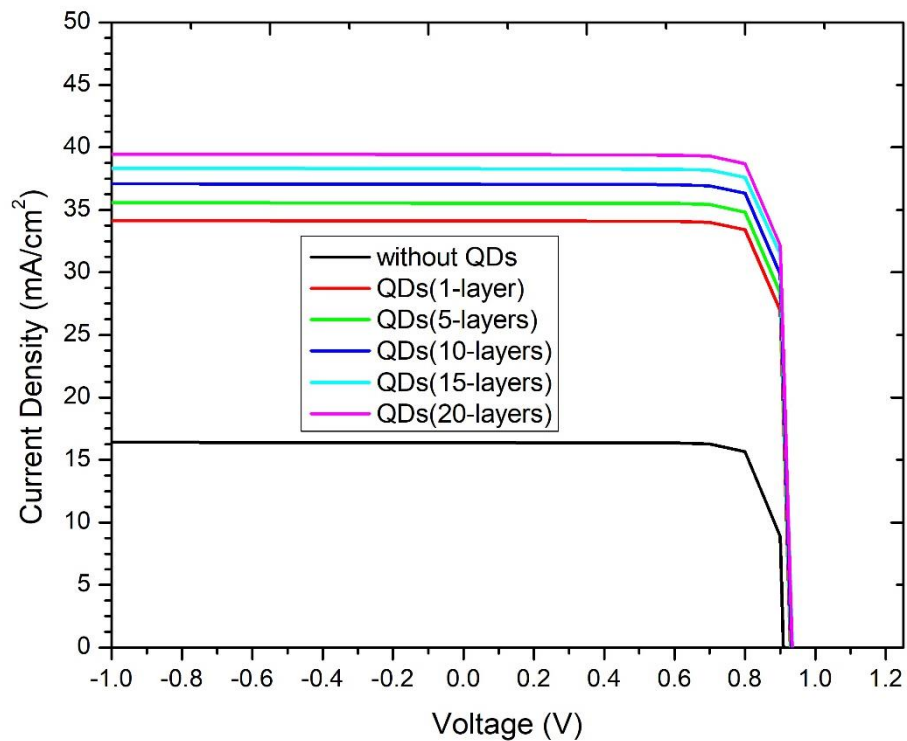
Figure (4.19) J-V characteristics for standard solar cell and for QDs solar cell with different number of layers.

These findings are aligned with the majority of numerical studies [14][90]. The device's absorption is increased with the addition of more QDs layers, which accounts for the improvement's significance, especially in the current density [90]. The associated outputs are seen in Table 4.7.

Table 4.7 The simulation results of standard solar cell and multi-layers of quantum dots solar cell.

Device	p-i-n without QD	1-layer QD	5-layers QD	10-layers QD	15-layers QD	20-layers QD
J_{sc} (mA/cm^2)	16.4047	34.1625	35.5917	37.1026	38.3309	39.4775
V_{oc} (Volts)	0.90884	0.92856	0.93004	0.931544	0.93456	0.9337
FF (%)	83.9773	84.2137	84.1527	84.07935	83.9353	83.9701
Efficiency (%)	12.5158	26.7046	27.8457	29.0493	30.0569	30.9402

Figure (4.20) illustrates the effect obtained on performance parameters before and after inserting QDs layers. The best result obtained when 20-layers of QDs is inserted. It is clear that J_{sc} increases when QDs layers are introduced inside the i-region of the p-i-n solar cell due to the additional pairs electron-hole photo-generated. V_{oc} slightly increases with the addition of QDs in accordance with the reference cell without QDs. As for **PCE** and according to Table 4.8, it can be seen a rise in efficiency with increasing number of QDs. **FF** is almost constant with inserting different numbers of QDs layers.
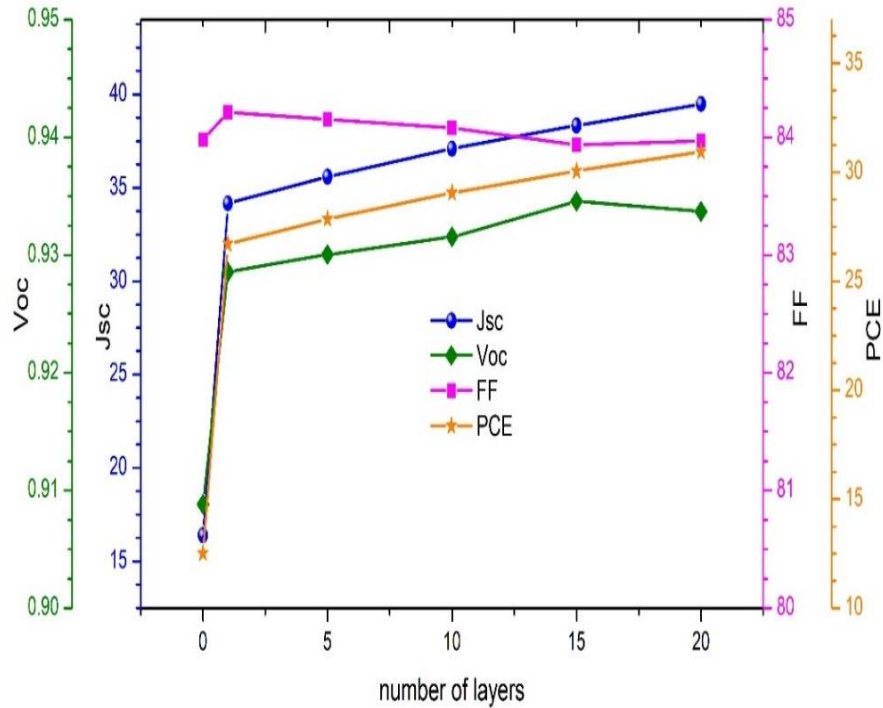
Figure (4.20) The Effect of increasing the no. of QDs layers on J_{sc}, V_{oc}, PCE and FF.

4.5 Power Curve:

Obtaining the electrical power is one of the most functions of solar cell. In this study, it has been calculated at all cases to find out the effect of adding QDs layers at the power. Figure (4.21) shows the electrical power of standard p-i-n solar cell and multi-layers (up to 20-layers) QDs solar cell. It can be seen that standard solar cell provides an electrical power of **12.52x10^{-12} W/cm^2**. As starting to insert the first layer of QDs in the i-region, the electrical power increases to **26.715x10^{-12} W/cm^2**. It continuously increases until it reaches **30.952x10^{-12} W/cm^2** at 20-layers of QDs solar cell.
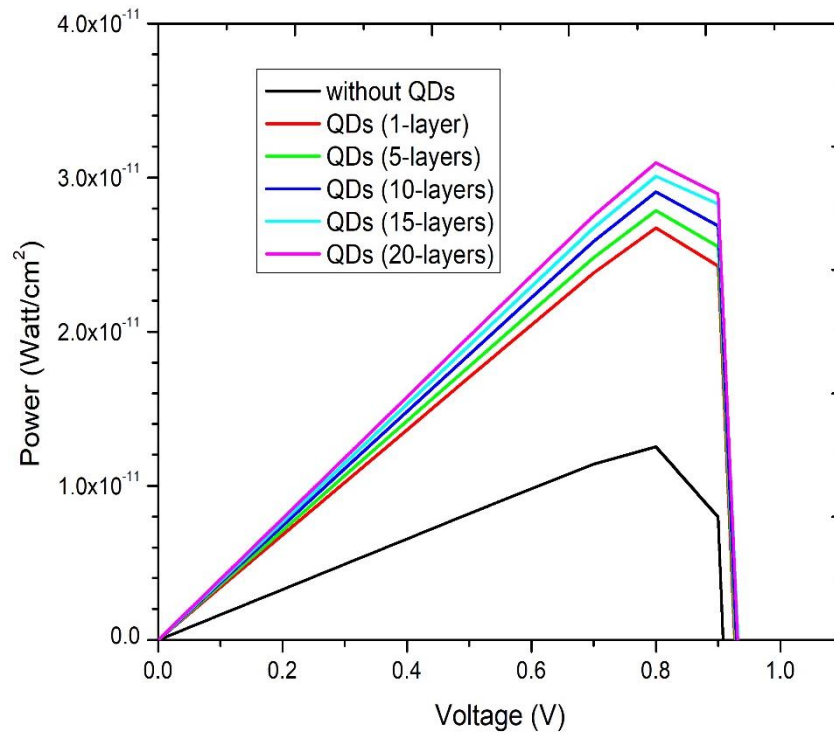
Figure (4.21) power curve for standard solar cell and multi-layers of QDs solar cell.

4.6 Spectral Response:

The most significant effect of quantum dots, as discussed in Chapter 2, is to assist solar cells in absorbing those photons with lower energy, which also means long wavelengths. A normal GaAs solar cell typically has a maximum photon absorption wavelength which is about 850 nm [78]. The use of quantum dots allows for the absorption of photons with a wavelength of between 300 nm and 900 nm.
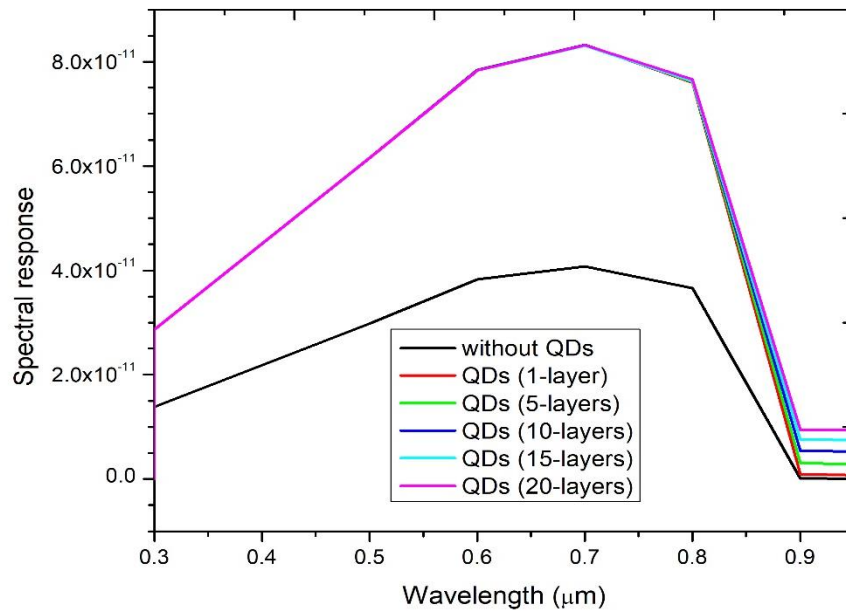
Figure (4.22) The spectral response of standard solar cell and multi-layers of QDs solar cell.

Figure (4.22) demonstrates that the conventional p-i-n solar cell's spectral response actually reaches zero at wavelengths around 900 nm., regarding the solar cells that contain 1, 5, 10, 15, and 20-layers of quantum dots. As shown in Figure (4.22), it can be noticed that the response of standard solar cell is low compared to the response of the solar cell in the presence of QDs layers. In addition, the response of the solar cell when inserting 1-layer up to 20-layers is the same in all cases. The solar cell has successfully absorbed photons in this wavelength range, resulting in the generation of photocurrent.

4.7 The Effect of Temperature on the Performance of Quantum Dots Solar Cell

Increasing the temperature of the solar cell negatively effects on its performance [91], and thus the productive power and the efficiency decrease. The majority of the characteristics of the semiconductor material are impacted by temperature increases because they cause the semiconductor band-gap to decrease [92]. The rising energy of the electrons in the material

can be the reason for the decrease in the semiconductor band-gap with temperature increase. Because of this, less energy is needed to break the link. Semi-empirical model proposed by Varshni can be used to characterize the temperature-dependent bandgap in semiconductors [93].

$$E_g(T) = E_g(0) - \frac{\alpha - T^2}{(\beta - T)} \qquad (4-1)$$

Where $E_g(0)$ is a bandgap value at T=0 K, α and β are constant values, which are unique for each material. The electron-phonon interaction and, to a lesser extent, the thermal expansion of the lattice with temperature are attributed to the temperature dependence of bandgap [93]. In the current work, the temperature is gradually increased (by steps of 10 degrees).

- **The Temperature effect on the performance of standard solar cell:**

For standard GaAs p-i-n solar cell, the temperature is increased from 310 K up to 360 K. Figure (4.23) shows the relation between the performance parameters of the solar cell and the temperature, where the solid line represents J_{sc} curve, the dash line is for V_{oc} curve, the dash dot line is for *FF* and *PCE* curve is represented by short dash line.
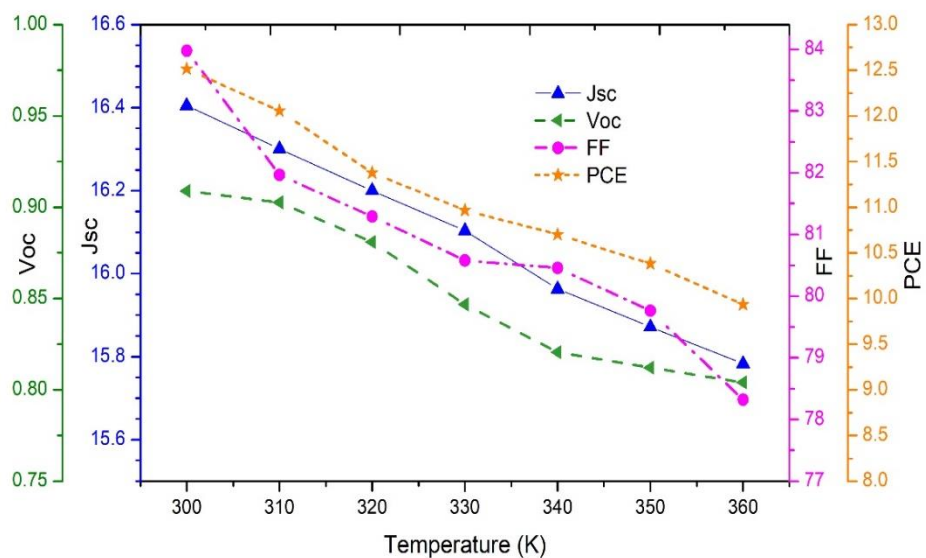
Figure (4.23) The performance parameters curves for standard GaAs solar cell.

It can be seen that J_{sc} is decreased from *16.4047 mA/cm²* at T=300 K to *15.7832 mA/cm²* at T=360 K. V_{oc} is decreased gradually with increasing the temperature from *0.90884 V* to *0.80396 V*. In term of **FF**, its value starts decreasing from *83.9773%* to *78.3218%*. As for **PCE**, it decreases with increasing temperature from *12.5158%* to *9.9347%*. It can be said that increasing the temperature of the standard solar cell negatively affects its performance as it reduces the bandgap and thus affects the coefficients of the material.

- **The Temperature effect on the performance of Quantum Dots solar cell with 1-layer**

The temperature is regularly increased, starting from 300 K up to 360 K to reveal the effect of high temperature on the performance of the quantum dots solar cell. Figure (4.24) depicts the performance parameters that are affected by increasing the temperature.
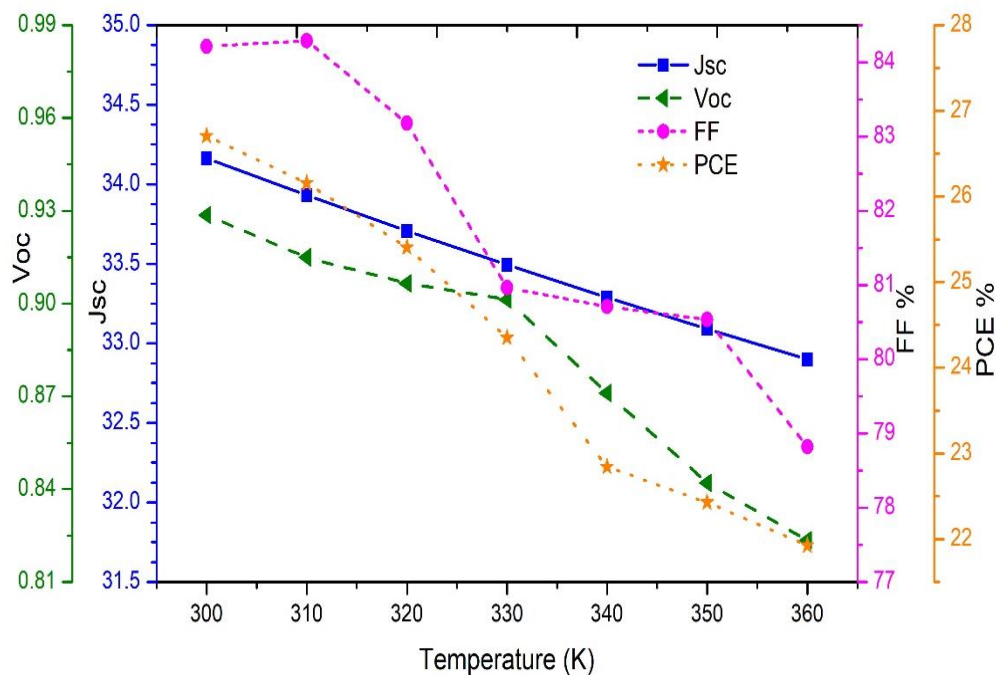
Figure (4.24) The performance parameters curves for quantum dots solar cell with 1-layer.

For QDs solar cell with 1-layer, J_{sc} is decreased from *34.1625 mA/cm²* to *32.8996 mA/cm²* with increasing the temperature. V_{oc} is decreased as increasing temperature from *0.92856 V* to *0.82353 V*. Likewise, *PCE* decreases while increasing temperature from *26.7046%* to *21.9282%*. As for *FF*, it slightly increases from *84.2137%* to *84.2888%* with increasing the temperature to 310 K, after that it starts being decreased with increasing the temperature to *78.822%* at T=360 K.

- **The Temperature effect on the performance of Quantum Dots solar cell with 10-layers**

The temperature is regularly increased to reveal the effect of high temperature on the performance of the quantum dots solar cell with 10-layers. Figure (4.25) presents the performance parameters that are affected by increasing the temperature.
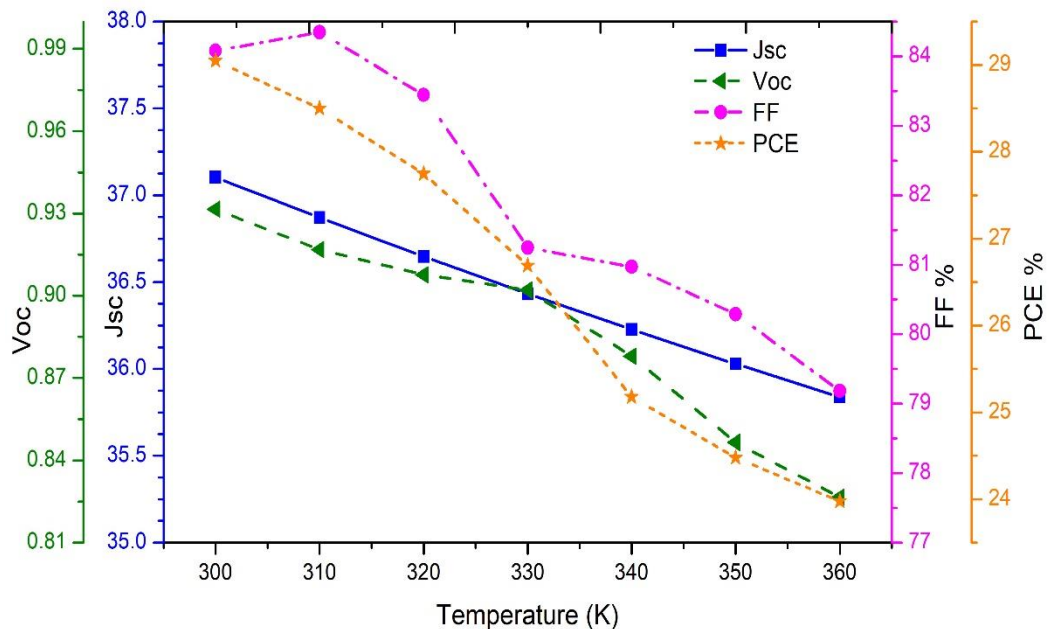
Figure (4.25) The performance parameters curves for quantum dots solar cell with 10-layer.

For QDs solar cell with 10-layer, J_{sc} is decreased with increasing the temperature from ***37.1026 mA/cm²*** to ***35.838 mA/cm²***. V_{oc} is decreased by increasing temperature from ***0.93154 V*** to ***0.82654 V***. Likewise, ***PCE*** decreases with increasing temperature from ***29.0493%*** to ***23.9762%***. As for ***FF***, it increases from ***84.0793%*** to ***84.3437%*** with increasing the temperature to 310 K, and then it starts to be decreased with increasing the temperature to ***79.18416%***.

- **The Temperature effect on the performance of Quantum Dots solar cell with 20-layers**

The temperature is increased gradually, starting from 310 K up to 360 K to show the effect of high temperature on the performance of the quantum dots solar cell with 20-layers. Figure (4.26) illustrates the performance parameters that are affected by increasing the temperature.
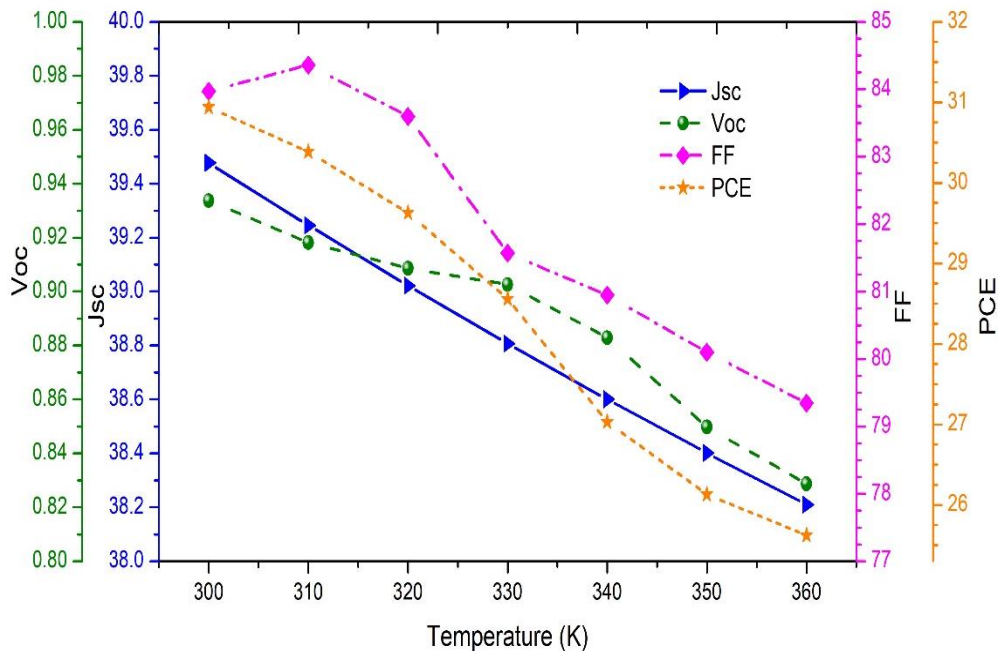
Figure (4.26) The performance parameters curves for quantum dots solar cell with 20-layer.

For QDs solar cell with 20-layers, J_{sc} decreases with increasing the temperature from **39.4775 mA/cm²** to **38.2097 mA/cm²**. V_{oc} is decreased by increasing temperature from **0.933705 V** to **0.82869 V**. In the same vein, **PCE** decreases with increasing temperature from **30.9402%** to **25.6224%**. As for **FF**, it increases at T=310 from **83.97019%** to **84.36107%** and then decreases with increasing the temperature to **79.3442%** at T=360 K. Table 4.9 shows the performance parameters values in each case (standard p-i-n solar cell, QDs solar cell with (1,10 and 20) layers) with increasing the temperature.

Table 4.8 The performance parameters at different temperature for standard solar cell and multi layers of QDs solar cell.

Temp.	Performance parameters	No. of layers			
		0	**1**	**10**	**20**
300	J_{sc}	16.4047	34.1625	37.1026	39.4775
	V_{oc}	0.90884	0.92856	0.93154	0.933705
	FF	83.9773	84.2137	84.0793	83.97019
	PCE	12.5158	26.7046	29.0493	30.9402
310	J_{sc}	16.3006	33.9302	36.8704	39.2451
	V_{oc}	0.902558	0.91489	0.91677	0.918136
	FF	81.9643	84.2888	84.3437	84.36107
	PCE	12.054	26.1557	28.499	30.386
320	J_{sc}	16.2001	33.7071	36.6471	39.0214
	V_{oc}	0.88084	0.90651	0.90771	0.908586
	FF	81.28817	83.1785	83.444	83.59804
	PCE	11.377	25.4064	27.7474	29.62813

Temp.	Performance parameters	No. of layers			
		0	**1**	**10**	**20**
330	J_{sc}	16.1033	33.4929	36.4327	38.8064
	V_{oc}	0.84676	0.90124	0.902029	0.90259
	FF	80.5771	80.96423	81.2458	81.57136
	PCE	10.96664	24.3532	26.6902	28.5609
340	J_{sc}	15.9632	33.2872	36.2266	38.5998
	V_{oc}	0.82056	0.871037	0.87798	0.88294
	FF	80.4559	80.7087	80.97717	80.94888
	PCE	10.702	22.8455	25.17638	27.03179
350	J_{sc}	15.8713	33.0896	36.0285	38.401
	V_{oc}	0.81212	0.842002	0.84654	0.849802
	FF	79.7605	80.5317	80.2892	80.101132
	PCE	10.382	22.4291	24.479	26.12993
360	J_{sc}	15.7832	32.8996	35.838	38.2097
	V_{oc}	0.80396	0.82353	0.82654	0.82869
	FF	78.3218	78.822	79.18416	79.3442
	PCE	9.9347	21.9282	23.9762	25.6224

Through Table 4.8, when comparing the effect of increasing temperature at PCE with increasing the number of QDs layers, it is noticed that PCE is decreased with increasing the temperature and it is noticeable when the number of QDs layers increases. Figures (4.27), (4.28) and (4.29) explains the relation between the layer's number of QDs versus (PCE, J_{sc} and V_{oc}) for different T.
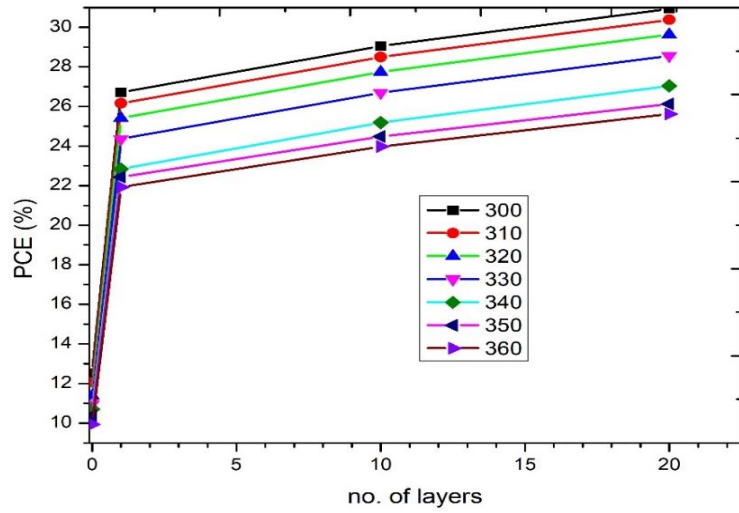
Figure (4.27) The no. of QDs layers versus PCE for different T.
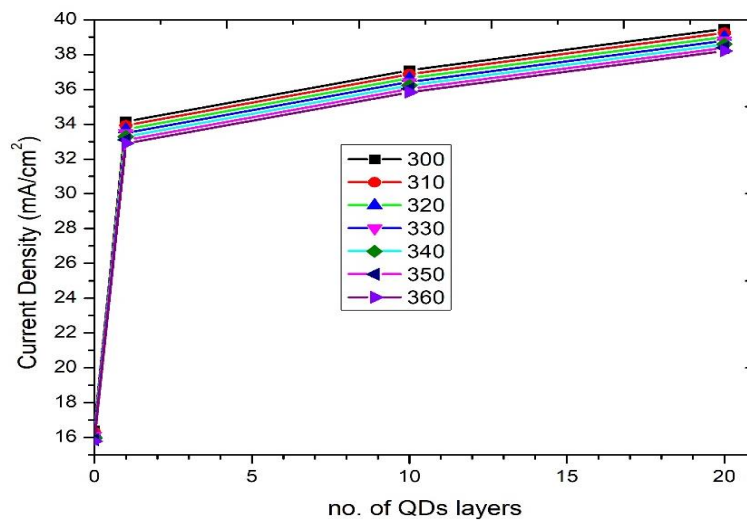
Figure (4.28) The no. of QDs layers versus J_{sc} for different T.
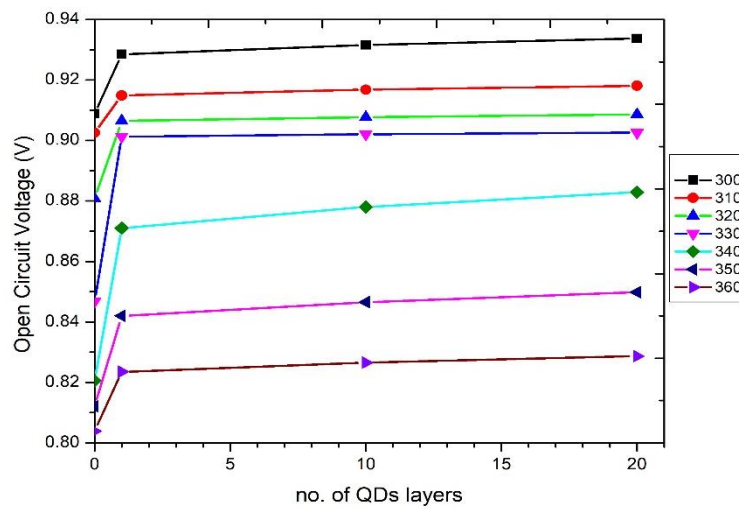
Figure (4.29) The no. of QDs layers versus V_{oc} for different T.
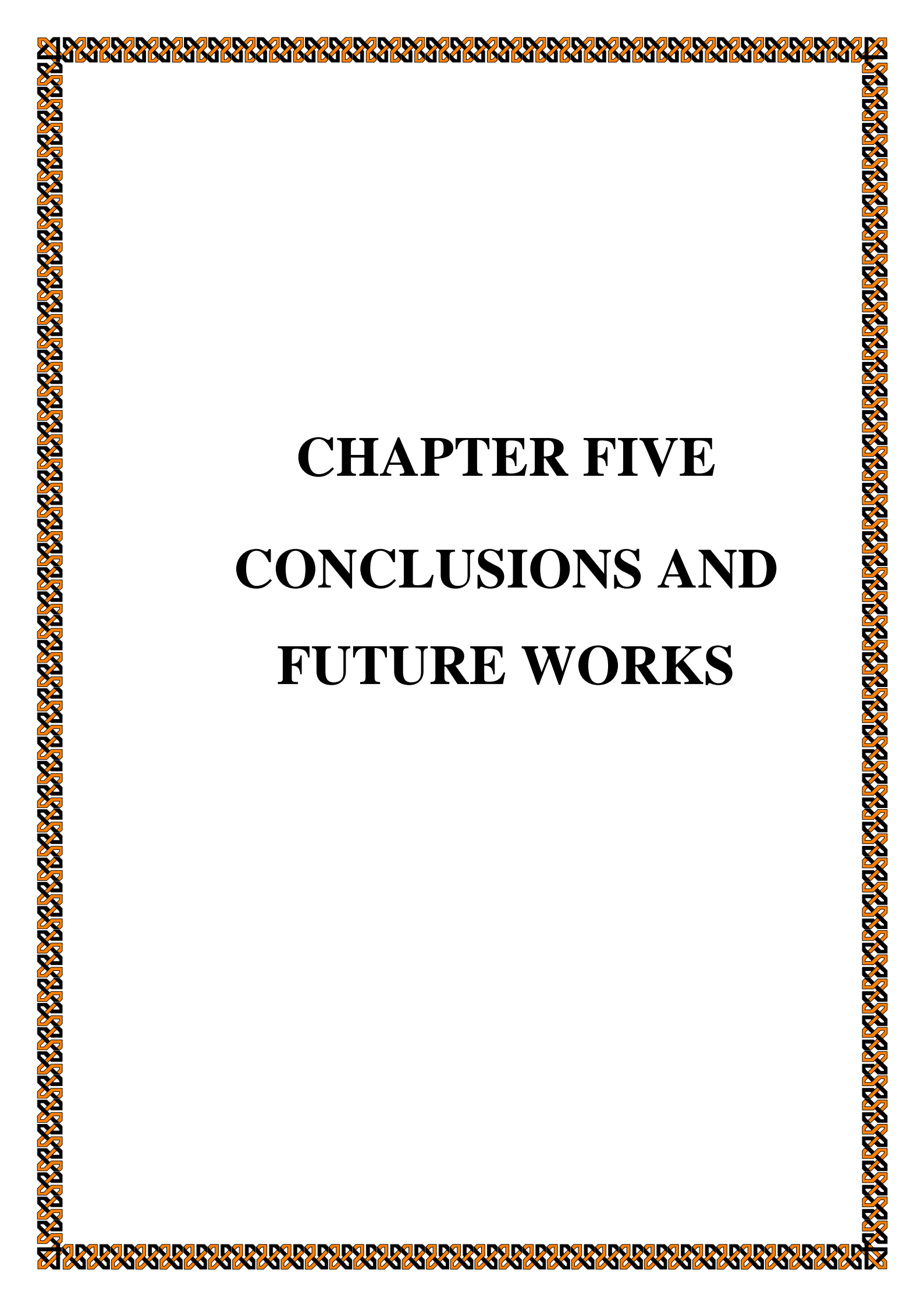
CHAPTER FIVE

CONCLUSIONS AND FUTURE WORKS

CHAPTER FIVE

CONCLUSIONS AND FUTURE WORKS

5.1 Conclusions:

The use of simulation software will facilitate a more thorough understanding of the fundamental ideas behind the operation of solar cells. Solar cells involve of several generations and each generation has its types. This study concentrated on the quantum dots solar cells.

Due to the simulation models' flexibility, this research added several factors for improving the performance of quantum dots solar cells gadgets before they are manufactured, which will save cost, time, and effort. Accordingly, SILVACO ATLAS software was employed to achieve the aforementioned factors.

The outcomes showed that the major factor in improving the performance of the solar cells is the insertion of QDs layers into the absorber layer. The results of the study revealed that:

1. It was analyzed the performance parameters of the proposed structure for standard p-i-n solar cell to investigate the impact of adding the quantum dots layers to the i-region layer. The results of the standard solar cell were compared with similar structure achieved by others for validation.

2. The performance parameters of the solar cell were improved by adding quantum dots layers into the i-region. The examining of adding quantum dots layers was achieved with a fixed thickness of the i-region at 410 nm.

3. It was noticed the improvement at the performance parameters due to increase of photo-generation of charge carriers. A noticeable

enhancement in the PCE was obtained where it is increased from 12.5158% to 26.7046%.

4. Increasing the number of quantum dots layers (5,10,15 and 20) produce a further improvement in the performance parameters of the solar cell because of adding more QD's layer led to increase in the photo-generation rate due to increase the absorption of incident photons.

5. It was obtained that the impact of adding the QD's layers on the SC performance appears slightly with layers' number higher than 10 layer and this could be ascribed to the saturation in the photon absorption by the quantum dot effect.

6. The impact of increasing the temperature at the performance parameters for standard p-i-n solar cell and for the solar cell with quantum dots layers was investigated. The range of temperature under study was increased from 300 K to 360 K. It was found that for standard solar cell the performance parameters decreased with increasing the temperature more than for quantum dots solar cell.

7. The power conversion efficiency was compared by adding quantum dots layers to the solar cell with increasing the temperature.

5.2 <u>Suggestions for Future Works:</u>

1. Studying the impact of different sizes of quantum dots on the performance of the solar cell.

2. Studying the influence of QD's distribution on the SC performance.

3. Studying the effect of defects with existence the QDs on the cell performance.
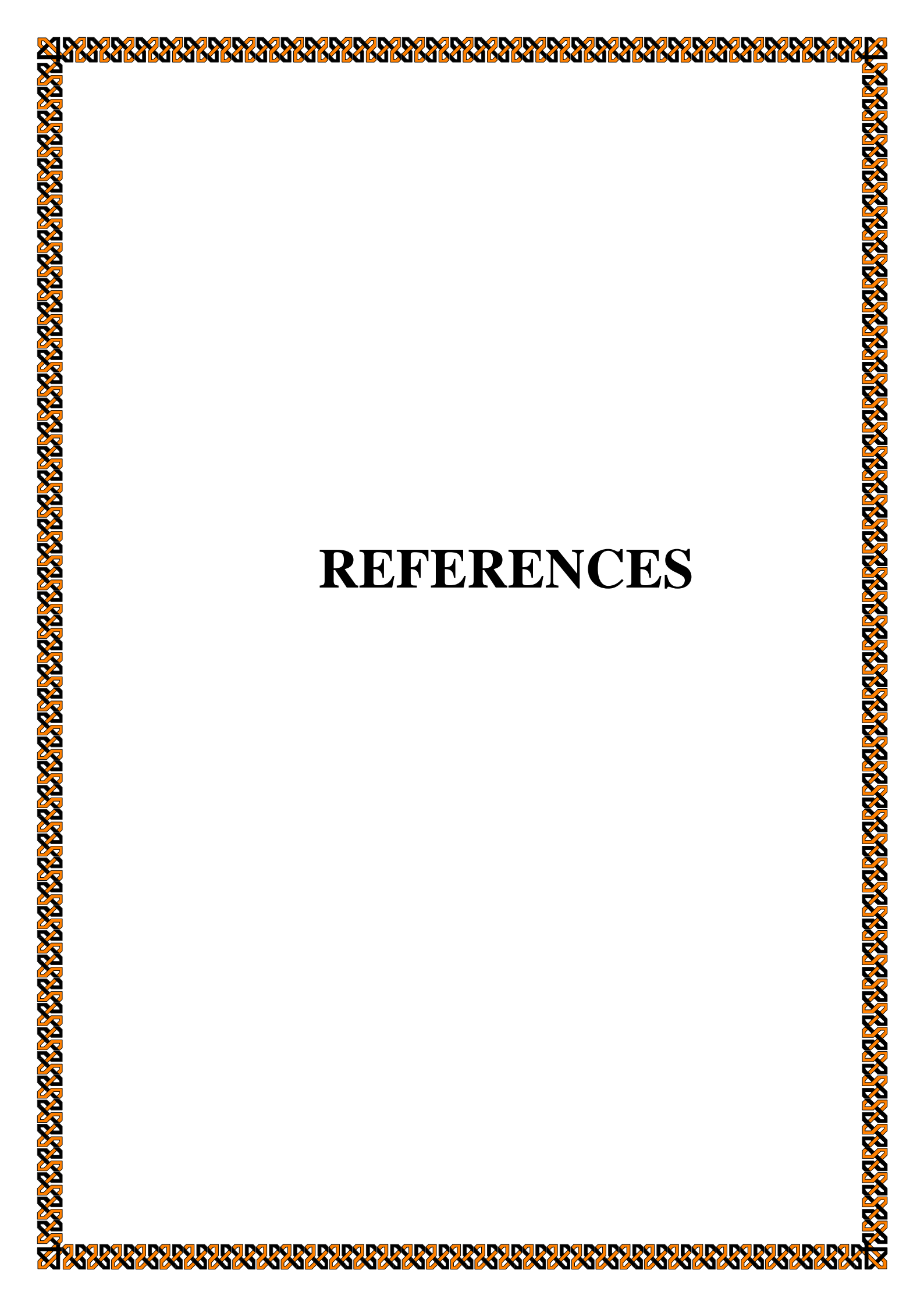
REFERENCES

REFERENCES

[1] A. Khatibi, F. Razi Astaraei, and M. H. Ahmadi, "Generation and combination of the solar cells: A current model review," *Energy Sci. Eng.*, vol. 7, no. 2, pp. 305–322, 2019, doi: 10.1002/ese3.292.

[2] T. K. Manna and S. M. Mahajan, "Nanotechnology in the development of photovoltaic cells," *2007 Int. Conf. Clean Electr. Power, ICCEP '07*, pp. 379–386, 2007, doi: 10.1109/ICCEP.2007.384240.

[3] K. A, T. K, S. Y, and M. T, "Organometal halide perovskites as visible-light sensitizers for photovoltaic cells," *J. Am. Chem. Soc.*, vol. 131, no. 17, pp. 6050–6051, 2009.

[4] Harvey Serreze, "Optimizing SC performance by simultaneous consideration of grid pattern design and interconnect configuration," in *Conference Record of the IEEE Photovoltaic Specialists Conference*, 1978.

[5] A. Rothwarf and K. W. Böer, "Direct conversion of solar energy through photovoltaic cells," *Prog. Solid State Chem.*, vol. 10, no. PART 2, pp. 71–102, 1975, doi: 10.1016/0079-6786(75)90007-2.

[6] M. Z. Jacobson and M. A. Delucchi, "A path to: Sustainable energy by 2030," *Sci. Am.*, vol. 301, no. 5, pp. 58–65, 2009, doi: 10.1038/scientificamerican1109-58.

[7] Y. Tsuo, J. Gee, P. Menna, and D. Strebkov, "Environmentally benign silicon solar cell manufacturing," *Photovolt. Sol. Energy Convers.*, no. July, pp. 1–7, 1998, [Online]. Available: http://www.nrel.gov/docs/legosti/FY98/23902.pdf

[8] S. V. N. and A. S. N. K. Govardhan Reddy, T. G. Deepak, G. S. Anjusree, b Sara Thomas, Sajini Vadukumpully, K. R. V.

Subramanian, "On Global Energy Scenario, Dye-sensitized Solar Cells and the Promise of Nanotechnology," *Phys. Chem. Chem. Phys.*, vol. 3, pp. 10715–10722, 2015, doi: 10.1039/b000000x.

[9] J. Yan and B. R. Saunders, "Third-generation solar cells: A review and comparison of polymer:fullerene, hybrid polymer and perovskite solar cells," *RSC Adv.*, vol. 4, no. 82, pp. 43286–43314, 2014, doi: 10.1039/c4ra07064j.

[10] V. K. Sethi, M. Pandey, and M. P. Shukla, "Use of Nanotechnology in Solar PV Cell," vol. 2, no. 2, pp. 77–80, 2011.

[11] L. Wang, Y. Wang, A. Gerger, A. Lochtefeld, K. Shreve, and A. Barnett, "Three terminal Si-Si:Ge solar cells," *Conf. Rec. IEEE Photovolt. Spec. Conf.*, pp. 000286–000289, 2011, doi: 10.1109/PVSC.2011.6185901.

[12] A. C. Varonides, "High Efficiency Multijunction Tandem Solar Cells with Embedded Short-Period Superlattices," *Proc. World Renew. Energy Congr. – Sweden, 8–13 May, 2011, Linköping, Sweden*, vol. 57, no. 570, pp. 2767–2773, 2011, doi: 10.3384/ecp110572767.

[13] Y. L. L. and H. T. Tzung-Luen Li, "High-performance quantum dot-sensitized solar cells based on sensitization with CuInS2 quantum dots/CdS heterostructure," *Energy Environ. Sci. View*, pp. 5315–5324, 2012, doi: 10.1039/c1ee02253a.

[14] Dong B, "Modeling and simulation of InAs/GaAs quantum dot solar cells in SILVACO TCAD". Master Thesis, In2014 IEEE 40th Photovoltaic Specialist Conference (PVSC) (pp. 0476-0478).

[15] I. B. Karki, "Effect of Temperature on the I-V Characteristics of a Polycrystalline Solar Cell," *J. Nepal Phys. Soc.*, vol. 3, no. 1, p. 35, 2016, doi: 10.3126/jnphyssoc.v3i1.14440.

[16] F. Benyettou, A. Aissat, M. A. Benamar, and J. P. Vilcot, "Modeling and Simulation of GaSb/GaAs Quantum Dot for Solar Cell," *Energy Procedia*, vol. 74, pp. 139–147, 2015, doi: 10.1016/j.egypro.2015.07.535.

[17] M. Mehrabian and S. Dalir, "Numerical simulation of CdS quantum dot sensitized solar cell using the Silvaco-Atlas software," *Opt. - Int. J. Light Electron Opt.*, 2016, doi: 10.1016/j.ijleo.2016.08.016.

[18] D. Chettri, T. J. Singh, and K. J. Singh, "InAs / GaAs Quantum Dot Solar Cell," *Int. J. Electron. Electr. Comput. Syst.*, vol. 6, no. 3, pp. 221–224, 2017.

[19] G. Kartopu, "Enhancement of the photocurrent and efficiency of CdTe solar cells suppressing the front contact reflection using a highly-resistive ZnO buffer layer," *Sol. Energy Mater. Sol. Cells*, vol. 191, no. August 2018, pp. 78–82, 2019, doi: 10.1016/j.solmat.2018.11.002.

[20] M. Moustafa and T. Alzoubi, "Numerical simulation of single junction ingan solar cell by scaps," *Key Eng. Mater.*, vol. 821 KEM, pp. 407–413, 2019, doi: 10.4028/www.scientific.net/KEM.821.407.

[21] L. Madani, "Numerical Simulation of InAs/GaAs Quantum well and Quantum dots solar cells," University of Mohamed Kheider of Biskra Exact, 2019.

[22] S. Royanian, A. Abdolahzadeh Ziabari, and R. Yousefi, "Efficiency Enhancement of Ultra-thin CIGS Solar Cells Using Bandgap Grading and Embedding Au Plasmonic Nanoparticles," *Plasmonics*, vol. 15, no. 4, pp. 1173–1182, 2020, doi: 10.1007/s11468-020-01138-2.

[23] A. I. Ankhi, M. R. Islam, M. T. Hasan, and E. Hossain, "Projected Performance of InGaAs/GaAs Quantum Dot Solar Cells: Effects of Cap and Passivation Layers," *IEEE Access*, vol. 8, pp. 212339–

212350, 2020, doi: 10.1109/ACCESS.2020.3039457.

[24] N. Rathore, N. L. Panwar, F. Yettou, and A. Gama, "A comprehensive review of different types of solar photovoltaic cells and their applications," 2021, doi: 10.1080/01430750.2019.1592774.

[25] A. M. Bagher, M. Mahmoud, A. Vahid, and M. Mohsen, "Types of Solar Cells and Application," vol. 3, no. 5, pp. 94–113, 2015, doi: 10.11648/j.ajop.20150305.17.

[26] Thomas S, Kalarikkal N, Oluwafemi OS, Wu J, editors. Nanomaterials for solar cell applications. Elsevier; 2019 Jun 12.

[27] P. Würfel, Physics of Solar Cells: From Principles to New Concepts, Wiley-WCH, Weinheim, 2005.

[28] B. S. M. S. Fahad Rasool , Micheal Drieberg , Nasreen Badruddin, "PV panel modeling with improved parameter extraction technique," *Elsevier*, 2017.

[29] Rappaport, Paul. "The photovoltaic effect and its utilization." Solar Energy 3, no. 4 (1959): 8-18.

[30] H. Zimmermann, Evenson, *Silicon optoelectronic integrated circuits*, Second Edi. Springer, 2004.

[31] T. Markvart and L. Castañer, *Principles of solar cell operation*. Elsevier Ltd, 2018. doi: 10.1016/B978-0-12-809921-6.00001-X.

[32] M. J. Fisher, "Optimization and Novel Applications of Luminescent Solar Concentrators by Submitted for the degree of From the Department of Physics," no. November, 2013.

[33] K. S. Rida, A. A. K. Al-waeli, and K. A. H. Al-asadi, "The impact of air mass on photovoltaic panel performance The impact of air mass on photovoltaic panel performance," no. December, 2016, doi:

10.18282/ser.v1.i1.41.

[34] M. T. C. Hussein A Kazem, "The Impact of Using Solar Colored Filters to Cover the PV Panel in Its Outcomes The Impact of Using Solar Colored Filters to Cover the PV Panel in Its Outcomes," *Sch. Bull. (A Multidiscip. J.*, no. August, 2016, doi: 10.21276/sb.2016.2.7.5.

[35] A. You, M. A. Y. Be, and I. In, "A New Silicon p-n Junction Photocell for Converting Solar Radiation into Electrical," vol. 676, no. January 1954, pp. 22–24, 2004.

[36] H. Shnishil, S. S. Chid, M. J. Yaseen, and T. J. Alwan, "Influence of Air Mass on the Performance of Many Types of PV Modulus in Baghdad," vol. 6, pp. 153–159, 2011, doi: 10.1016/j.egypro.2011.05.018.

[37] Y. H. Khattak, "Modeling of High Power Conversion Efficiency Thin Film Solar Cells," phD Thesis, Universitat Politècnica de València, 2019.

[38] A. Goetzberger, J. Knobloch, and B. Voss, *Crystalline silicon solar cells*, vol. 1. Wiley Online Library, 1998.

[39] S. S. LI, *Semiconductor Physical Electronics*. springer, 1993. doi: 10.1007/978-1-4613-0489-0.

[40] C. Kwak, "Improving the sustainability of organic and perovskite photovoltaic cells," phD Thesis,University of Sheffield, 2016.

[41] H. Ullah, B. Marí, and H. Cui, "Investigation on The Effect of Gallium on The Efficiency of CIGS Solar Cells Through Dedicated Software," vol. 453, pp. 1497–1501, 2014, doi: 10.4028/www.scientific.net/AMM.448-453.1497.

[42] S. Fonash, *solar cell devices physics*. Elsevier, 2010.

[43] S. Kundu, N. Gupta, and P. Kumar, "Review of Solar Photovoltaic Maximum Power Point Tracking Techniques," no. November, 2017, doi: 10.1109/IICPE.2016.8079494.

[44] A. W. Bett, F. Dimroth, G. Stollwerck, and O. V. Sulima, "III-V compounds for solar cell applications," *Appl. Phys. A Mater. Sci. Process.*, vol. 69, no. 2, pp. 119–129, 1999, doi: 10.1007/s003390050983.

[45] Z. Liu, W. Ma, and X. Ye, *Shape control in the synthesis of colloidal semiconductor nanocrystals*. Elsevier Inc., 2018. doi: 10.1016/B978-0-12-804069-0.00002-2.

[46] O. Lopez-Rojas and J. García Guzmán, "A review on quantum dot solar cells: Properties, materials, synthesis and devices," *2019 IEEE Int. Conf. Eng. Veracruz, ICEV 2019*, 2019, doi: 10.1109/ICEV.2019.8920641.

[47] U. Aeberhard, "Simulation of nanostructure-based high-efficiency solar cells : challenges , existing approaches and future directions," no. c, pp. 1–11, 2013.

[48] A. Luque and A. Martí, "Increasing the Efficiency of Ideal Solar Cells by Photon Induced Transitions at Intermediate Levels," *Phys. Rev. Lett.*, vol. 78, no. 26, pp. 5014–5017, 1997, doi: 10.1103/PhysRevLett.78.5014.

[49] A. Martí, "Production of photocurrent due to intermediate-to-conduction-band transitions: A demonstration of a key operating principle of the intermediate-band solar cell," *Phys. Rev. Lett.*, vol. 97, no. 24, pp. 1–4, 2006, doi: 10.1103/PhysRevLett.97.247701.

[50] A. Scaccabarozzi, S. Adorno, S. Bietti, M. Acciarri, and S. Sanguinetti, "Evidence of two-photon absorption in strain-free quantum dot GaAs/AlGaAs solar cells," *Phys. Status Solidi - Rapid Res. Lett.*, vol. 7, no. 3, pp. 173–176, 2013, doi: 10.1002/pssr.201206518.

[51] R. Tamaki, Y. Shoji, Y. Okada, and K. Miyano, "Spectrally resolved interband and intraband transitions by two-step photon absorption in ingaas/gaas quantum dot solar cells," *IEEE J. Photovoltaics*, vol. 5, no. 1, pp. 229–233, 2015, doi: 10.1109/JPHOTOV.2014.2368712.

[52] T. Nozawa, H. Takagi, K. Watanabe, and Y. Arakawa, "Direct Observation of Two-Step Photon Absorption in an InAs/GaAs Single Quantum Dot for the Operation of Intermediate-Band Solar Cells," *Nano Lett.*, vol. 15, no. 7, pp. 4483–4487, 2015, doi: 10.1021/acs.nanolett.5b00947.

[53] S. Tomic and T. S. and Y. Okada, "In-plane coupling effect on absorption coefficients of InAs/GaAs quantum dots arrays for intermediate band solar cell," *Prog. Photovoltaics Res. Appl.*, vol. 20, no. 1, pp. 6–11, 2015, doi: 10.1002/pip.

[54] S. M. Willis, "Defect mediated extraction in InAs / GaAs quantum dot solar cells," *Sol. Energy Mater. Sol. Cells*, vol. 102, pp. 142–147, 2012, doi: 10.1016/j.solmat.2012.03.010.

[55] N. S. Beattie, "Analysis of InAs/GaAs quantum dot solar cells using Suns-Voc measurements," *Sol. Energy Mater. Sol. Cells*, vol. 130, pp. 241–245, 2014, doi: 10.1016/j.solmat.2014.07.022.

[56] K. Tanabe, D. Guimard, D. Bordel, and Y. Arakawa, "High-efficiency InAs/GaAs quantum dot solar cells by metalorganic chemical vapor deposition," *Appl. Phys. Lett.*, vol. 100, no. 19, 2012, doi: 10.1063/1.4714767.

[57] A. Luque, A. Martí, and A. J. Nozik, "Solar cells based on quantum dots: Multiple exciton generation and intermediate bands," *MRS Bull.*, vol. 32, no. 3, pp. 236–241, 2007, doi: 10.1557/mrs2007.28.

[58] P. Guyot-Sionnest, "Colloidal quantum dots," *Comptes Rendus Phys.*, vol. 9, no. 8, pp. 777–787, 2008, doi: 10.1016/j.crhy.2008.10.006.

[59] A. Luque and A. Martí, "Electron-phonon energy transfer in hot-carrier solar cells," *Sol. Energy Mater. Sol. Cells*, vol. 94, no. 2, pp. 287–296, 2010, doi: 10.1016/j.solmat.2009.10.001.

[60] A. J. Nozik, "Multiple exciton generation in semiconductor quantum dots," *Chem. Phys. Lett.*, vol. 457, no. 1–3, pp. 3–11, 2008, doi: 10.1016/j.cplett.2008.03.094.

[61] L. M. Nikolenko and V. F. Razumov, "Colloidal quantum dots in solar cells," *Russ. Chem. Rev.*, vol. 82, no. 5, pp. 429–448, 2013, doi: 10.1070/rc2013v082n05abeh004337.

[62] Z. Ahmad, M. A. Najeeb, R. A. Shakoor, S. A. Al-Muhtaseb, and F. Touati, "Limits and possible solutions in quantum dot organic solar cells," *Renew. Sustain. Energy Rev.*, vol. 82, no. April, pp. 1551–1564, 2018, doi: 10.1016/j.rser.2017.07.001.

[63] D. Litvinov, A. Rosenauer, D. Gerthsen, P. Kratzert, M. Rabe, and F. Henneberger, "Influence of the growth procedure on the Cd distribution in CdSe/ZnSe heterostructures: Stranski-Krastanov versus two-dimensional islands," *Appl. Phys. Lett.*, vol. 81, no. 4, pp. 640–642, 2002, doi: 10.1063/1.1496133.

[64] A. J. N. Joseph M. Luther, Matt Law, Matthew C. Beard, Qing Song, Matthew O. Reese, Randy J. Ellingson, "Schottky Solar Cells Based on Colloidal Nanocrystal Films," *NANO Lett. 8*, vol. 8, 2008.

[65] Anwar, H., Arif, I., Javeed, U., Mushtaq, H., Ali, K. and Sharma, S.K., 2020. Quantum Dot Solar Cells. Solar Cells: From Materials to Device Technology, pp.235-258.

[66] X. W. Andras G. Pattantyus-Abraham, Illan J. Kramer, Aaron R. Barkhouse, I. R. Gerasimos Konstantatos,, Ratan Debnath, Larissa Levina, M. K. Nazeeruddin, M. Gratzel, and and E. H. Sargent, "Depleted-Heterojunction Colloidal Quantum Dot Solar Cells," *Am. Chem. Soc.*, vol. 4, 2010.

[67] Jasim, K.E., 2015. Quantum dots solar cells. Solar cells-new approaches and reviews, 1, pp.303-331.

[68] J. D. Bude and K. Hess, "Thresholds of impact ionization in semiconductors," no. March 2014, 1992, doi: 10.1063/1.351434.

[69] D. Harrison, R. A. Abram, and S. Brand, "Characteristics of impact ionization rates in direct and indirect gap semiconductors," *J. Appl. Phys.*, vol. 85, no. 12, pp. 8186–8192, 1999, doi: 10.1063/1.370658.

[70] Ellingson, Randy J., Matthew C. Beard, Justin C. Johnson, Pingrong Yu, Olga I. Micic, Arthur J. Nozik, Andrew Shabaev, and Alexander L. Efros. "Highly efficient multiple exciton generation in colloidal PbSe and PbS quantum dots." *Nano letters* 5, no. 5 (2005): 865-871.

[71] Zhao Z. Optical Characterization of InAs/GaAs 1-x Sb x Quantum-Dot Structures. Master Thesis, University of California, Los Angeles; 2018.

[72] L. E. Brus and L. E. Brus, "Electron – electron and electronhole interactions in small semiconductor crystallites : The size dependence of the lowest excited electronic state," vol. 4403, no. 1984, 2011, doi: 10.1063/1.447218.

[73] V. Aroutiounian, "Quantum dot solar cells," *Appl. Phys.*, vol. 2268, no. 2001, 2012, doi: 10.1063/1.1339210.

[74] A. J. Nozik, "Quantum Dot Solar Cells," *Compr. Nanosci. Technol.*, vol. 1–5, pp. 257–275, 2011, doi: 10.1016/B978-0-12-374396-1.00129-X.

[75] A. Fedoseyev, M. Turowski, A. Raman, and A. A. Balandin, "Multiscale Models of Quantum Dot Based Nanomaterials and Nanodevices for Solar Cells," no. January 2018, 2008, doi: 10.1007/978-3-540-69387-1.

[76] Nasr, A. and Aly, A.E.M.M., 2016. Performance Evaluation of Quantum-Dot Intermediate-Band Solar Cells. Journal of Electronic Materials, 45, pp.672-681.

[77] Aihara, T., Tayagaki, T., Nagato, Y., Okano, Y. and Sugaya, T., 2018. Design and characterization of InGaP-based InP quantum dot solar cells. Japanese Journal of Applied Physics, 57(8S3), p.08RF04.

[78] C. G. Bailey, "Open-Circuit Voltage Improvement of InAs / GaAs Quantum-Dot Solar Cells Using Reduced InAs Coverage," vol. 2, no. 3, pp. 269–275, 2012.

[79] I. Inxga, "Influence of Geometrical Shape on the Characteristics of the Multiple Influence of Geometrical Shape on the Characteristics of the Multiple InN / In x Ga 1 − x N Quantum Dot Solar Cells," no. May, 2021, doi: 10.3390/nano11051317.

[80] M. Kunrugsa,"Two-dimensional simulation of GaAsSb/GaAs quantum dot solar cells," *J. Phys. D*, 2018.

[81] R. N. B. Paranthaman, M. Parans, Winnie Wong-Ng, *Semiconductor materials for solar photovoltaic cell*. springer, 2016.

[82] P. Henry, *atlas_users1*. 2010.

[83] Bouhdjar, A., 2016. Study and numerical simulation of (a-Si: H/μc-Si: H) heterojunction solar cells. Etude et simulation numérique des cellules solaires à hétérojonction (a-Si: H/μc-Si: H (Doctoral dissertation, Université Mohamed Khider-Biskra).

[84] F. B. A. Aissat, "Electrical Properties Of InAsP/Si Quantum Dot Solar Cell," *Int. J. Hydrogen Energy*, 2017.

[85] D. M. Jihene Zribi, Bouraoui Ilahi, Bernard Paquette, Abdelatif Jaouad, Olivier Th´eriault, Karin Hinzer, Ross Cheriton, Gilles Patriarche, Simon Fafard, Vincent Aimez, Richard Ar`es, "Effect of Dot-Height Truncation on the Device Performance of Multilayer InAs/GaAs Quantum Dot Solar Cells," *IEEE J. Photovoltaics*, 2016.

[86] J. W. and E. T. S. Gaan, Guowei He, and R. M. Feenstra, "Electronic States of InAs/GaAs Quantum Dots by Scanning Tunneling Spectroscopy," *Appl. Phys. Lett.*, 2010.

[87] C. G. Bailey and C. G. Bailey, "Optical and Mechanical Characterization of InAs / GaAs Quantum Dot Solar Cells," 2012.

[88] A. L. A. Martí, a N. López, E. Antolín, E. Cánovas, "Emitter degradation in quantum dot intermediate band solar cells," *Am. Inst. Phys.*, 2007, doi: 10.1063/1.2747195.

[89] F. C. Mariangela Gioannini, Ariel P. C´edola, Member, IEEE, Natale Di Santo, Francesco Bertazzi, "Simulation of Quantum Dot Solar Cells Including Carrier Intersubband Dynamics and Transport," *IEEE J. Photovoltaics*, 2013, doi: 10.1109/JPHOTOV.2013.2270345.

[90] Belghachi, A., 2015. Theoretical calculation of the efficiency limit for solar cells. Solar Cells-New Approaches and Reviews, pp.47-76.

[91] B. S. Swapnil Dubey, Jatin Narotam Sarvaiya, "Temperature Dependent Photovoltaic (PV) Efficiency and Its Effect on PV Production in the World A Review," in *PV Asia Pacific Conference*, Elsevier, 2013. doi: 10.1016/j.egypro.2013.05.072.

[92] J. Halpern, "Metals and Semiconductors," in *CHEM 2000: Chemistry for Engineers*, LibreTexts, 2023.

[93] C. B. H. Ehsan Vadiee, Yi Fang, Chaomin Zhang, Alec M. Fischer, Joshua J. Williams, Emma J. Renteria, Ganesh Balakrishnan, "Temperature Dependence of GaSb and AlGaSb Solar Cells," *sciencedirect*, 2018.

الملخص

أدى تطوير الطاقة المتجددة الى حاجة ملحة لاستخدام الخلايا الشمسية، ومع ذلك فان الضعف في كفاءة تحويل الطاقة للخلايا الشمسية التقليدية، وجه الدراسات الحديثة الى الخلايا الشمسية ذات الكفاءة العالية في تحويل الطاقة.

الخلايا الشمسية ذات النقاط الكمومية هي واحدة من أكثر الخلايا الواعدة وهي تنتمي الى الجيل الثالث من الخلايا الشمسية، يتضمن العمل الحالي تحقيق المحاكاة في تأثير ادخال طبقات النقاط الكمومية في معايير أداء الخلية الشمسية، تم تنفيذ هيكل (p-i-n) خلية شمسية قياسية وقد تم استخدام مادة (GaAs) في هذا التركيب، إذ تمثل طبقة (p) طبقة (نقل الفجوة) وتمثل طبقة (i) (الطبقة النقية) طبقة الامتصاص اما بالنسبة لطبقة (n) فتمثل طبقة (نقل الالكترون) وتم استخدام مادة (InAs) في طبقات النقاط الكمومية (QD).

في هذا العمل، يتم الحفاظ على سمك طبقة (i) ثابتة اثناء إضافة طبقات النقاط الكمومية بداخلها؛ لتحقيق هذا الهدف تم استخدام برنامج (SILVACO - TCAD) لتنفيذ الخلية الشمسية القياسية والخلية الشمسية ذات النقاط الكمومية، تظهر نتائج المحاكاة ان الطريقة المقترحة لإضافة طبقة واحدة من (QDs) وزيادة عدد الطبقات الى (5،10،15،20) على التوالي، أدت الى تحسين أداء الخلية الشمسية وتفوقت على الخلية الشمسية القياسية من حيث (J_{sc}, V_{oc}, FF, PCE).

من خلال مقارنة نتائج الخلية الشمسية القياسية بنتائج إضافة طبقة واحدة من (QDs) يظهر تحسنا في أداء (SC) مع زيادة في الكفاءة من (12.5158%) الى (26.7046%)، إضافة المزيد من طبقات (QD's) ترتفع الكفاءة ولكن هذه الزيادة تصل الى مرحلة التشبع بعد إضافة أكثر من (10) طبقات، وأفضل قيمة للكفاءة نحصل عليها تصل الى (29.0493%) مع إضافة 10 طبقات من (QD's).

تمت دراسة تأثير درجة الحرارة على أداء الخلية الشمسية القياسية مع وجود طبقات (QDs). تظهر النتائج ان درجة الحرارة تؤثر سلبا على أداء الخلية الشمسية حيث مع زيادة درجة الحرارة تنخفض كفاءة الخلية حتى بوجود طبقات (QDs) حيث تصل قيمتها الى (25.224%) عند وصول درجة الحرارة الى (360) درجة.

<div dir="rtl">

إقرار لجنة المناقشة

نشهد بأننا أعضاء لجنة التقويم والمناقشة قد اطلعنا على هذه الرسالة الموسومة **(تصميم ومحاكاة الخلايا الشمسية ذات النقطة الكمومية عالية الكفاءة على مبدأ تقنية البلورات النانوية)** وناقشنا الطالبة **(ايمان محسن احمد)** في محتوياتها وفيما له علاقة بها بتاريخ   /   / 2024 وقد وجدناها جديرة بنيل شهادة الماجستير/علوم في اختصاص هندسة الالكترونيك.

التوقيع:

رئيس اللجنة: أ.د. خالد خليل محمد

التاريخ: /   / 2024

التوقيع:

عضو اللجنة: أ.م.د. محمد طارق ياسين

التاريخ: /   / 2024

التوقيع:

عضو اللجنة: أ.م.د. احمد محمد احمد

التاريخ: /   / 2024

التوقيع:

عضو اللجنة (المشرف): أ.د قيس ذنون نجم

التاريخ: /   / 2024

التوقيع:

عضو اللجنة (المشرف): أ.م.د عمر إبراهيم السيف

التاريخ: /   / 2024

قرار مجلس الكلية

اجتمع مجلس كلية هندسة الالكترونيــات بجلستــه .... المنـعقدة بتاريخ: /   / 2024 وقرر المجلس منح الطالبة شهادة الماجستير علوم في اختصاص هندسة الالكترونيك

مقرر المجلس: أ.م.د. بلال علاءالدين جبر

التاريخ: /   / 2024

رئيس مجلس الكلية: أ.د. خالد خليل محمد

التاريخ: /   / 2024

</div>

تصميم ومحاكاة الخلايا الشمسية ذات النقطة الكمومية عالية الكفاءة على مبدأ تقنية البلورات النانوية

رسالة تقدمت بها

ايمان محسن احمد

إلى

مجلس كلية هندسة الإلكترونيات ـ جامعة نينوى

وهي جزء من متطلبات نيل شهادة الماجستير

علم في هندسة الالكترونيك

بإشراف

الأستاذ

الدكتور قيس ذنون الجواري

الأستاذ المساعد

الدكتور عمر إبراهيم السيف

جامعة نينوى

كلية هندسة الالكترونيات

قسم الإلكترونيك

تصميم ومحاكاة الخلايا الشمسية ذات النقطة الكمومية عالية الكفاءة على مبدأ تقنية البلورات النانوية

ايمان محسن احمد

رسالة الماجستير في

الهندسة الالكترونية

بإشراف

الأستاذ

الدكتور قيس ذنون الجواري

الأستاذ المساعد

الدكتور عمر إبراهيم السيف